AN ABSTRACT OF THE DISSERTATION OF

Chadi Sayde for the degree of Doctor of Philosophy in Water Resources Engineering presented on March 22, 2012.

Title: Improving Soil Water Determination in Spatially Variable Field Using Fiber Optic Technology and Bayesian Decision Theory

Abstract approved:

Marshall J. English   John S. Selker

Achieving and maintaining sustainability in irrigated agriculture production in the era of rapidly increasing stress on our natural resources require, among other essential actions, optimum control and management of the applied water. Thus, a significant upgrade of the currently available soil water monitoring technologies is needed. The primary goal of this work was to reduce the uncertainties of spatially variable soil water in the field. Two approaches are suggested: 1) The Bayesian decision model that implicitly accounts for spatial variability at minimal cost based on limited field data, and 2) The Actively Heated Fiber Optic (AHFO) method that explicitly accounts for spatial variability with high sampling density at relatively low cost per measurement point.

The Bayesian decision model uses an algorithm to integrate information embodied in independent estimates of soil water depletion to derive a posterior estimation of soil

water status that has the potential to reduce the risk of costly errors in irrigation scheduling decisions. The sources of information are obtained from an ET based water balance model, soil water measurements, and expert opinion. The algorithm was tested in a numerical example based on a field experiment where soil water depletion measurements were made at 43 sites in an agricultural field under center pivot irrigation. The results showed that the estimates of the average soil water depletion in the field obtained from the posterior distributions of soil water depletion proved to outperform simple averaging of n soil water depletion measurements, up to n = 35 measurements. For $n < 3$, the model also provided a 39% average reduction in risk of error derived from non-representative measurements.

The AHFO method observes the heating and cooling of a buried fiber optic (FO) cable through the course of a pulse application of energy as monitored by a distributed temperature sensing (DTS) system to reveal soil water content simultaneously at sub-meter scale along the FO cable that can potentially exceeds kilometers in length. A new and simple interpretation of heat data that takes advantage of the characteristics of FO temperature measurements is presented. The results demonstrate the feasibility of AHFO method application to obtain <0.05 m^3m^{-3} error distributed measurements of soil water content under laboratory controlled conditions. The AHFO method was then tested under field conditions using 750 m of FO cables buried at 30, 60, and 90 cm depths in agricultural field. The calibration curve relating soil water content to the thermal response of the soil to a heat pulse was developed in the lab. It was successively applied to the 30 and 60 cm depths cables, while the 90 cm depth cable illustrated the challenges of soil heterogeneity for this technique. The method was used to map with high spatial (1m) and temporal (1hr) resolution the spatial variability of soil water content and fluxes induced by the non-uniformity of water application at the surface.

Improving Soil Water Determination in Spatially Variable Field using Fiber Optic Technology and Bayesian Decision Theory

by

Chadi Sayde

A DISSERTATION

submitted to

Oregon State University

in partial fulfillment of

the requirements for the

degree of

Doctor of Philosophy

Presented March 22, 2012

Commencement June 2012

Doctor of Philosophy dissertation of Chadi Sayde presented on March 22, 2012

APPROVED:

Co-Major Professor, representing Water Resources Engineering

Co-Major Professor, representing Water Resources Engineering

Director of the Water Resources Graduate program

Dean of the Graduate School

I understand that my dissertation will become part of the permanent collection of Oregon State University libraries. My signature below authorizes release of my dissertation to any reader upon request.

Chadi Sayde, Author

ACKNOWLEDGEMENTS

A special word of sincere appreciation is extended to my major professors Prof. Marshall English and Prof. John Selker. I am very grateful for your helpful comments, guidance, and advices during my research. This research would not have been possible without your support and your facilitation to "think outside the box".

Prof. Alix Gitelman served as my statistic minor advisor and I gratefully acknowledge her guidance. Additionally, I would like to thank my other graduate committees Prof. Richard Cuenca and Prof. Pence Deborah for serving on my committee and for their helpful comments. I would like also to express gratitude for the Department Head John Bolte for his support.

I would like to thank agencies that supported the work on which the dissertation was based including the National Science Foundation (grants NSF-EAR-0930061, NSF-EAR-07115494) and the Oregon Experiment Station.

Mr. Kent Madison deserves special thanks for his generous contribution of time, land, experience, and friendship.

I have been very fortunate to have friends and department mates who were all so incredibly friendly and supportive: Javier, Ryan, Daniel, Travis, Ari, Maria, Chris, Charles, Carole, Yutaka, Erika, Barb, Carb, Judy, Mary Anne, Jim, Joy and Scott…..

I would like also to thank those who made this thesis possible such as my parents and my sisters who gave me the moral support.

I am thankful for my son Gio who filled my life with love and adventure. You are always able to put a big smile on my face, each single day.

Finally, I acknowledge my wife, best friend, and colleague Laureine for her continued confidence and support during the whole journey. I will always treasure the hours spent together in the field, lab, and office, and the nights that you spent listening to me talking about my project. It is impossible to completely express my thanks.

CONTRIBUTION OF AUTHORS

John Selker was the principal investigator for the research related to the AHFO method (2nd and 3rd manuscripts). He provided invaluable expertise, experimental oversight, manuscript editing and organized the funds for those projects.

Marshall English was very involved for years in these projects, provided very constructive guidance, manuscript editing and financial support. He was the principal investigator for the Bayesian model (1st manuscript).

Alix Gitelman, a statistician at Oregon State University, provided guidance in the 1st manuscript particularly with ways to present Bayesian statistical model.

Scott Tyler and Richard Cuenca helped to improve review of the 2nd manuscript by providing invaluable advices.

Laureine El Khoury was extensively involved in the installations, data collection, and analysis of these researches. Christopher Gregory, Maria Gil Rodriguez, Javier Benitez, and Leonord Rodriguez helped in the lab experiments. Maria Gil Rodriguez was very supportive on various aspects of the data processing using Matlab. Charles Hillyer was very helpful in his programming skills by generating the outputs of Irrigation Management Online.

TABLE OF CONTENTS

TABLE OF CONTENTS (Continued)

LIST OF FIGURES

LIST OF FIGURES (Continued)

LIST OF TABLES

1. General Introduction

1.1 Uncertainty in Soil Moisture Measurements

The fundamental objective of scientific irrigation scheduling is accurate tracking of crop-available water in the soil. A variety of techniques are employed to measure soil water content, which is then used to calculate the amount of available water remaining in the root zone. But measurements of soil water content are inherently uncertain, and because crop water availability is defined in terms of the remaining 'available capacity' in the root zone the uncertainty of measured soil moisture is compounded by the natural variability of soil water holding characteristics and inexact knowledge of crop root zones and water uptake patterns.

The net effect is that estimates of field-wide crop water availability derived from soil moisture measurements are quite uncertain. Some degree of uncertainty is intrinsic to the measurement technique used. Additional uncertainty derives from soil heterogeneity and uneven distribution of applied water.

A point measurement of soil water content will often not be representative of average conditions, nor will it provide any information about the variability of soil water content. Additionally, the uncertainty of computed values of crop available water will be compounded by wide variations in total holding capacities.

1.2 Dealing with Uncertainty

When water supplies are not limited the problem of measurement uncertainty is often circumvented by maintaining soil moisture at higher than critical levels, relying on point measurements of soil moisture to decide when to irrigate, and maintaining some soil water in reserve as a hedge against uncertainty. But with the accelerating competition for water and resulting increases in opportunity costs of water, the practice of holding soil moisture in reserve will become progressively more expensive. That implies a need for more accurate ways of estimating crop water availability in heterogeneous fields.

More accurate determinations can be derived by replication, i.e., by taking measurements at several points in the field. The common assumption is that the variance of measured depletion is reduced inversely with the square of the number of replicated measurements. However the validity of this assumption is limited by two factors:

- Individual measurements are not always statistically independent. Different soil types encompassed within a single field imply patterned variations in water holding characteristics.
- Non-uniform applications of irrigation water, compounded by redistribution of surface runoff and preferential subsurface flows may result in systematic variations in soil water distributions. Consequently, soil moisture

measurements taken within definable sub-sectors of a field may be highly correlated.

- Uncertainties of crop root zone and uptake patterns are not reduced by replication of soil moisture measurements. The uncertainty of available capacity remains a confounding factor.

The cost of replication is also another important factor. Because the accuracy of measurements is more or less inversely proportional to cost, the irrigation manager faces a Hobson's choice. The high cost of more accurate measurements may preclude taking multiple measurements; lower cost methods characterized by low accuracy require multiple measurements to be effective.

1.3 Alternative Approaches-Objectives

The primary goal of this work is develop alternative approaches for reducing the uncertainties of spatially variable soil water contents in the field. Two approaches are suggested:

1. The Bayesian decision model that implicitly accounts for spatial variability with virtually no additional cost.
2. The Actively Heated Fiber Optic (AHFO) method that explicitly account for spatial variability with relatively low cost per measurement point and replica.

For the first approach, the specific objective is to explore the concept of using a Bayesian algorithm to integrate information embodied in independent estimates of soil water depletion generated from an ET based model with the information derived from soil moisture measurements in the field as well as additional subjective information to derive a posterior estimation of soil water status that has the potential to provide a better basis for irrigation decisions. An irrigation decision that will be based on:

1. More accurate estimation of the average condition of soil water in the field.
2. Reduced risk of relaying on measurements or modeling outputs that are substantially non representative of the average condition of soil water in the field.

The Bayesian decision model approach is detailed in Chapter 2.

For the second approach, the objectives are first to test, under controlled conditions, the feasibility of using a novel approach for analyzing the thermal response of buried fiber optic cable to a heat pulse in order to retrieve high temporal (< 1 hr) and spatial (< 1 m) resolution distributed measurements of soil water content. The feasibility analysis of the AHFO method is presented in Chapter 3.

Then, condition the capability of the AHFO method to capture with high spatial and temporal resolution the spatial variability of soil water content and fluxes is tested under field. The AHFO field testing methodology and results are presented in Chapter 4.

2. A Bayesian Decision Model for Reducing the Uncertainty of Soil Water Determinations

Chadi Sayde, Alix Gitelman, and Marshall English

Journal of Irrigation and Drainage Engineering
American Society of Civil Engineers
1801 Alexander Bell Drive
Reston Virginia 20191

To be submitted

2.1 Abstract

Scientific irrigation scheduling often relies on calculated evapotranspiration (*ET*) to estimate daily soil water depletion. Since the resulting estimates of soil water content are uncertain, and become increasingly uncertain as *ET* estimation errors accumulate over a period of time, it is common practice to measure soil water periodically to correct the soil water content estimates. But soil water content measurements are also subject to substantial error. While both *ET*-based estimates and field measurements of soil water content provide useful information, neither is sufficiently accurate for purposes of precise irrigation management.

An algorithm for minimizing uncertainty of soil water depletion determinations is presented. Based on Bayesian decision analysis, the algorithm integrates information from ET estimates and soil water content measurements to derive $\hat{\delta}_i$, the posterior estimate of soil water content at each particular location in the field. $\hat{\delta}_i$ has the potential to provide a better basis for irrigation decisions. An indicator was also developed to identify potential problems with the various sources of the model inputs. The algorithm was tested in a numerical example where soil water depletion measurements were made at 43 sites. These provided a basis for evaluating the performance of the model. For determining average condition of soil water depletion in the field, the estimates derived from $\hat{\delta}_i$ proved to outperform simple averaging of n soil water depletion measurements. For n<4, the model also provided a 39% average

reduction in risk of error derived from extremely non representative measurements of the average conditions of soil water depletion, i.e., measurements or combination of n measurements that are outside an error band of ± 50% range of the true average soil water depletion.

2.2 Introduction

In any irrigation management decision irrigation managers need to answer the three fundamental questions: 1) How much water to apply?, 2) When to apply it?, and 3) How to apply it? [*Fereres et al.,* 2003].

From a conventional irrigation management perspective, the answers for the three former questions are strategically shaped by the objective of minimizing yield losses through: 1) satisfying all plant evaporative demands, 2) before crop water-stress occurs and 3) in >90% of the field [*English et al*., 2002]. The answers are usually formulated by quantitative approaches [*Fereres et al.,* 2003] such as direct soil water measurements and monitoring, and soil water balance modeling. A variety of techniques are employed to determine soil water content, which is then used to calculate the amount of available water remaining in the root zone. All of these techniques are subject to error, and because crop water availability is defined in terms of the remaining fraction of 'available capacity' in the root zone, the uncertainty of an estimated or measured soil water content is compounded with the natural variability of soil water holding characteristics and inexact knowledge of crop root zones and water uptake patterns. Several methods are usually employed to mitigate the effects of uncertainty associated with soil water depletion determinations when conventional irrigations scheduling methods are employed. For instance, the threshold of soil water content at which an irrigation event will be initiated is usually set higher than the true water stress threshold level at which crop yields will be reduced, in order to minimize the risk of crossing the stress threshold [*Schmitz and Sourell*, 2000]. Likewise, the target soil water refill level is often set lower than field capacity to avoid overfilling the root zone profile. Using such uncertainty mitigation techniques, conventional irrigation management can maximize crop yield while minimizing associated risks. But such strategies for mitigating uncertainty can be expensive, and are inconsistent with economically optimized irrigation scheduling strategies such as deficit irrigation [*English et al*., 2003].

The accelerating competition for water and resulting decreases in availability and increases in opportunity costs of water have motivated the emergence of a fundamentally new paradigm for irrigation management that seeks to maximize net economic returns to water rather than maximizing yields [*English*, 1996; 2002] especially in arid and semi-arid regions [*Debaeke and Aboudrare*, 2004]. Generally, deficit irrigation is an effective strategy for maximizing returns to water [*English*, 1990; *Fereres and Soriano*, 2006; *Geerts and Raes*, 2009]. Deficit irrigation involves deliberate under-irrigation of some land at some times during the irrigation season soil water content is allowed to fall below the soil plant water-stress threshold level and crop stress and potential yield reduction are expected.

Optimum management will therefore require accurate tracking of crop-available water in the soil to enable carefully controlled levels of soil water depletion. Thus, uncertainty mitigation techniques routinely used in conventional irrigation scheduling are no longer applicable, and consequently, errors in implementation of optimal irrigation strategies are practically inevitable. Such errors can eventually lead to sub-optimal irrigation management, reduced net returns, increased economic risk [*English*, 1981] and increased environmental impacts [*English*, 2002].

Irrigation managers currently seek to reduce the uncertainty by methods that vary in reliability and precision. Some involve scientific measurement, but the irreducible uncertainties associated with all practical, currently available scientific measurement techniques are generally substantial. To reduce these uncertainties much more measurement replicas in the field are needed than what is currently employed in the field of irrigation management. This requires additional investments that can only be justified economically by high value crops, extreme water resources stress and costs, or by very tight regulatory constraints on non-point sources pollution driven by agricultural water application. Other methods are more or less subjective, including unverified simulation and professional judgment, but such subjective methods may embody valuable information. The argument we make here is that valuable information gleaned from multiple sources, including both imperfect measurements and subjective information, may be combined for a more useful estimate of soil water depletion than is possible with any single source. But all such information is intrinsically uncertain, and that uncertainty must be accounted for in the analysis.

This paper will focus on a methodology to reduce the uncertainty, of some of the already commercially available methods for determination of soil water depletion.

English et al. [2008] and *Sayde et al*. [2008] proposed an analytical approach to reduce the uncertainty of estimated crop available water with virtually no additional cost, utilizing a Bayesian decision model to integrate information embodied in different estimators of soil water depletion. In their approach, the uncertainties of two common methods of estimating soil water depletion, one based on cumulative estimated *ET* the other on soil water measurements, are quantified. Then the probability distributions of the two estimators are incorporated into a posterior probability distribution of depletion that provides a better basis for assessing average plant available water in the field. However, their approach did not account for the spatial variability of actual crop water uptake and applied water, which can lead to subsequent variability in soil water depletion across the field.

In this paper, we propose an analytical method to reduce the uncertainty in determinations of soil water depletion while accounting for its variability in the field. A normal-normal Bayesian model will be used to combine estimates of soil water depletion from two sources: 1) soil water measurements, and 2) an irrigation scheduling model that accounts for the spatial variability of soil physical properties and non-uniformity of antecedent soil water content (due to uneven uptake and non-uniform application). The irrigation Management Online (IMO) model will be used as the evapotranspiration (*ET*) and irrigation scheduling model in this paper.

2.3 The Bayesian Model

The objective of this work is to provide a mechanism for explicitly accounting for and reducing the uncertainty in soil water depletion estimates when formulating optimum irrigation strategies. To this end, estimates of soil water depletion from both the IMO model (the *ET* model) and soil water measurements will be treated as random variables rather than deterministic quantities. The probability distributions of each will be combined in a Bayesian analysis to derive a posterior distribution of depletion, which will, on the one hand, provide a better basis for irrigation decisions, and on the other hand, adjust the soil water distribution estimates generated by the IMO model to provide better initial estimates of soil water distribution for the day that follows a soil water measurement.

The following is a list of parameters used in the model formulation:

δ_i	True soil water depletion at location *i*	(mm)
D_i	Measured soil water depletion at location *i*	(mm)
σ_{Di}^2	Variance in D_i due to measurement errors at location *i*	(mm)
ω	True field-average soil water depletion	(mm)
τ^2	True spatial variance of soil water depletion in the field	(mm^2)
m	Modeled field-average soil water depletion from IMO	(mm)
s^2	Modeled spatial variance of soil water depletion in the field from IMO	(mm^2)
α^2	Coefficient of confidence in the IMO model outputs	(mm^2)
ϕ_i	True maximum amount of water stored in the crop root zone at field capacity at location *i*	(mm)

θ_i	True soil water content at location i	(mm)
M_i	Measured soil water content (mm) at location *i*	(mm)
M_{FCi}	Measured soil water content at field capacity at location *i*	(mm)
ξ_i	random error in soil water measurement at location *i*	(mm)
σ_i^2	Variance of ξ_i	(mm^2)
ξ_{FCi}	random error in soil water measurement at field capacity at location *i*	(mm)
σ_{FCi}^2	Variance of ξ_{FCi}	(mm^2)
$\hat{\delta}_i$	Posterior estimate of δ_i	(mm)
$\hat{\sigma}^2_{\hat{\delta}i}$	Posterior variance of $\hat{\delta}_i$	(mm^2)
$\hat{\omega}$	Estimated average soil water depletion in the field	(mm)
$\hat{\tau}^2_{\omega}$	Variance of $\hat{\omega}$	(mm^2)
$\overline{D}_i$	Sample average of D_i across the field	(mm)
$\sigma^2_{\overline{D}i}$	Variance of $\overline{D}_i$	(mm^2)
$\overline{\lambda}_p$	Difference between $\hat{\omega}$ and m	(mm)
$\overline{\lambda}_m$	Difference between $\hat{\omega}$ and $\overline{D}_i$	(mm)
N	Total number of D_i	

2.3.1 The model structure

A normal Bayesian model with known variance and normal prior for the mean is suggested to estimate δ_i, the true soil water depletion at a particular location (*i*) in the field. The advantage of this model is that it accounts for both the spatial variability of soil water depletion across the field (by allowing each location its own mean), and the uncertainty of soil water depletion measurements (i.e. the measured error) while keeping the computational costs manageable.

The structure of the model is presented in Figure 2.1. Here we assume that at a particular moment in time, the prior distribution of δ_i in the field follows a normal distribution $N(m, s^2 + \alpha^2)$ where m is the IMO simulated average soil water depletion in the field. s^2 the variance of the IMO simulated soil water depletion in the field and α^2 is a coefficient added to s^2 to reflect the uncertainty in the IMO model outputs. A full description of the prior distribution can be found in section 2.3.3.

D_i is the measured soil water depletion at location (i). Assuming that the measurement instrument is unbiased we take σ_{Di}^2 to be the error of a particular measurement, D_i. We assume that D_i follows a normal distribution (as indicated in section 2.3.2) so that:

$$D_i \,|\, \delta_i, \sigma_{Di}^2 \sim N(\delta_i, \sigma_{Di}^2) \qquad \text{Eq. 2.1}$$

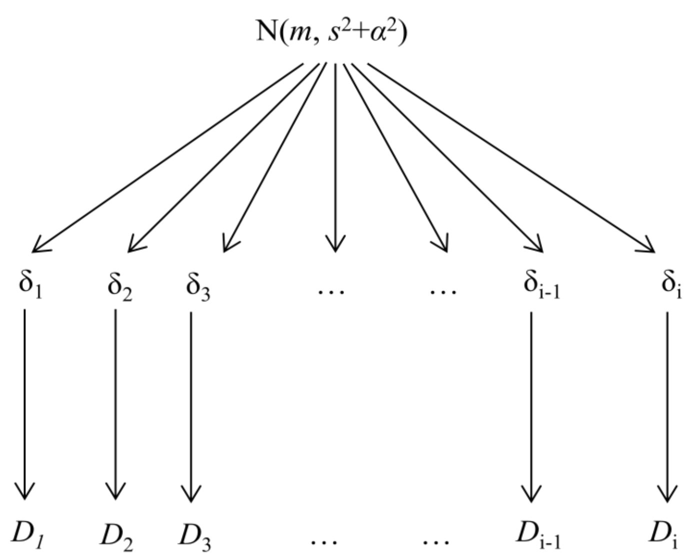

Figure 2.1 Structure of the normal model

Our objective is to obtain an estimate of the average soil depletion in the field for irrigation management decisions. This will be obtained in two steps: 1) First, posterior estimate and variance for each δ_i is calculated by using the normal Bayesian model to combine the measured soil water depletion data and a prior distribution for the δ_i 's obtained from IMO. Then 2) the various posterior estimates of δ_i obtained in the previous step are used to calculate an estimated mean of the soil water depletion in the field (i.e. an approximate posterior field average soil water depletion) as well as the uncertainty in this estimated mean.

In the following sections we will first describe, in section 2.3.2, how the D_i probability distribution is obtained. Then in section 2.3.3, we will address the prior distribution characteristics and the IMO model description that is used to generate the prior. Finally in section 2.3.4, we present the posterior distribution formulation and the use of the posterior distributions of the δ_i to calculate an approximate posterior estimate of field-average soil water depletion and its related uncertainty.

2.3.2 Probability distributions of measured soil water depletion

Measured soil water depletion is derived from the difference between the measured maximum amount of water stored at field capacity (M_{FC}) and measured current soil water content (M). Estimates of depletion derived from soil water measurements may be quite uncertain. In fact, in addition to the uncertainty associated with measuring M_{FC} and M, both are measured at random points in a heterogeneous field, and integrated through an uncertain root zone. Soil water depletion is known to vary across a field. This is mainly due to 1) heterogeneity of water application and 2) the spatial heterogeneity of crop-available water and crop development, and the consequent variability of crop ET associated with areas of low water availability.

The main sources of uncertainties associated with the determination of soil water depletion at a particular location in the field are: 1) errors in measurement of current soil water content, 2) uncertainty in M_{FC}.

We define ϕ_i to be the true maximum amount of water stored in the crop root zone at field capacity at a particular location (i) in the field, and θ_i to be the true soil water content (mm) at a given time. Then δ_i, the true soil water depletion at location i, can be expressed as:

$$\delta_i = \phi_i - \theta_i \qquad \text{Eq. 2.2}$$

ϕ_i, and θ_i are usually unknowns, and we rely on measurements to determine the soil water depletion at a particular location. But, every measurement imbeds errors that need to be characterized in order to be used effectively in determination of soil water depletion.

In this context we will assume that D_i is obtained from subtracting M_i, the measured soil water content (mm) at location i , from M_{FCi} the measured soil water content at field capacity at location i such as:

$$D_i = M_{FCi} - M_i \qquad \text{Eq. 2.3}$$

To account for the uncertainty in soil water measurements, M_i is expressed as:

$$M_i = \theta_i + \xi_i \qquad \text{Eq. 2.4}$$

Where ξ_i is a random error with $\xi_i \sim N(0,\sigma_i^2)$

Here, σ_i^2, the variance of random errors at a particular point in the field, usually comes from: I) instrument error, II) calibration error and III) integration error (including the uncertainty of root zone depth). For example, in the case of neutron probe measurements (the instrument we will focus on here), the instrument error is associated with the count measurement precision. The calibration variance is associated with the use of single calibration curve for all locations, and errors arising from the calibration process itself [*Hupet et al.,* 2004]. The integration variance is associated with the numerical technique used to integrate measurements through the root zone [*Haverkamp et al*., 1984]. Detailed statistical methods to quantify the uncertainty in neutron probe soil water measurements are detailed in *Haverkamp et al*. [1984] and *Hupet et al.* [2004].

To account for the uncertainty in the field capacity measurements, M_{FCi} can be expressed as:

$$M_{FCi} = \phi_i + \xi_{FCi} \qquad \text{Eq. 2.5}$$

where:

- ξ_{FCi} is a random (measurement) error such that $\xi_{FCi} \sim N(0,\sigma_{FCi}^2)$. The same methodology described above can be used to quantify σ_{FCi}^2.

Ideally, a specific value of M_{FCi} is obtained at each location (i). This can be achieved by direct measurement of soil water content when location i is assumed to be at field capacity. However, in most cases such measurement is difficult and expensive to obtain under field conditions, leading the irrigation manager to use a single value of soil water content at field capacity. In this case additional sources of uncertainty are to be expected in the determination of soil water depletion at any location in the field. Characterizing and accounting for these additional sources of uncertainty will be discussed in the results and discussion sections.

Again, the objective is to obtain a statistical distribution of the uncertain measured soil water depletion (D_i) to be used in the Bayesian model. This can be obtained by deriving the expected value and the variance of D_i in Equation 2.3. Being the difference of two normally distributed parameters (M_i and M_{FCi}) assumed to be independent for the sake of simplicity, then D_i follow a normal distribution as follows:

$$D_i \sim N(\delta_i, \sigma_{Di}^2) \qquad \text{Eq. 2.6}$$

where:

$$\sigma_{Di}^2 = \sigma_{FCi}^2 + \sigma_i^2 \qquad \text{Eq. 2.7}$$

2.3.3 Prior distribution of soil water depletion in the field

The prior distribution of soil water depletion across the field is obtained using IMO simulations. IMO is a web-based advisory service for optimum irrigation management. It is designed to assist irrigation managers with planning and implementing optimum irrigation strategies when water supplies are limited or expensive.

IMO uses a soil water balance model, tracking irrigation and precipitation inputs, estimating potential crop *ET*, adjusting the potential *ET* to account for low soil water or wet surface conditions, and application non-uniformity. It has two components:

1. A preseason planner that allows the irrigation mangers to test the performance of different cropping patterns and irrigation scheduling strategies.
2. A near real-time irrigation scheduler that automatically downloads near real-time data from weather stations and incorporates measured soil water to provide irrigation scheduling advice during the growing season.

This application is different from most other scheduling tools in that it is focused on maximizing net economic returns from irrigation rather than simply maximizing yield. Of particular relevance is that IMO explicitly models the spatial n heterogeneity of soil physical properties and soil water availability, the key parameters of interest here.

IMO simulates the spatial variability of the applied water (*AW*), available water holding capacity (*AWHC*), and soil depths (*RD*) using a Monte-Carlo method to assign random values of AW, *AWHC* and *RD* to a set of random monitoring points within a field. Using a water balance approach, these spatially variable factors are combined with algorithms for estimation of spray loss, *ET*, infiltration and percolation to estimate field scale variability of plant available water and soil water depletion.

The IMO model outputs that we are interested in are *m*, the simulated average soil water depletion in the field, and s^2, the variance of the simulated soil water depletion in the field. A parameter, α^2, is added to s^2 to reflect the uncertainty in the IMO model outputs. For the scope of this paper, we assumed that α^2 is a user input based on an educated guess. Nevertheless, IMO could be adapted to calculate an α^2 value for each time step by accounting for the various sources of uncertainties associated with its input parameters and algorithms involved in the simulations. Two general objections might be raised from incorporating “subjective” information into the analysis; first, that such information lacks scientific rigor, and second that judgment can vary from one individual to another. But by using expert judgment the analyst is introducing valuable additional information that could not otherwise be incorporated into the analysis. The loss of objectivity and lack of consistency that may result must be viewed as reasonable tradeoffs for the additional information introduced to the analysis [*English and Orlob*, 1978]. In addition this additional information is used in a decision making context, which is the purpose of developing this Bayesian decision model in the first place. This is fundamentally different from the scientific inquiry context where analysts prefer not to take the risk of biasing their results by adding subjective information [*English and Orlob*, 1978].

In the follow-up example in section 2.3.4, the educated guess for α^2 will be based on *Sayde et al.* [2008] analysis of the uncertainly in ET and ET_c in the region where the test field is located.

The assumed prior distribution of δ_i is:

$$P(\delta_i | m, \alpha^2, s^2) \sim N(m, s^2 + \alpha^2) \qquad \text{Eq. 2.8}$$

2.3.4 The posterior distribution of soil water depletion and an approximate posterior estimated field average soil water depletion

Using Bayes rule to combine the data distribution $P(D_i | \delta_i, \sigma^2_{Di})$ and the prior distribution $P(\delta_i | m, \alpha^2, s^2)$, the posterior distribution of δ_i is given up to a constant of proportionality as:

$$P(\delta_i | D_i, m, \sigma^2_{Di}, s^2, \alpha^2) \propto P(\delta_i | m, s^2, \alpha^2) \times P(D_i | \delta_i, \sigma^2_{Di}) \qquad \text{Eq. 2.9}$$

Using the assumption that both data distribution and prior distribution are normal, we obtain:

$$p(\delta_i \mid D_i, m, \sigma_{Di}^2, s^2, \alpha^2) \propto$$

$$\frac{1}{\sqrt{2\pi(s^2+\alpha^2)}}\exp\left[-\frac{1}{2(s^2+\alpha^2)}(\delta_i - m)\right] \times \frac{1}{\sqrt{2\pi\sigma_{Di}^2}}\exp\left[-\frac{1}{2\sigma_{Di}^2}(D_i - \delta_i)^2\right] \quad \text{Eq.2.10}$$

After performing the necessary calculation (see Appendix A) we obtain the estimated posterior distribution of δ_i as follows:

$$P\left(\hat{\delta}_i \middle| D_i, m, s^2, \alpha^2\right) \sim N\left(\hat{\delta}_i, \hat{\sigma}_{\hat{\delta}i}^2\right) \quad \text{Eq. 2.11}$$

where:

$$\hat{\delta}_i = \frac{\dfrac{m}{s^2+\alpha^2} + \dfrac{D_i}{\sigma_{Di}^2}}{\dfrac{1}{s^2+\alpha^2} + \dfrac{1}{\sigma_{M\delta i}^2}} \quad \text{Eq. 2.12}$$

and

$$\frac{1}{\hat{\sigma}_{\hat{\delta}i}^2} = \frac{1}{s^2+\alpha^2} + \frac{1}{\sigma_{Di}^2} \quad \text{Eq. 2.13}$$

$\hat{\delta}_i$ can be combined to calculate a approximate posterior distribution of field average soil water depletion, as follows:

$$\hat{\omega} = \frac{\sum_{i=1}^{n} \frac{\hat{\delta}_i}{\hat{\sigma}_{\delta i}^2}}{\sum_{i=1}^{n} \frac{1}{\hat{\sigma}_{\delta i}^2}} \qquad \text{Eq. 2.14}$$

and,

$$\hat{\tau}_{\omega}^2 = \frac{1}{\sum_{i=1}^{n} \frac{1}{\hat{\sigma}_{\delta i}^2}} \qquad \text{Eq. 2.15}$$

where:

- $\hat{\omega}$ is the estimated average soil water depletion in the field
- $\hat{\tau}_{\omega}^2$ is the estimated variance of $\hat{\omega}$
- *n* is the number of measurement locations that are averaged

2.3.5 Assessing the model output

In order to provide decision makers with additional information that reflects the degree of belief in the posterior estimates, an indicator is developed to identify potential problems with the various sources of inputs. This indicator can be potentially used for the IMO model calibration. Here, we argue that there is no established measure of credible interval for the Bayesian model outputs. Absent any such measure of credibility we cannot judge whether the posterior distribution is a reliable basis for decision making. An appropriate measure of credibility can indicate whether the approximate posterior distribution is reasonably consistent with the original input information; if the approximate posterior distribution is consistently and substantially different from either the measurements or the prior (IMO modeling outputs), this will indicate that a problem exists in either or both sources of information, in which case a careful assessment of those sources of information is warranted, and the posterior output should be used with extra caution.

One way to identify potential problems with the model outputs is to use the approximate posterior outputs to judge the likelihood of observing the measured and prior values. An example of this procedure is to look at both the estimated differences ($\bar{\lambda}_p$) between the mean of the approximate posterior distribution and the mean of the prior distribution, and the estimated differences $\bar{\lambda}_m$ between the mean of the approximate posterior distribution and the mean of $\bar{D}_i$ distribution. Here $\bar{D}_i$ is the weighted average of n D_i :

$$\bar{D}_i = \frac{\sum_{i=1}^{n} \frac{D_i}{\sigma_{Di}^2}}{\sum_{i=1}^{n} \frac{1}{\sigma_{Di}^2}} \qquad \text{Eq. 2.16}$$

and,

$$\sigma_{\overline{D}i}^{2} = \frac{1}{\sum_{i=1}^{n} \frac{1}{\sigma_{Di}^{2}}} \qquad \text{Eq. 2.17}$$

As normality is assumed for the measured, prior, and approximate posterior distributions then, $\bar{\lambda}_p \sim N(m\text{-}\hat{\omega}, \sigma_p{}^2)$ and $\bar{\lambda}_m \sim N(\overline{D}i - \hat{\omega}, \sigma_m{}^2)$, Where:

$$\sigma_p{}^2 = \sigma_{Di}{}^2 + \hat{\tau}_{\omega}^2 \qquad \text{Eq. 2.18}$$

and,

$$\sigma_m{}^2 = \alpha^2 + s^2 + \hat{\tau}_{\omega}^2 \qquad \text{Eq. 2.19}$$

Then, $\bar{\lambda}_p$ and $\bar{\lambda}_m$ distributions can be used to verify that the probability of observing the zero difference value (the value which would indicate there is no difference between the means under the criteria that are tested) is within a certain range "*d*". Here, *d* is left to the user judgment. Note that, in principle, the variances of the two "differences" distributions should decreases with increasing *n,* and thus allowing testing the difference between the parameters over stricter interval.

This methodology can also be used to calibrate the IMO model. For instance if a time series of soil water depletion measurements is available, IMO input parameters can be calibrated such as to observe at every time step a probability of *zero difference* between the posterior means and IMO generated prior that is in a certain range *d*.

2.3.6 An alternative Bayesian model to estimate the average soil water depletion in the field

The Bayesian model described in the previous paragraphs treats every D_i independently to obtain one particular posterior distribution for each one of the D_i. The advantage of such technique is that it will potentially allow each D_i to have its own prior distribution in case additional information is available on the spatial location of the measurement. An example of the potential additional information is the farmer/irrigation manager judgement on how representative a particular measurement location is in relation to the patterns of depletion across a particular field.

If spatial information on each of the D_i cannot be obtained, an alternative hierarchical normal-normal model can also be employed to generate a posterior distribution estimate of the field average soil water depletion. The structure of the model is detailed in Figure 2.2.

In this model we have:

$D_i \,\big|\, \delta_i \,, \sigma_{Di}^2 \sim N(\delta_i \,, \sigma_{Di}^2)$ σ_{Di}^2 assumed known

$\delta_i \,\big|\, \omega \,, \sigma_\delta^2 \sim N(\omega \,, \sigma_\delta^2)$ $\sigma_\delta^2 = s^2$ assumed known from IMO

$\omega \sim N(m \,, \alpha^2)$ *m* assumed known from IMO

α^2 user input

Then the posterior distribution of ω, can be expressed as (see Appendix 2 for full derivation for the posterior distribution):

$$f\left(\omega \,\middle|\, \widetilde{D}\right) \sim N(\widehat{\omega}, \widehat{\alpha}^2)$$

With:

$$\widehat{\omega} = \frac{\frac{m}{\alpha^2} + \sum_{i=1}^{n} \frac{D_i}{\sigma_{Di}^2 + \sigma_\delta^2}}{\frac{1}{\alpha^2} + \sum_{i=1}^{n} \frac{1}{\sigma_{Di}^2 + \sigma_\delta^2}} \qquad \text{Eq.2.20}$$

And,

$$\widehat{\alpha}^2 = \frac{\frac{m}{\alpha^2} + \sum_{i=1}^{n} \frac{D_i}{\sigma_{Di}^2 + \sigma_\delta^2}}{\frac{1}{\alpha^2} + \sum_{i=1}^{n} \frac{1}{\sigma_{Di}^2 + \sigma_\delta^2}} \qquad \text{Eq.2.21}$$

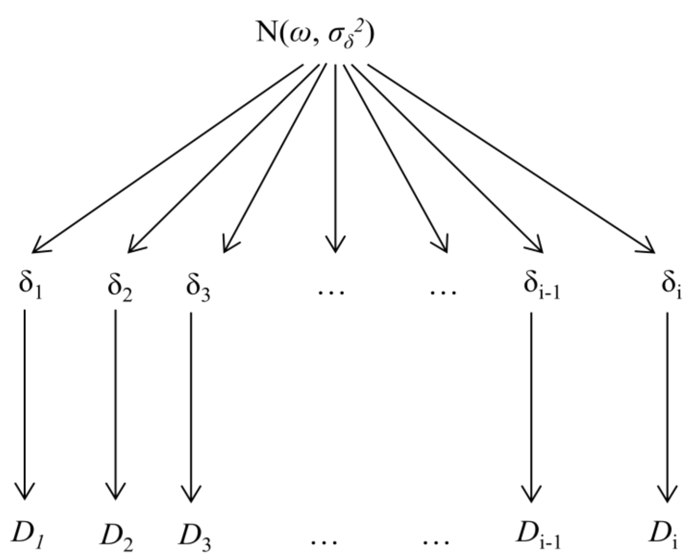

Figure 2.2 Structure of the hierarchical normal-normal model

2.4 A Numerical Example

The analytical approach outlined above is illustrated in a case study for mid-season irrigation of a winter wheat field on a cooperating farm near Echo, Oregon. The objective of the numerical example is to gain some insights on how the model performs, and what are its limitations.

The data used in the numerical example are from a non-published field experiment to study the yield response to different irrigation treatments. In the experiment, the field was divided in three sections. In section 1 (~15.4 ha), water was applied to meet the evaporative demands. In section 2 (~15.4 ha), the center pivot speed was adjusted to apply 60% of the water application in section 1. Section 3 (~25.1 ha), was divided into eight zones of application treatments by adjusting the center pivot speed at each of the eight zones. The eight treatments are: 110, 90, 85, 80, 70, 50, 30, and 0% of the water applied in section 1 in each single irrigation event.

In this numerical example, we will use the data of soil water monitoring network installed in section 1 to illustrate the spatial variability of soil water depletion measured in the field. The soil monitoring network consisted of fifty 1.5” PVC tube distributed in section 1 and monitored periodically by a neutron probe (CPN 503DR). The locations of the access tube are illustrated in Figure 2.2. Soil water measurements were taken at 15cm increments in depth. Each measurement consisted of a 16 seconds reading time. A calibration equation to transfer the measured neutron count ratio into soil water value was developed specifically for this field.

Field capacity measured in the field at the beginning of the irrigation season showed significant spatial variability (Figure 2.3). This can be explained mainly by the large variation in soil depth in the field (Figure 2.4).

Out of the 50 access tubes installed in section 1, 43 will be used in the analysis. The remaining 7 were not installed when the field capacity values were obtained or were not measured on the 27th of May, the day that we will focus on for this numerical example

,

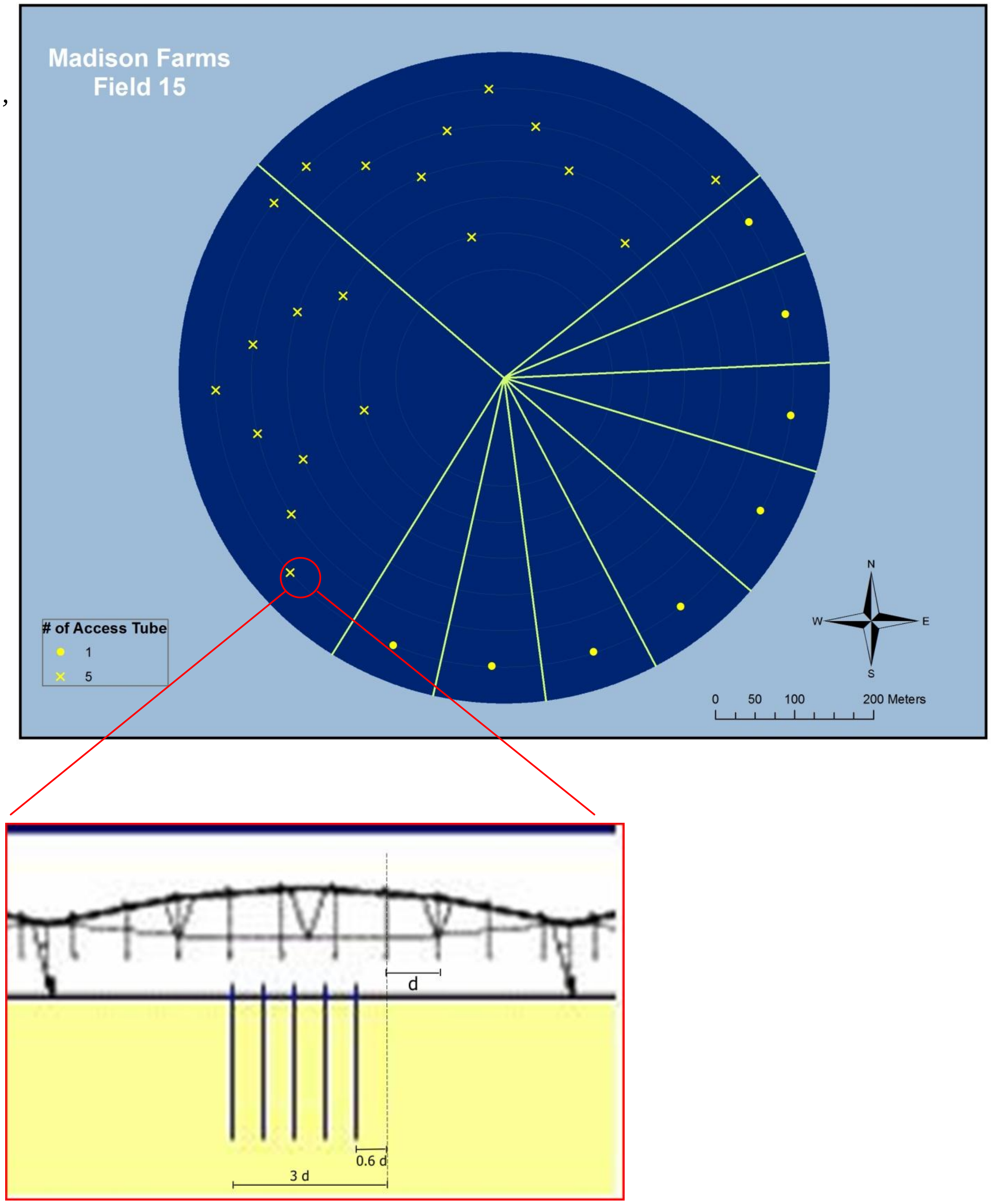

Figure 2.3 Location of the neutron probe access tubes in the field.

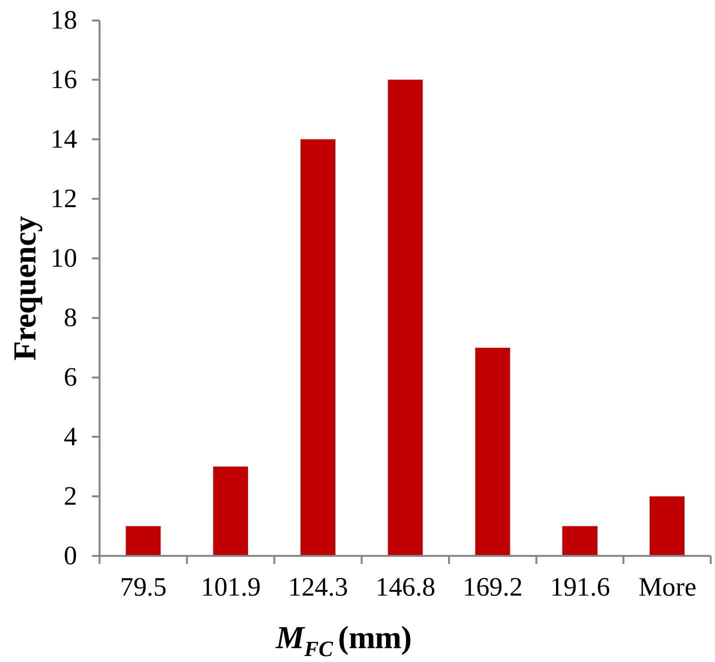

Figure 2.4 Distribution of measured soil water content at field capacity

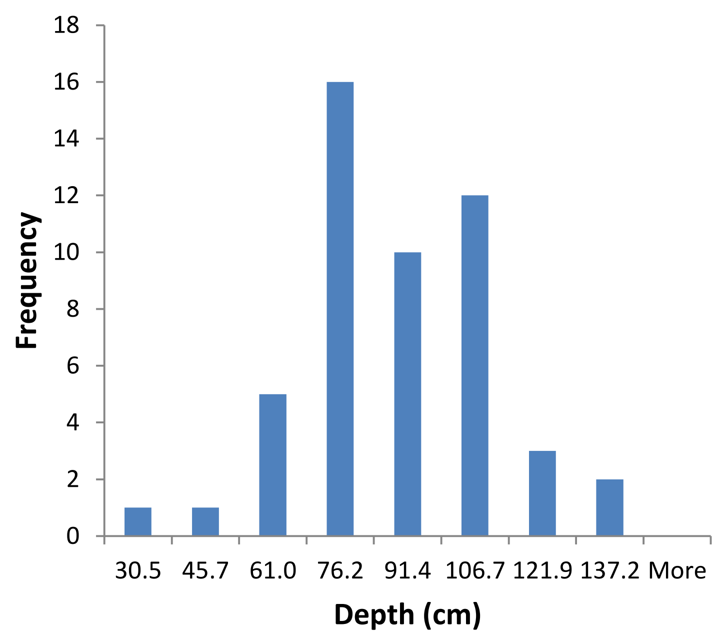

Figure 2.5 Distribution of measured soil depth

Though the objective of the irrigation treatment in Section 1 was to meet all evaporative demands, this was not possible due to several water shortages, including the time period between May 24 and May 27. The effect of the water shortages is clearly visible in the IMO simulation of both soil water budget (Figure 2.5) and ET_c (Figure 2.6). On May 27, a soil water measurement event was conducted in section 1. The results of this soil water measurement event will be used to calculate soil water depletions (Figure 2.7) that will be refer to as measured depletions in the following sections.

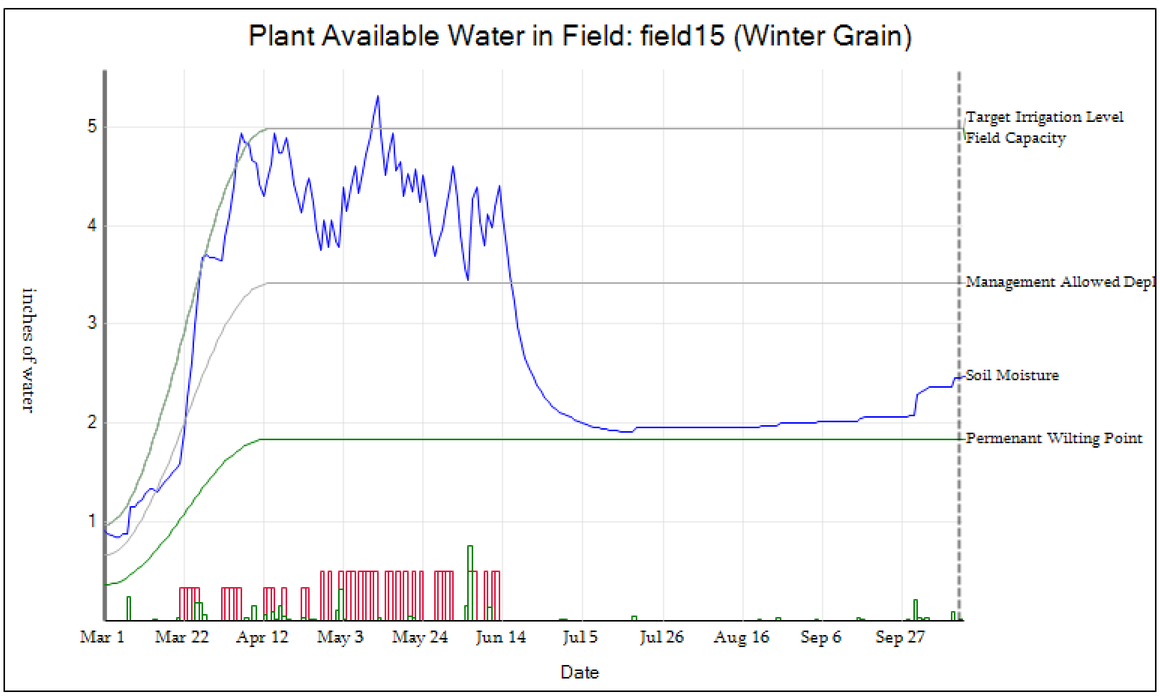

Figure 2.6 Estimated soil root zone water contents from IMO simulations (blue line), applied water (red bars), and precipitation (green bars) as shown in IMO output plots.

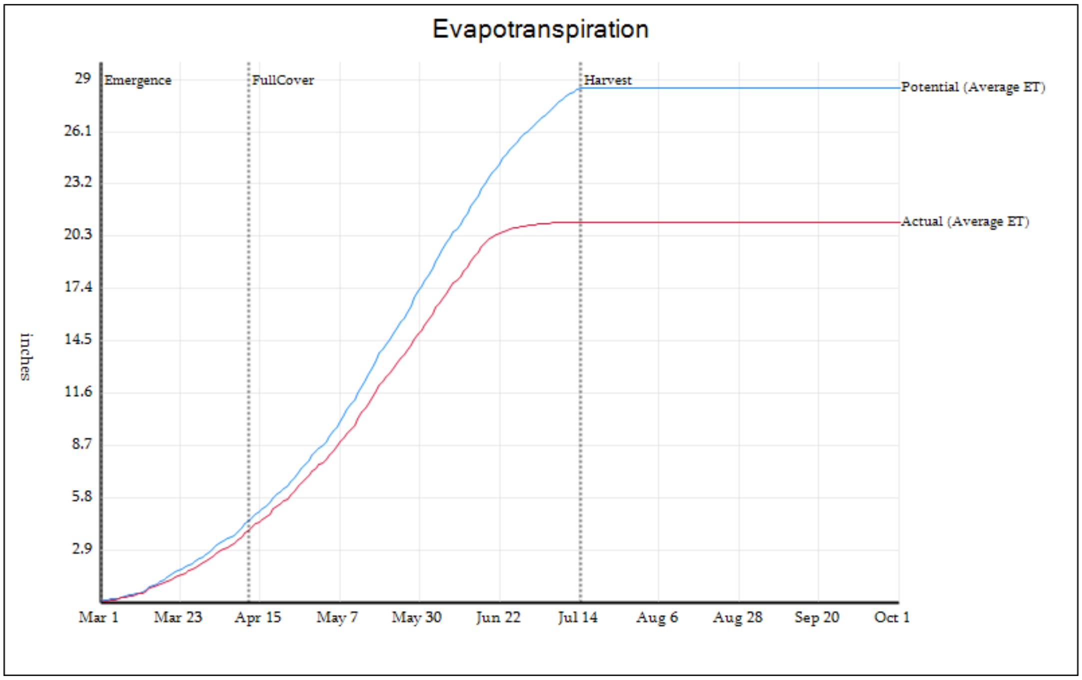

Figure 2.7 Cumulative potential and actual average ET simulated by IMO.

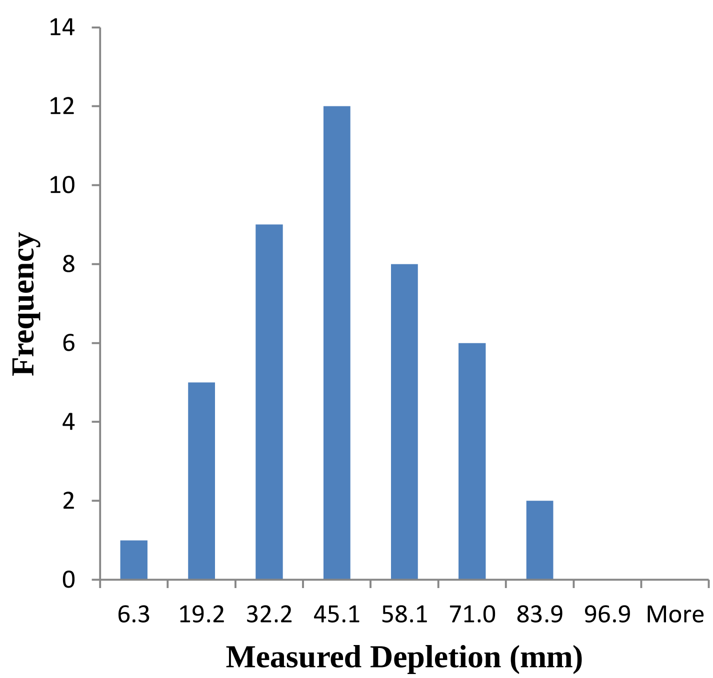

Figure 2.8 Measured Depletion on the 27th of May

Input Parameters:

On the 27th of May, the IMO simulated spatial variability of depletion is presented in Figure 2.8. The average and variance calculated from 300 monitoring points' simulations are:

$$m = 38.8 \text{ mm} \quad \text{and } s^2 = 56.2 \text{ mm}^2$$

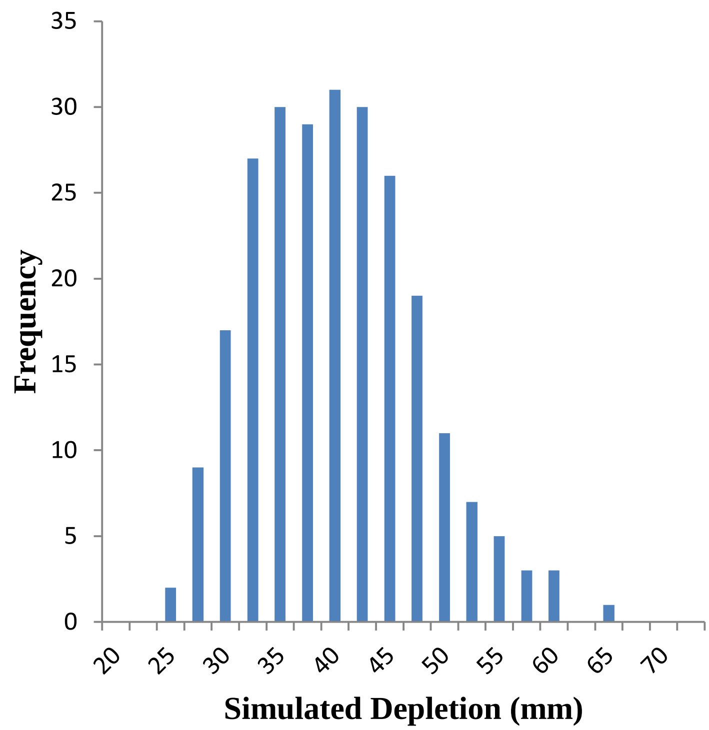

Figure 2.9 Distribution of the simulated soil water depletion from IMO

An α^2 value of 21.8 mm^2 is used in Equation 2.8 though Equation 2.15. This value is obtained from the analysis of the uncertainly in ET and ET_c estimates in the area where the field is located. The standard deviation of the simulated cumulative ET_c was

15% of the mean (see *Sayde et al*., 2008 for more details). As depletion is directly associated to ET_c, we assumed α^2 is equal $(0.15 \times m)^2$.

The values of soil water depletion measurements (D_i) and their associated σ_{FCi}^2, σ_i^2, and σ_{Di}^2 on the 27th of May are shown in Table 2.1. The different variance components are calculated using the method detailed in *Haverkamp et al*. [1984] and *Hupet et al*. [2004].

Table 2.1 D_i and $\hat{\delta}_i$ values, and their associated uncertainties for each measurement location on the 27th of May

Tube #	D_i	σ_{FCi}^2	σ_i^2	σ_{Di}^2	$\hat{\delta}_i$	$\hat{\sigma}_{\delta i}^2$
1.1	56.5	20.2	11.3	31.5	51.3	22.6
1.2	49.8	14.5	11.3	25.8	46.9	19.5
1.3	26.9	2.9	1.6	4.4	27.5	4.2
1.4	30.0	15.2	12.4	27.5	32.1	20.5
1.5	44.0	2.7	2.2	4.9	43.7	4.6
3.1	14.4	4.4	3.8	8.2	16.6	7.5
3.2	6.3	5.3	4.0	9.3	9.6	8.3
3.3	28.6	8.2	6.5	14.8	30.1	12.5
3.4	20.6	4.1	3.1	7.3	22.0	6.7
3.5	8.4	4.4	3.9	8.3	11.2	7.5
4.1	19.1	3.5	2.8	6.3	20.5	5.8
4.2	24.8	6.0	4.9	10.9	26.4	9.6
4.4	32.4	3.2	3.6	6.8	32.8	6.3
4.5	10.4	6.0	5.8	11.9	14.0	10.3
5.1	33.1	5.1	6.4	11.5	33.7	10.1
5.2	59.0	6.4	8.4	14.8	55.8	12.5
5.3	57.8	6.7	10.3	17.0	54.3	14.0
5.4	68.1	5.7	10.2	16.0	63.1	13.3
5.5	43.4	5.1	7.7	12.9	42.7	11.1
6.1	61.0	4.8	7.4	12.1	58.0	10.5
6.2	31.4	5.2	6.3	11.5	32.2	10.0
6.3	52.9	5.0	6.5	11.5	51.1	10.0
6.4	34.8	4.5	5.5	10.0	35.2	8.9

Table 2.1 (Continued) D_i and $\hat{\delta}_i$ values, and their associated uncertainties for each measurement location on the 27th of May

Tube #	$\boldsymbol{D_i}$	$\boldsymbol{\sigma_{FCi}}^2$	$\boldsymbol{\sigma_i}^2$	$\boldsymbol{\sigma_{Di}}^2$	$\hat{\delta}_i$	$\hat{\sigma}^2_{\tilde{\delta}i}$
6.5	62.2	5.5	8.9	14.4	58.6	12.2
7.1	47.6	5.7	8.2	13.9	46.2	11.8
7.2	78.9	4.7	9.8	14.6	72.6	12.3
7.3	56.6	5.5	9.3	14.8	53.7	12.5
7.4	63.4	5.0	9.1	14.0	59.7	11.9
7.5	51.4	4.9	7.8	12.6	49.5	10.9
8.1	53.3	8.4	16.4	24.7	49.7	18.9
8.2	83.9	6.3	16.6	22.9	73.7	17.8
8.3	36.9	3.6	16.5	20.1	37.2	16.1
8.4	44.1	3.0	16.6	19.6	42.9	15.7
8.5	15.7	4.6	16.4	20.9	20.4	16.6
9.1	39.9	3.5	5.5	9.0	39.7	8.1
9.2	61.9	3.6	7.9	11.5	58.9	10.1
9.3	41.9	4.3	6.9	11.2	41.4	9.8
9.4	42.5	3.3	4.9	8.2	42.1	7.5
9.5	41.5	4.3	5.7	9.9	41.2	8.8
10.1	31.2	4.4	5.8	10.2	32.0	9.1
10.2	32.5	4.9	6.0	10.9	33.2	9.6
10.3	31.5	3.7	5.1	8.8	32.1	7.9
10.4	21.7	4.4	5.5	10.0	23.6	8.9

Posterior output:

The estimated posterior $\hat{\delta}_i$ and $\hat{\sigma}^2_{\tilde{\delta}i}$ values, calculated using Equation 2.12 and Equation 2.13 respectively, are presented in Table 2.1.

What we expect of the Bayesian decision model output are 1) a more accurate estimation of soil water depletion status in the field and 2) a reduced risk of serious estimation errors derived from a measurement or combination of measurements that is extremely non-representatives of the average soil water depletion in the field. The performance of the Bayesian model was assessed with these two criteria in mind based on the May 27th field measurements.

The probability of observing n soil water depletion measurements with a weighted average (by their variance) that falls outside a certain range of error (R) around the true average soil water depletion in the field was calculated. That probability was then compared to the corresponding probability that an average of n posterior soil water depletion estimates would fall outside that range. Here we assume that the weighted average of the 43 soil water depletion measurements is the true average soil water depletion is the field. This comparison was performed for n ranging from 1 to 39.

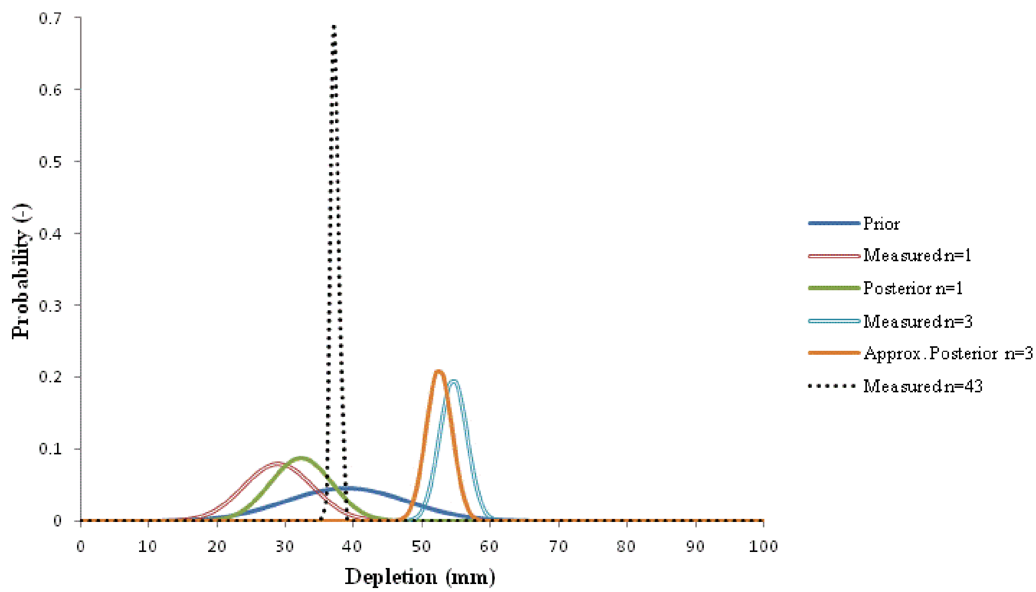

Figure 2.10 Example of the prior, measured, and approximate posterior distributions

To test the improved accuracy in determination of average soil water depletion, R was set to ± 10% of true soil water depletion (the true value being the weighted average of 43 soil water depletion measurements).The percentages of 2000 randomly generated combinations of n soil water depletion measurements and 2000 randomly generated combinations of n posterior depletion estimates that have average depletion values located outside *R* was calculated. This calculation was repeated for *n* ranging from 1 to 39 measurement locations and 1 to 39 posterior depletion estimates.

The same methodology was used to assess the performance of the Bayesian model in reducing the risk of obtaining a measurement or combination of measurements that are extremely non-representatives of the field average soil water depletion. The only difference is that for purposes of this assessment *R* was set to ±50%. Here we argue that if the average of *n* measurements (and reciprocally the average of *n* posterior depletion estimates) falls outside the range of ±50% of the true water depletion then it can be considered extremely non-representatives of the field average soil water depletion. Using such data to schedule irrigations based on average soil water depletion will significantly increase the risk of substantially under or over irrigating the majority of the field.

The results show that for a high number of measurements made in the fields, there was little or no improvement in accuracy or risk reduction reported from the use of the Bayesian decision model (Figures 2.10 and 2.11). But in practice, multiple measurements are expensive, and irrigation managers usually rely on very few measurements to assess soil water status and decide the timing and the depth of the next irrigation events. Thus, there is advantage in using the Bayesian decision model in this case, where the greatest improvement in risk reduction is observed at low numbers of measurement combinations (Figures 2.10 and 2.11).

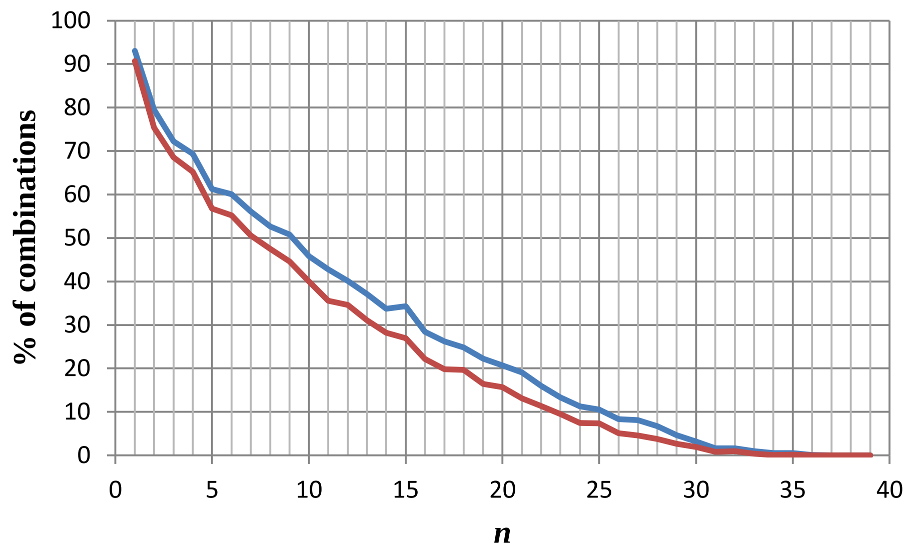

Figure 2.11 Percent of $n\ D_i$ combinations (blue line) and $n\,\hat{\delta}_i$ combinations (red line) that are outside an error band of ± 10% range of the 43 measured depletion average values.

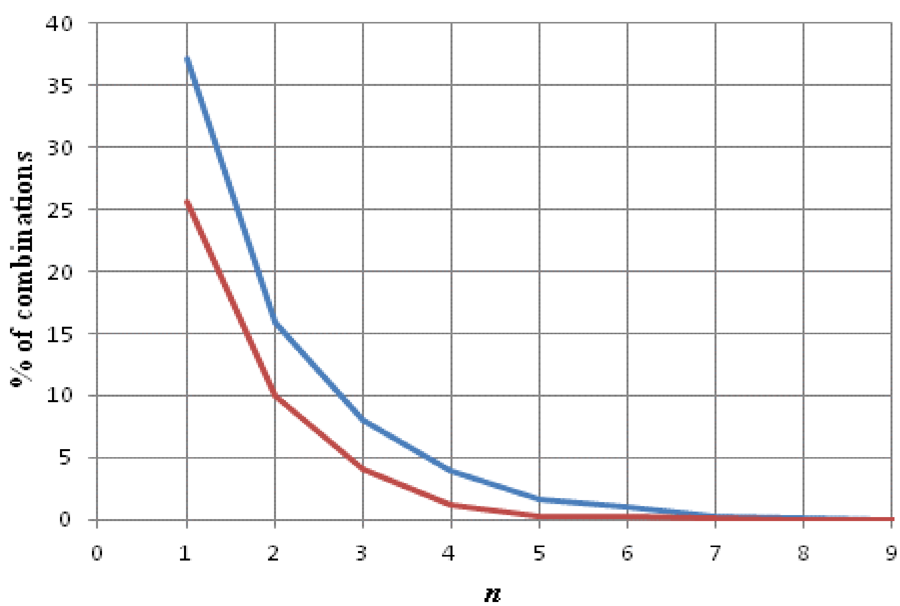

Figure 2.12 Percent of nD_i combinations (blue line) and n $\hat{\delta}_i$ combinations (red line) that are outside an error band of ± 50% range of the 43 measured depletion average values.

Again, what we are suggesting here is a new approach that helps irrigation managers make use of multiple sources of information conjunctively to improve their irrigation scheduling decisions. The Bayesian model, presented in this work, is basically a first attempt to tackle this approach and to provide guidance for future work. In particular, future work should address the following issues:

- *The normality assumptions suggested for the different parameters employed in the model*. How will the model perform if the normality assumption is breached for any of its parameters? And how to deal with it?
- *The assumption that the soil water depletion measurements are unbiased*. This can be true in the case of the above numerical example because of the site specific soil water measurement calibration employed. But bias in neutron probe measurements is commonly observed in irrigation management. Such bias is often due to the use of generic calibration curves that are not representative of a particular local soil.
- *The assumptions that Individual measurements are statistically independent*. Generally the chances of correlation increases with decreasing spacing between measurements. A refined version of the model should deal with the non independence by accounting for correlation between measurements.
- There are additional sources of information that could be integrated in this analysis that might provide additional insights on the status of soil water depletion in the field. Specifically, we would expect that most experienced farmers could judge how representative a particular measurement location is

in relation to the patterns of depletion across a particular field e.g. a particular farmer might judge a particular measurement site to represent average, or dry, or wet sections of a field. In principle such subjective information represents additional information that could be utilized by a simulation model that explicitly accounts for spatial variability in the field (e.g. IMO). This would allow us to generate stratified prior distributions that reflect defined conditions in the field (e.g. driest 25%, average, wettest 25%, etc…). Another advantage of including such information is that it will allow additional flexibility for decision makers to adapt wide range of irrigation scheduling strategies instead of the targeting the average condition in the field as the current version of the model implicitly suggest.

2.5 Conclusions

Estimators of soil water depletion commonly used in the practice of irrigation scheduling are characterized by pervasive uncertainty. The Bayesian method outlined here provides a way to explicitly account for and reduce the uncertainties of those estimators, while making full use of the information embedded in those estimators.

The analysis highlights the usefulness of water balance models, such as IMO, that explicitly account for the variability of soil physical properties and non-uniformity of applied water. Insights derived from the analysis lead to an important general conclusion, that scientific irrigation scheduling can be made more effective by accounting for the uncertainties of both ET estimates and soil water determinations (including both soil water content and the soil characteristics to which soil water measurements are referenced). The paper has presented an analytical procedure for reducing uncertainty by explicitly incorporating it into the analysis. Analytical tools for irrigation scheduling need not only estimate the most probable levels of depletion; they must also quantify the uncertainties of such predictions.

The task of quantifying the uncertainty of soil water measurements and soil characteristics may be challenging. Given the pervasive modeling and observation of ET, modeling of the uncertainty of ET may require relatively small additional investment of time. But it may be much more difficult to devise economical techniques for quantifying the uncertainty of measured soil water depletion. A variety of techniques for characterizing and mapping the spatial variability and uncertainty of soil water measurements might be used, such as distributed networks of point measurements, remote sensing and Actively Heated Fiber-Optics method (AHFO).

2.6 References

Abourached, C., C. Hillyer, C. Sayde, M. English, and J. Bosch. 2007. A web-based advisory service for optimum irrigation management. ASABE Paper No. 072253. Minneapolis, MN.: ASABE.

Charlesworth, P. 2005. Soil water monitoring. Irrigation Insights No. 1, CSIRO. *Land & Water Australia* (2nd Edition) 96p.

Debaeke, P., Aboudrare, A., 2004. Adaptation of crop management to water-limited environments. *Eur. J. Agron*. 21:433–446.

English, M. 1981. The uncertainty of crop models in irrigation optimization. *Agricultural Water Management* 32(1):1-14.

English, M., 1990. Deficit irrigation. I. Analytical framework. *J. Irrig. Drain E. ASCE* 116:399–412.

English, M. and Orlob, G. 1978. Decision theory applications and irrigation optimization. *Technical Completion report Contribution No. 174*, University of California.

English, M. and S. Navaid Raja. 1996. Perspectives on deficit irrigation. *Transactions of the American Society of Agricultural Engineers* 24(4): 917–921and 928.

English, M. J., K. H. Solomon, and G. J. Hoffman. 2002. A paradigm shift in irrigation management. *Journal of Irrigation and Drainage Engineering* 128(5):267-277.

English, M., C. Sayde, A. Gitelman, and L. Khoury. 2008. A feedback system to optimize crop water use estimates in irrigation scheduling. In *World Environmental & Water Resources Congress*, May 13-16, 2008, Honolulu, Hawaii.

Fereres, E., and M. A. Soriano. 2006. Deficit irrigation for reducing agricultural water use. *Journal of Experimental Botany* 58(2):147-159, doi:10.1093/jxb/erl165.

Fereres E, Goldhamer DA, Parsons LR. 2003. Irrigation water management of horticultural crops. Historical review compiled for the American Society of Horticultural Science's 100th Anniversary. *HortScience*, 38:1036-1042.

Geerts, S., and D. Raes. 2009. Deficit irrigation as an on-farm strategy to maximize crop water productivity in dry areas. *Agricultural Water Management* 96(9): 1275-1284, doi: 10.1016/j.agwat.2009.04.009.

Haverkamp, R., M. Vauclin, and G. Vachaud. 1984. Error analysis in estimating soil water content from neutron probe measurements. 1. Local standpoint. *Soil Sci.* 137:78–90.

Hupet, F., P. Bogaert, and M. Vanclooster. 2004. Quantifying the local scale uncertainty of estimated actual evapotranspiration. *Hydrol. Processes* 18: 3415–3434, doi:10.1002/hyp.1504.

Hillyer C., English M., Sayde C., Hutchinson K., and Busch J. 2009. A Web-Based Advisory Service For Optimum Irrigation Management. World Environmental & Water Resources Congress, *ASCE*, Kansas City, MO.

Hillyer C., and Robinson P., 2010. Envisioning The Next Generation Of Irrigation Schedulers. 5th National Decennial Irrigation Conference Proceedings, *ASABE*, St. Joseph, Michigan, Phoenix, Arizona.

Sayde, C., L. Khoury, A. Gitelman, and M. English. 2008. Optimizing estimates of soil water for irrigation scheduling. *ASABE* Paper No. 084699. St. Joseph, MI.: ASABE.

Steele, D. D., T. F. Scherer, L. D. Prunty, and E. C. Stegman. 1997. Water balance irrigation scheduling: Comparing crop curve accuracies and determining the frequency of corrections to soil water estimates. *Trans. ASAE* 13(5):599-599.

Schmitz, M., and H. Sourell. 2000. Variability in soil water measurements. *Irrigation Science*, 19:147–151.

3. Feasibility of Soil Moisture Monitoring with Heated Fiber Optics

Chadi Sayde, John S. Selker, Marshall J. English

Water Resources Research
American Geophysical Union
Vol. 46, PP. 8, 2010 Abstract

3.1 Abstract

Accurate methods are needed to measure changing soil water content from meter to kilometer scales. Laboratory results demonstrate the feasibility of the heat pulse method implemented with fiber-optic temperature sensing to obtain accurate distributed measurements of soil water content. A fiber-optic cable with an electrically conductive armoring was buried in variably saturated sand and heated via electrical resistance to create thermal pulses monitored by observing the distributed Raman backscatter. A new and simple interpretation of heat data that takes advantage of the characteristics of fiber-optic temperature measurements is presented. The accuracy of the soil water content measurements varied approximately linearly with water content. At volumetric moisture content of 0.05 m^3/m^3 the standard deviation of the readings was 0.001 m^3/m^3, and at 0.41 m^3/m^3 volumetric moisture content the standard deviation was 0.046 m^3/m^3. This uncertainty could be further reduced by averaging several heat pulse interrogations, and through use of a higher performance fiber-optic sensing system.

3.2 Introduction

Soil water accumulation, storage, and depletion play a central role in the hydrologic cycle and the global water balance. Though many accurate methods are available for point measurement of soil water content, there are currently no precise *in-situ* methods for measurement of soil water content from meter to kilometer scales. The goal of this article is to demonstrate the feasibility of the Active Heat pulse method with Fiber Optic temperature sensing (AHFO) to obtain precise, distributed measurements of soil water content across these spatial scales and over a broad range of soil water contents.

The ability of fiber-optic Distributed Temperature Sensing (DTS) systems to retrieve temperature readings each meter along fiber-optic cables in excess of 10,000 m in length at high temporal frequency has afforded many important opportunities in environmental monitoring [e.g., *Selker et al.*, 2006a, 2006b; *Tyler et al*., 2008; *Westhoff et al*., 2007; *Tyler et al*., 2009; *Freifeld et al*., 2008]. Recently, *Steele-Dunne et al.* [2009] demonstrated the feasibility of using the thermal response to the diurnal temperature cycle of buried fiber-optic cables for distributed measurements of soil thermal properties and soil moisture content. Unlike the AHFO method, the *Steele-Dunne et al*. [2009] method does not require an external source of energy. Nevertheless, its application remains challenging under conditions where the thermal response to the diurnal temperature cycle is not large enough to allow accurate estimation of soil moisture content (e.g., under dense vegetative canopy, at depths beyond the top few centimeters of the soil column, cloudy days, or other surface-energy flux limited systems).

The principle of temperature measurement along a fiber-optic cable is based on the thermal sensitivity of the relative intensities of backscattered Raman Stokes and anti-Stokes photons that arise from collisions with electrons in the core of the glass fiber [see *Tyler et al*., 2009]. A laser pulse, generated by the DTS unit, traversing a fiber-optic cable will result in Raman backscatter at two frequencies, referred to as Stokes and anti-Stokes. The DTS quantifies the intensity of these backscattered photons and elapsed time between the pulse and the observed returned light. The intensity of the Stokes backscatter is largely independent of temperature, while anti-Stokes backscatter is strongly dependent on the temperature at the point where the scattering process occurred. Temperature can be inferred from the Stokes/anti-Stokes ratio. The computed temperature is attributed to the position along the cable from which the light was reflected, computed from the time of travel for the light [*Grattan and Sun*, 2000].

Heat pulse methods are well established for the determination of soil thermal properties, soil water content and water movement. These methods usually apply a line source of energy to the soil with the resulting temperature fluctuation monitored by one or more parallel probes [*Bristow et al*., 1994]. The rate of radial transmission of heat depends on the soil bulk density, mineralogy, particle shape, and—principally—soil water content [e.g., *Shiozawa and Campbell*, 1990]. Geometries where the thermal observations are co-located with the heated probe are referred to as single probe methods [*de Vries and Peck*, 1958; *Shiozawa and Campbell*, 1990; *Bristow et al*., 1994]. Heat pulse methods have also been widely implemented in multi-probe geometries, with one or more sensing probes in proximity of the heat source [e.g., *Lubimova et al*., 1961; *Jaeger*, 1965; *Larson*, 1988; *Campbell et al*., 1991; *Bristow et al*., 1993, 1994; *Heitman et al*., 2003; *Ren et al*., 2003; *Ren et al*., 2005].

Many analytical and numerical methods have been developed for the interpretation of heat pulse experiments in soils. Typically, the solutions assume an infinitely small radius and infinitely long line-source geometry. The thermal properties of soil are calculated from the heat-pulse response via the solution of the radial heat conduction equation [*Carslaw and Jaeger*, 1959]. During heating, a pulse of duration t_0 (s) is applied to an infinite line heat source in a homogeneous isotropic medium which is taken to be at uniform initial temperature. The solution for the resulting temperature change following the commencement of heating is given by [*de Vries and Peck*, 1958; *Shiozawa and Campbell*, 1990; and *Bristow et al*., 1994]:

$$\Delta T(r,t) = -\frac{q'}{4\pi\kappa\rho c} Ei\left(\frac{-r^2}{4\kappa t}\right) \qquad \text{for } 0 < t \le t_0 \qquad \text{Eq. 3.1}$$

and during cooling

$$\Delta T(r,t) = \frac{q'}{4\pi\kappa\rho c}\left[Ei\left(\frac{-r^2}{4\kappa(t-t_0)}\right) - Ei\left(\frac{-r^2}{4\kappa t}\right)\right] \qquad \text{for } t > t_0 \qquad \text{Eq. 3.1}$$

Where q' is the energy input per unit length per unit time (J $m^{-1}s^{-1}$), ρ is the density of the medium (kg m^{-3}), c is the specific heat of the medium (J kg^{-1} °C^{-1}), r is the distance from the line source (m), $\kappa = \lambda/\rho c$ is the thermal diffusivity (m^2s^{-1}), λ is the thermal conductivity (W m^{-1} °C^{-1}), and Ei donates the exponential integral.

In this implementation of the line-source transient method, the radius of the heat source is assumed to be infinitely small. A correction factor can be added to the long-time solution to account for the non-zero radius of the heat source. The validity of such a correction decreases with an increase of the probe radius [*Blackwell*, 1954]. To account for the finite dimensions of the cable, the cylindrical transient method can be used as described by *Jaeger* [1965] for a perfectly conducting cylinder with constant heat supply per unit length per unit time (q'):

$$\Delta T = \frac{2q'\alpha^2}{\pi^3\lambda\rho c}\int_0^\infty \frac{\left\{1-\exp\left(-\tau u^2\right)\right\}du}{u^3\Delta(u)} \qquad \text{Eq. 3.2}$$

Where:

$$\Delta(u) = \left[uJ_0(u) - (\alpha - hu^2)J_1(u)\right]^2 + \left[uY_0(u) - (\alpha - hu^2)Y_1(u)\right]^2 \qquad \text{Eq. 3.3}$$

$$\tau = \kappa t/a2 \qquad \text{Eq. 3.5}$$

$$\alpha = 2\pi a2\rho c/S \qquad \text{Eq. 3.6}$$

$$h = \lambda/aH \qquad \text{Eq. 3.7}$$

with a being the heat-source radius (m), S the heat capacity per unit length of the cylinder (J m^{-1} °C^{-1}), $1/H$ the thermal contact resistance per unit area between the perfect conductor and the surrounding material (m^2 °C W^{-1}), and $J_n(u)$ and $Y_n(u)$ the Bessel functions of u of order n of the first and second kind (dimensionless).

Most of the existing heat pulse method literature focuses first on calculating λ and ρc from the thermal responses of the soil to a heat pulse. From these values, the soil moisture content is then inferred, since both λ and ρc of the soil monotonically increase with increasing water content. The well-known advantage of using the dual-probe method for soil water determination is that both thermal conductivity and volumetric heat capacity can be accurately obtained from a single measurement, while the single probe method is primarily sensitive to the thermal conductivity [e.g., *de Vries*, 1952, 1963; *Campbell*, 1985; *Kluitenberg et al.*, 1993; *Bristow et al.*, 1994]. The main advantage of obtaining the volumetric heat capacity of the soil is that it allows estimation of the change in soil water content without information on soil-specific thermal properties [*Bristow et al.*, 1993]. Some have tried to directly correlate soil moisture content to the temperature rise during heating [e.g., *Shaw and Baver*, 1940; *Youngs,* 1956]. A disadvantage of such methods is that a calibration curve that relates soil moisture content to temperature change is needed for each soil type, and for each probe design.

Systems using more than two probes provide additional information (e.g., direction of flux), and are an active area of investigation [e.g., *Bristow et al*., 2001; *Mori et al*., 2003, 2005; *Hopmans et al*., 2002; *Ren et al*., 2000; *Green et al*., 2003; *Kluitenberg et al*., 2007]. Concerns regarding the accuracy of the different heat pulse methods remain, related to soil bulk density [*Tarara and Ham*, 1997], soil mineralogy [*Bristow*, 1998], contact resistance between the probe and the surrounding material [*Blackwell*, 1954], and temperature sensitivity [*Olmanson and Ochsner*, 2006].

The use of actively heated fiber-optic cable for observation of subsurface water movement has been demonstrated [e.g., *Perzlmaier et al*., 2004, 2006; *Aufleger et al*., 2005], though for determination of soil water content it was concluded that (1) the method could only distinguish qualitatively between dry, wet and saturated soils [*Perzlmaier et al*., 2004, 2006; *Weiss*, 2003], and (2) small changes in soil water content could not be detected at levels above 6% volumetric water content [*Weiss*, 2003]. *Weiss* [2003] concluded that only with dramatic improvement of the signal-to-noise ratio of the DTS instrumentation could sufficiently accurate thermal conductivity be obtained by a DTS heat pulse method to quantify soil water content above this level.

Although we agree that better DTS performance improves accuracy, here we argue that the DTS method can quantify moisture content more precisely than suggested previously by using a different approach to data interpretation. Both *Weiss* [2003] and *Perzlmaier et al*. [2004] used the long-time approximation of either the line-source or the cylindrical-source transient methods to calculate the thermal conductivity of the soil, deriving the thermal conductivity from the slope and intercept of a line fit to the temperature response following an extended heat pulse. They then computed the moisture content using a calibration equation. Unfortunately, this fitting routine made use of data which varied little between moisture contents (particularly the fitted slope). Our approach was, in part, motivated by their data, where it was evident that though the slope of heating was rather insensitive to water content, the overall magnitude of the temperature change was quite sensitive to moisture content. This is partially due to the impact of the early-time data that is not fully incorporated into the late-time analysis. In addition, there is an intrinsic improvement in sensitivity found in integral methods compared to derivative (slope) approaches.

Recent work has shown that more robust estimates of soil thermal properties are obtained using analyses that fit the entire data set of temperature change with time to a model [*Mortensen et al*., 2006]. In this article we do not attempt to optimize the data interpretation, but rather demonstrate the power of a simple interpretation methodology that appears to make better use of information contained in the heat pulse data obtained with a DTS system. Opportunities for optimization of this method are many fold, and will be the topic of further research.

3.3 Materials and Methods

We seek a response variable that monotonically varies with soil water content and is suited to the characteristics of the DTS measurement method. To this end, we propose quantifying the thermal response of the soil to the heat pulse in the form of cumulative temperature increase over a certain period of time:

$$T_{cum} = \int_0^{t_0} \Delta T \, dt \qquad \text{Eq. 3.8}$$

where T_{cum} is the cumulative temperature increase [°C.s] during the total time of integration t_0 [s], and ΔT is the DTS reported temperature change from the pre-pulse temperature [°C]. T_{cum} is a function of the soil thermal properties. Higher heat capacity and higher thermal conductivity, both of which monotonically increase with soil water content (θ), increase the rate at which heat is conducted away from the probe and reduce the integral for sufficiently long heat pulses. Thus, there exists a 1-to-1 function relating T_{cum} to θ (under conditions where flow can be taken to be negligible) for a given soil, heating rate, integration time, and fiber-optic cable characteristics.

One may ask about the advantage of the integrated parameter compared to the maximum temperature increase approach described in *Shaw and Baver* [1940] and *Youngs* [1956]. The variance of the computed parameter is minimized by taking advantage of the fact that the DTS readings are fundamentally based upon cumulative photon counting. The standard deviation of DTS temperature measurements reduces with the square root of reading time [*Selker et al*., 2006]. This method allows use of relatively long reading times (photon integration) and low sampling rates. In fact, the value of T_{cum} is largely unaffected by sampling rate since the DTS will internally compute this integral as it reports lower time resolution data requiring, for example, a less expensive DTS recording instrument. It will be shown later that T_{cum} allows for more accurate estimation of soil water content than ΔT in our experimental setup.

The high-speed DTS unit used in this experiment (Sensortran DTS 5100 M4) allows high frequency data collection for comparison of more traditional interpretations of the integral method. This DTS unit recorded temperature every 0.5 m along the fiber-optic cable, with a spatial resolution of 1 m for each measurement. The average reading frequency was 0.2 Hz.

A 0.61 m diameter sand column was supported by a 1.46 m tall smooth-interior, corrugated-exterior HDPE pipe (Figure 3.1). The bottom of the pipe was sealed with a rubber membrane, and an outlet was installed 0.05 m above the membrane seal. A 0.012 m diameter perforated hose was fitted to the inside of the drainage port and wound in a spiral laying flat on the bottom of the rubber seal to provide an easily controlled lower boundary condition. The drainage was actively controlled using a peristaltic pump.

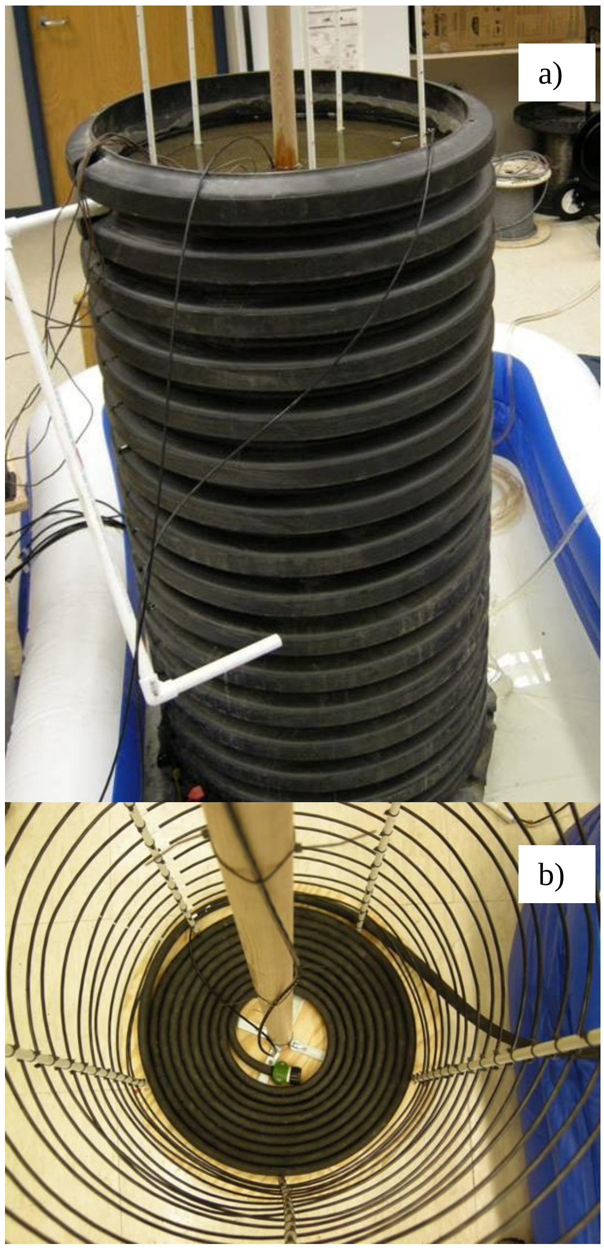

Figure 3.1 Images showing a) the sand column and b) fiber-optic section (in helical coils) before inserting into the sand column.

Within the column, 31.5 m of BruSteel (Brugg Cable, Brugg, Switzerland) fiber-optic cable was distributed in a helicoidal geometry supported by five vertical 0.006 m diameter fiberglass rods (Figure 3.1). The 3.8 x 10^{-3} m outer diameter cable made twenty-one 0.48-m diameter helical coils, spaced 0.06 m vertically, starting 0.05 m from the bottom and ending at the surface of the sand (1.30 m from the bottom). The fiber-optic cable employed was composed of two optical fibers encased in a central stainless steel capillary tube (OD 1.3 x 10^{-3}m / ID 1.07 x 10^{-3}m) surrounded by stainless steel strands (12 4.2 x 10^{-4}m OD stainless steel wires), all of which were enclosed in a 2 x 10^{-4} m thick nylon jacket. The metal components were used as an electrical resistance heater (0.365 Ω/m).

Air-dried medium sand (d_{50} = 0.297 mm) was added in 0.30 m deep lifts with vibration of the entire column using a rubber mallet to settle the sand between lifts. No further settling was observed during the remainder of the experiment. The total depth of sand in the column was 1.30 m with 0.12 m of the HDPE pipe extending beyond the top of the sand.

Computation of T_{cum} requires a precise value of the temperature before the start of the heat pulse. A 5-minute DTS reading preceding each heat pulse was used as the baseline temperature. Thereafter, a 44.5-m section of the cable (including the section in the sand column) was heated by connecting the stainless steel windings at both ends of the heated section to a variable voltage AC current source (Staco® Variable Autotransformer Type 3PN1010). The drop in voltage along the 12 AWG copper connecting wires was ~ 0.1% of the total, and thus was assumed to be negligible. A digital timer with a precision of ± 0.01% (THOMAS® TRACEABLE® Countdown Controller 97373E70) controlled the duration of the heat pulse. A wide range of combinations of power and time were tested, though in this article we discuss only the results of 2-minute heat pulses at 20 W/m (120.2 VAC) which appeared to provide an appropriate balance of temperature response and duration relative to the DTS resolution. The measurements were repeated three times. T_{cum} was calculated using the data obtained over the entire heating period of 120 sec. The temperature increase observed at the end of the heating period (ΔT_{120s}) will also be reported to compare its performance in predicting soil water content with that of T_{cum}. We chose to employ ΔT_{120s} because among all values of ΔT for heating and cooling it had the highest signal-to-noise ratio. A reference temperature reading was obtained from a 33-m coil of fiber-optic cable kept in an ice-filled water bath (0 °C) (Figure 3.2).

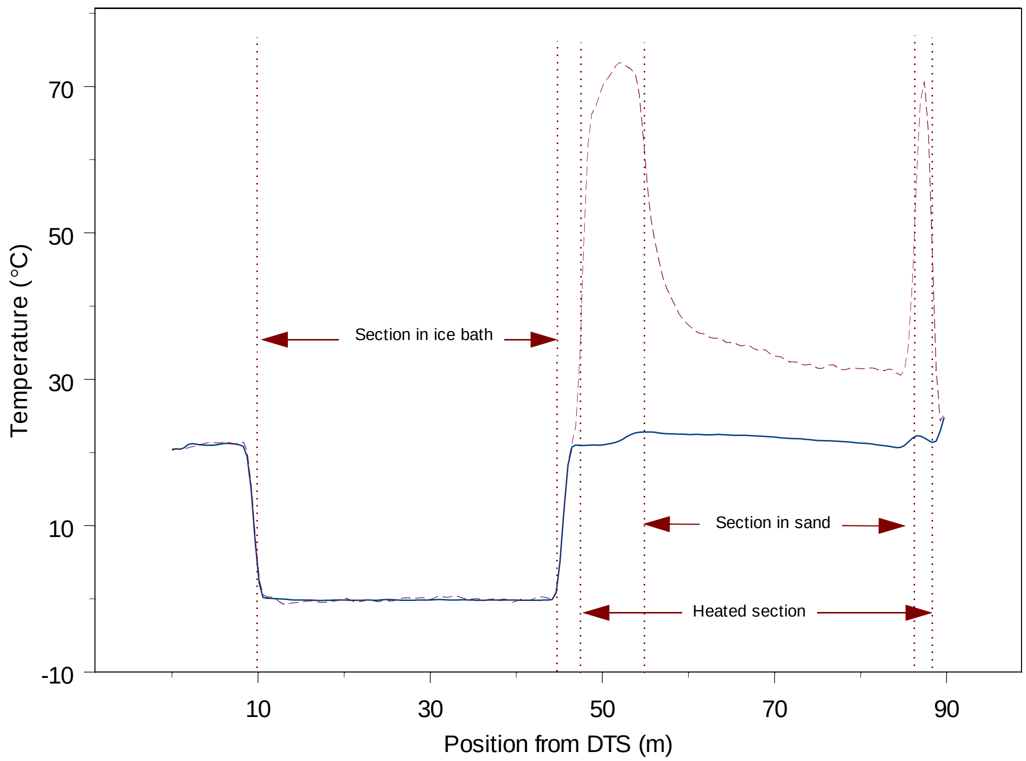

Figure 3.2 Temperature readings along the fiber-optic cable before (solid line) and at the end (dotted line) of a 2-minute – 20 W/m heat pulse for drained soil column condition. The before temperature is obtained by averaging all readings during the 5 minutes directly proceeding the heat pulse start.

DTS readings were taken in dry, saturated and drained conditions. The drained condition was obtained one month after establishing the water table at 0.4 m above the bottom. Following the final DTS measurements in the drained column, triplicate volumetric samples were obtained from eight depths between the sand surface and the water table (spanning 0.9 m) for calibration.

3.4 Results and Discussions

Volumetric soil moisture content of samples taken from the drained column varied from 4% to 41% (saturated), with a sharp transition 0.3 m above the water table, typical of sands (Figure 3.3). Repeatable, distinct values of T_{cum} were obtained up to saturation (Figure 3.3). The slope in the θ - T_{cum} and θ - ΔT_{120s} relationships decreased with water content (Figures 3.4 and 3.5), suggesting lower sensitivity at higher water contents, as found in previous studies [e.g., *Weiss*, 2003].

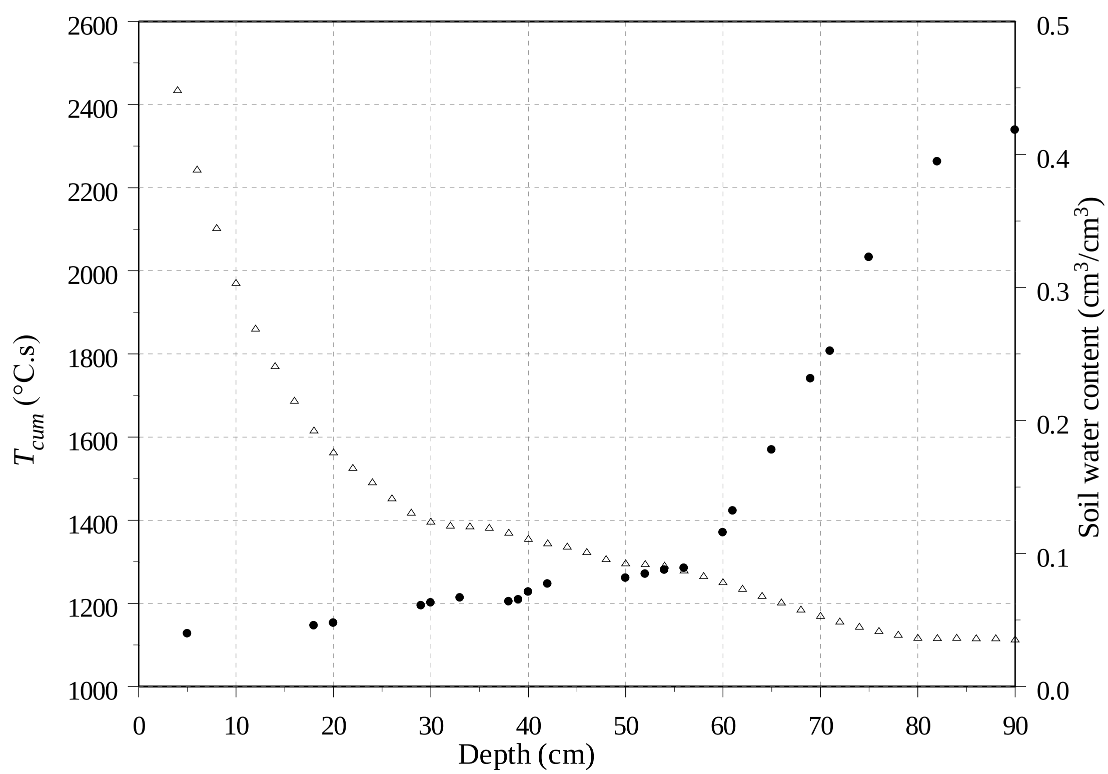

Figure 3.3 Measured soil water content (circles), and cumulative temperature increase (triangles) as function of depth for a 2-minute - 20 W/m heat pulse.

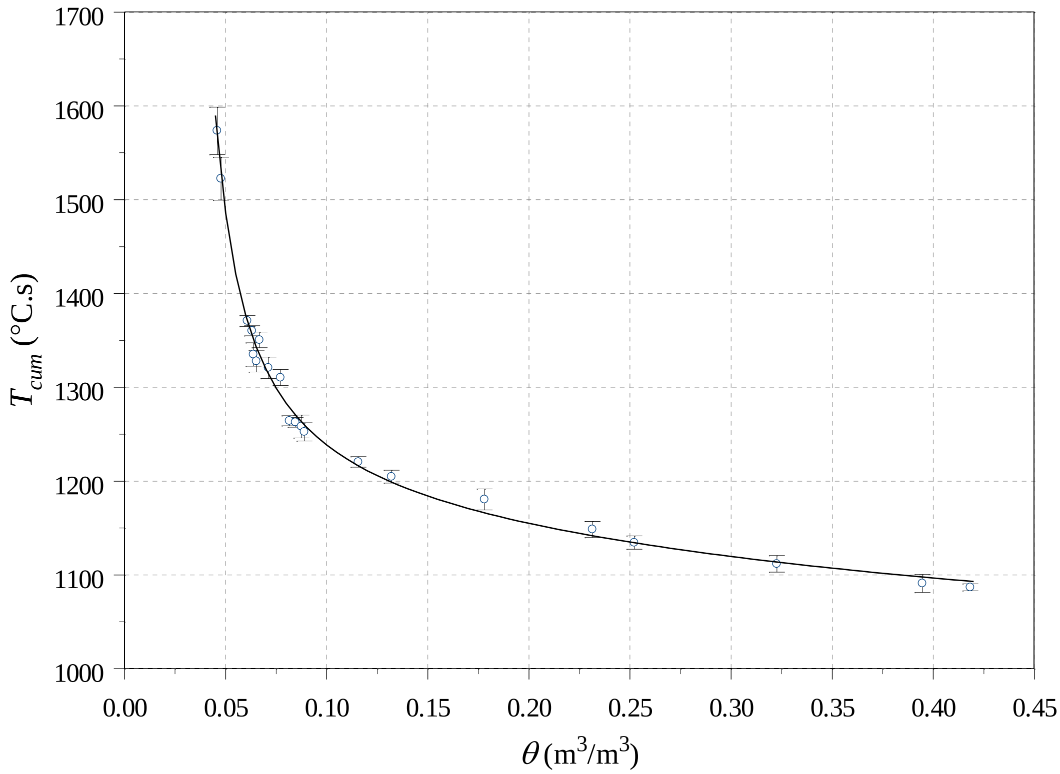

Figure 3.4 Average cumulative temperature increase (T_{cum}) integrated over 120 seconds as function of soil water content (θ) for three 2–minute - 20 W/m heat pulses and fitted function. For each soil water content value, the error bars are obtained from the standard deviation of three repetitions. The R^2 of the fitted function is 0.994.

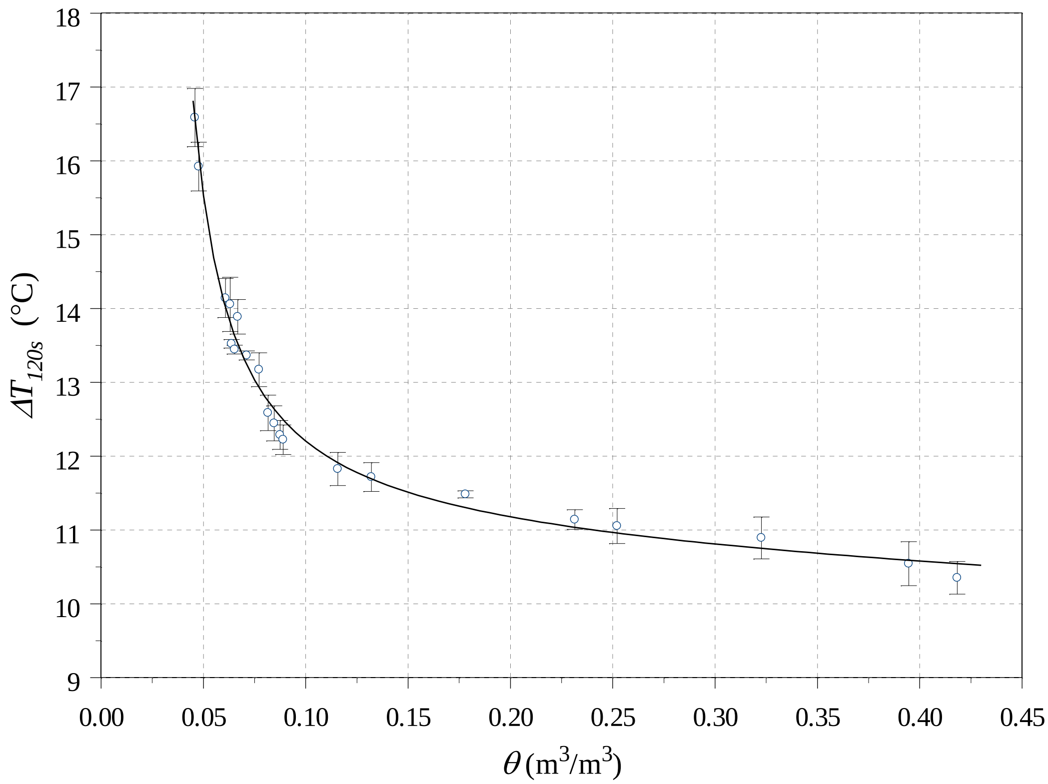

Figure 3.5 Average temperature increase at 120 seconds (ΔT_{120s}) as function of soil water content (θ), for three 2–minute - 20 W/m heat pulses and fitted function. For each soil water content value, the error bars are obtained from the standard deviation of three repetitions. The R^2 of the fitted function is 0.987.

To estimate the error in soil water content (θ) obtained from T_{cum}, a function $f(\theta)$ was fitted to the T_{cum} vs. θ data using least-squares regression (Figure 3.4). For each value of θ, the estimated error (σ_θ) was calculated as:

$$\sigma_\theta = \frac{\sigma_{T_{cum}}}{\left|\frac{df(\theta)}{d\theta}\right|} \qquad \text{Eq. 3.9}$$

Where $\sigma_{T_{cum}}$ is the standard deviation of T_{cum}, $\frac{df(\theta)}{d\theta}$ is the local slope of the T_{cum} response evaluated at θ.

In general, the standard deviation of DTS-measured temperature depends on the distance from the DTS recording unit, increasing with light loss as it potentially travels kilometers of distance from the unit [e.g., *Tyler et al.*, 2009]. However, over shorter cable distances, such as the 50 m span employed here, this effect is negligible. Therefore, the standard deviation of T_{cum}, $\sigma_{T_{cum}}$, should only depend on the performance of the DTS system. In this experiment, $\sigma_{T_{cum}}$ was computed as the average of all standard deviations of T_{cum} observed along the 30-m cable section in the sand column. The same method was employed to estimate the error in soil water content obtained from ΔT_{120s}. The error analysis shows that σ_{θ} obtained from either T_{cum} or ΔT_{120s} increased approximately linearly with soil water content (Figure 3.6). As expected, the error in soil water content obtained from T_{cum} was much smaller than that obtained from ΔT_{120s} (Figure 3.6). This error could be further reduced by increasing the signal-to-noise ratio, which could be accomplished by averaging several heat-pulse results, using a more precise DTS unit, increasing the heating intensity, or increasing the duration of heating.

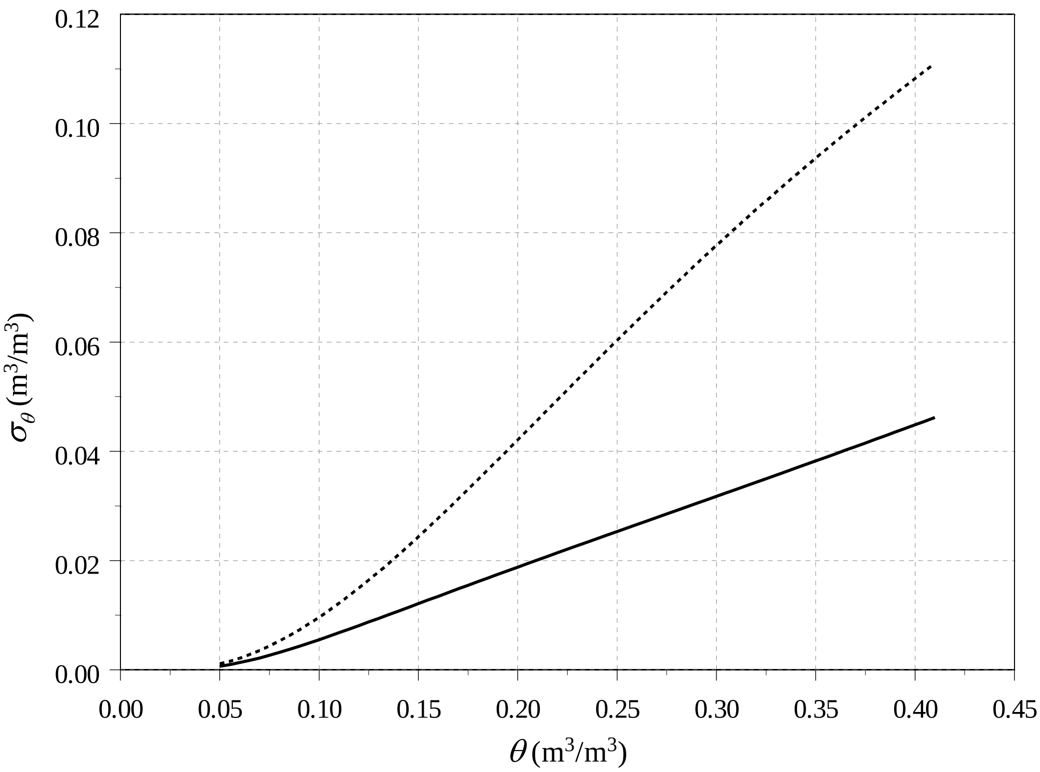

Figure 3.6 Calculated error (σ_θ) in soil water content derived from T_{cum} (solid line), and from ΔT_{120s} (dotted line), as function of soil water content (θ).

A large heat pulse could cause water to evaporate and/or diffuse away from the cable [*Farouki*, 1986]. To avoid this, and to minimize the energy required to complete a measurement, it is desirable to reduce both the magnitude and duration of temperature increase. An important advantage of the integral method is that a relatively good estimate of soil water content can be obtained with a brief heat pulse. In this experiment, the maximum cable temperature never exceeded 17 °C over the ambient soil temperature (Figure 3.5). The injected energy was less than 2.4 kJ/m, compared to the 11.7 kJ/m for *Weiss* [2003] and the greater than 72 kJ/m employed by *Perzlmaier* *et al*. [2004]. The much shorter heating interval employed here (120 s), compared to 626 s used by *Weiss* [2003] and 7200 s by *Perzlmaier et al*. [2004], greatly reduces the potential for such disturbance. That said, *Weiss* [2003] indicated that his approach did not give rise to water displacement, and our experiment showed no change in T_{cum} with replication, suggesting there were no significant distortions due to the heat pulse measurements. Sequential measurements did not show persistent cumulative heating in our experiments, but this would ultimately provide a practical limit to the feasible sampling frequency using this method. Fortunately, this cumulative heating can easily be measured with DTS.

Currently marketed DTS systems have both a ten-fold higher speed of reading performance and four times better spatial resolution than that employed here. The magnitude of the heat pulse required to obtain a particular level of precision is scaled linearly with reading speed, thus we have by no means explored the instrumentation limitations on accuracy or energetic requirements of the DTS approach.

While the laboratory results are encouraging, field measurements of soil water content using the DTS-based heat pulse method are expected to bring additional sources of uncertainty. Expected primary sources of error include poor contact between the probe and soil, and the spatial variability of soil thermal properties.

Finally, in addition to varying with moisture content, T_{cum} is expected to be a function of the convective flow of water around the heated cable. An increase in convective flow will further increase the rate at which heat is dissipated away from the probe and thereby reduce T_{cum}. Thus, this method has the potential to not only detect soil water content but also to monitor water fluxes in saturated soils, as demonstrated by *Perzlmaier et al*. [2004], with long heated durations. The ability to use shorter pulses based on the method proposed here allows greater separation between measurements of moisture content and flux.

3.5 Conclusions

We have shown that the heat pulse method using coaxial heating and a DTS system is feasible for determination of soil water content across a much broader range of values than previously reported. This result was found by using a response metric that has not been previously employed: the time integral of temperature deviation. This strategy is especially appropriate to the DTS method wherein precision of temperature reporting is a direct function of the interval of photon integration. Though we have used high temporal resolution in the DTS measurements, this method can provide the same level of precision with less expensive, slower DTS instruments since the data can be integrated in time for analysis. Further, using more sensitive DTS systems, the technique could be more accurate and use shorter, lower energy heat pulses which may be of importance in remote application of the method.

While this study demonstrates feasibility, additional work is required to develop optimal heating and interpretation strategies for DTS-based heat pulse methods, building upon the rich literature related to needle heat pulse systems. The key finding of this work is to confirm the potential to employ DTS systems to monitor soil water content at temporal resolutions well under one hour and at high spatial resolution (≤ 1 m). In principle, this DTS method could monitor soil moisture along cables exceeding 10,000 m in extent. This would allow for concurrent observation of thousands of adjacent locations, which will likely provide new insights into the spatial structure of infiltration and evaporation. Such measurements could be transformative in our understanding of soil hydrology in natural and managed systems at field and watershed scales. Many challenges remain (e.g., installation in the presence of stones and roots), calling for significant further effort in developing this methodology. For example, we presented only results from a single-probe DTS approach, though multiple probe approaches using DTS are expected to be of utility just as they have been in other soil heat-pulse applications.

3.6 Acknowledgements

The authors gratefully thank Atuc Tuli, Jan Hopmans, Jim Wagner, Mark Hausner, and Christine Hatch for their very helpful conversations about this method. We also wish to express our appreciation to *Water Resources Research* reviewers, Editor, and

Associate Editor for their valuable suggestions and comments concerning this manuscript. We acknowledge the National Science Foundation (grants NSF-EAR-0930061, NSF-EAR-07115494) and the Oregon Experiment Station for their critical financial support.

3.7 References

Aufleger, M., Conrad, M., Perzlmaier, S., and Porras, P. 2005. Improving a Fiber Optics Tool for Monitoring Leakage. *Hydro Review Worldwide*, 13(4):18-23.

Blackwell, J. H. 1954. A transient-flow method for determination of thermal constants of insulating materials in bulk. *J. Appl. Phys.*, Vol. 25, pp. 137–144.

Bristow, K. L., Campbell, G. S., and Calissendorff, C. 1993. Test of a heat-pulse probe for measuring changes in soil water content. *Soil Sci. Soc. Am. J.,* 57:930-4.

Bristow, K. L., R. D. White, and G. J. Kluitenberg. 1994. Comparison of single and dual probes for measuring soil thermal properties with transient heating. *Australian Journal of Soil Research*, 32:447-464.

Bristow, K. L. 1998. Measurement of thermal properties and water content of unsaturated sandy soil using dual-probe heat-pulse probes. *Agricultural and Forest Meteorology*, 89:75-84.

Bristow, K.L., G.J.Kluitenberg, C.J.Goding, and T.S. Fitzgerald. 2001. A small multi-sensor probe for measuring soil thermal properties, water content and electrical conductivity. *Comput. Electron. Agric.,* 31:265–280.

Campbell, G. S. 1985. Soil Physics with BASIC. Elsevier: New York.

Campbell, G. S., Calissendorff, K., and Williams, J. H. 1991. Probe for measuring soil specific heat using a heat-pulse method. *Soil Sci. Soc. Am. J.*, 55: 291-3.

Carslaw, H.S. and Jaeger, J.C., Conduction of Heat in Solids, Oxford Univ. Press, NJ, 1959, pp. 262.

Coleman, T.F. and Y. Li. 1996. An Interior, Trust Region Approach for Nonlinear Minimization Subject to Bounds, *SIAM Journal on Optimization,* Vol. 6, pp. 418- 445.

Farouki, O.T. 1986. Thermal properties of soils. Series on rock and soil mechanics. Vol. 11. Trans Tech Publications, Clausthal-Zeller- feld, Germany.

Freifeld, B.M., Finsterle, S., Onstott, T.C., Toole, P., Pratt, M. 2008. Ground surface temperature reconstructions: Using in situ estimates for thermal conductivity acquired with a fiber-optic distributed thermal perturbation sensor. *Geophysical Research Letters*, Vol. 35, L14309, doi:10.1029/2008GL034762.

Grattan, K.T.L. and Sun T. 2000. Fiber optic sensor technology: an overview. *Sens. Actuat. A.*; 82: 40-61.

Green, S., B. Clothier, and Jardine B. 2003, Theory and Practical Application of Heat Pulse to Measure Sap Flow, *Agron. J.*, *95*(6):1371-1379.

Heitman, J. L., J. M. Basinger, G. J. Kluitenberg, J. M. Ham, J. M. Frank and P. L. Barnes. 2003. Field Evaluation of the Dual-Probe Heat-Pulse Method for Measuring Soil Water Content. *Vadose Zone J.*, 2:552-560.

Hopmans, J. W., J. Simunek, and K. L. Bristow. 2002. Indirect estimation of soil thermal properties and water flux using heat pulse probe measurements: Geometry and dispersion effects. *Wat. Resour. Res.* 38(1), DOI 10.1029/2000WR000071.

Jaeger, J. C. 1965. Application of the theory of heat conduction to geothermal measurements. In 'Terrestrial Heat Flow.' (Ed. W. H. K. Lee.) American Geophysical Union Monograph. Vol. 8, pp. 7-23.

Kluitenberg, G. J., Ham, J. M., and Bristow, K. L. 1993. Error analysis of the heat pulse method for measuring soil volumetric heat capacity. *Soil Sci. Soc. Am. J.*, 57:1444-1451.

Kluitenberg, G. J., Ochsner, T. E., and Horton, R. 2007. Improved Analysis of Heat Pulse Signals for Soil Water Flux Determination, *Soil Sci. Soc. Am. J.*, *71*(1): 53-55.

Larson, T. H. 1988. Thermal measurement of soils using a multineedle probe with a pulsed point-source. *Geophysics*, 53:266-70.

Lubimova, H. A., Lusova, L. M., Firsov, F. V., Starikova, G. N. and Shushpanov, A. P. 1961. Determination of surface heat flow in Mazesta (USSR*). Annali di Geophys.* XIV, 157-67.

Mori, Y., Hopmans, J. W., Mortensen, A. P., and Kluitenberg, G. J. 2003, Multi-Functional Heat Pulse Probe for the Simultaneous Measurement of Soil Water Content, Solute Concentration, and Heat Transport Parameters, *Vadose Zone J.*,2(4): 561-571.

Mori, Y., Hopmans, J. W., Mortensen, A. P., and Kluitenberg, G. J. 2005. Estimation of Vadose Zone Water Flux from Multi-Functional Heat Pulse Probe Measurements, *Soil Sci. Soc. Am. J.*, 69(3):599-606.

Mortensen, A.P., Hopmans, J.W., Mori, Y., and Simunek, J. 2006. Multi-functional heat pulse probe measurements of coupled vadose zone flow and transport. *Adv. Water Resour.* 29:250–267.

Olmanson, O.K., and Ochsner, T.E. 2006. Comparing ambient temperature effects on heat pulse and time domain reflectometry soil water content measurements. *Vadose Zone J.*, 5:751–756.

Perzlmaier, S., Aufleger, M., and Conrad, M. 2004. Distributed fibre optic temperature measurements in hydraulic engineering. - Prospects of the heat-up method. In: Proceedings of the 72nd ICOLD Annual Meeting - Workshop on Dam Safety Problems and Solutions-Sharing Experience, Seoul, South Korea, May 16-22, 2004, Korean National Committee on Large Dams (KNCOLD), Seoul.

Perzlmaier, S., Straßer, K.-H., Strobl, Th., and Aufleger, M. 2006. Integral Seepage Monitoring on Open Channel Embankment Dams by the DFOT Heat Pulse Method. 22nd ICOLD, Barcelona. Q. 86 – R. 12.

Ren, T., Kluitenberg, G. J., and Horton, R. 2000. Determining soil water flux and pore water velocity by a heat pulse technique. *Soil Sci. Soc. Am. J.*, 64:552-560.

Ren, T., T. Y. Ochsner and R. Horton. 2003. Development of Termo-Time Domain Reflectometry for Vadose Zone Measurements. *Vadose Zone J.*, 2:544-551.

Ren, T., Z. Ju, Y Gong and R. Horton. 2005. Comparing Heat-Pulse and Time Domain Reflectometry Soil Water Contents from Thermo-Time Domain Reflectometry Probes. *Vadose Zone J.*, 4:1080-1086.

Selker, J.S., Thévenaz, L., Huwald, H., Mallet, A., Luxemburg, W., van de Giesen, N.,Stejskal, M., Zeman, J., Westhoff, M., and Parlange, M.B. 2006a. Distributed Fiber Optic Temperature Sensing for Hydrologic Systems. *Wat. Resour. Res.*, 42, W12202, doi:10.1029/2006WR005326.

Selker, J., N. van de Giesen, M. Westhoff, W. Luxemburg, M. B. Parlange. 2006b. *Geophysical Research Letters*, 2006, 33, L24401, doi:10.1029/2006GL027979.

Shaw, B. and L.D. Baver. 1940. An electrothermal method for following moisture changes on the soil in situ. Proc. Soil Sci. Soc. Am. 4:78-83.

Shiozawa, S., and G.S. Campbell. 1990. Soil thermal conductivity. *Remote Sens. Rev.*, 5:301–310.

Steele-Dunne, S. C., M. M. Rutten, D. M. Krzeminska, M. Hausner, S. W. Tyler, J. S. Selker, T. A. Bogaard, and N. C. van de Giesen. Feasibility of Soil Moisture Estimation using Passive Distributed Temperature Sensing. *Water Resour. Res.*, doi:10.1029/2009WR008272. 2009.

Tarara, J. M., and J. M. Ham. 1997. Measuring soil water content in the laboratory and field with dual-probe heat-capacity sensors. *Agronomy Journal*, 89:535-542.

Tyler, S., Burak, S., McNamara, J., Lamontagne, A., Dozier, J., Selker, J. 2008. Spatially Distributed Temperatures at the Base of Two Mountain Snowpacks Measured with Fiber Optic Sensors. *I. J. Glaciology*. 54(187):673-679. 2008.

Tyler, S. W., J. S. Selker, M. B. Hausner, C. E. Hatch, T. Torgersen, C. E. Thodal, and G. Schladow. Environmental Temperature Sensing using Raman Spectra DTS Fiber-Optic Methods. *Wat. Resour. Res*., doi:10.1029/2008WR007052. 2009.

de Vries, D.A. 1952. A nonstationary method for determining thermal conductivity of soil in situ. *Soil Sci.*, 73:83-9.

de Vries, D A., and Peck, A. J. 1958. On the cylindrical probe method of measuring thermal conductivity with special reference to soils. Part 1. Extension of theory and discussion of probe characteristics. *Aust. J. Phys.,* 11: 255-71.

de Vries, D.A. 1963. Thermal properties of soils. Physics of Plant Environment. Ed. W.R. Van Wijk. pp. 210-35. North-Holland: Amsterdam.

Weiss, J. D. 2003. Using Fiber Optics to Detect Moisture Intrusion into a Landfill Cap Consisting of a Vegetative Soil Barrier. *J. Air & Waste Manage. Assoc.*, 53:1130-1148.

Westhoff, M.C., Savenije, H. H. G., Luxemburg, W. M. J, Stelling, G. S., van de Giesen, N. C., Selker, J. S., Pfister, L., and Uhlenbrook, S. 2007. A distributed stream temperature model using high resolution temperature observations. *Hydrol. Earth Syst. Sci.*, 11:1469–1480.

Youngs, E.G. 1956. A laboratory method of following moisture content changes. Trans. 6th Int. Congr. Soil Sci., Paris I:89-93.

4. Mapping the Variability of Soil Water Content and Fluxes in the Field Using Actively Heated Fiber Optic (AHFO) Method

Chadi Sayde and John Selker

To be submitted to
Water Resources Research
American Geophysical Union

4.1 Abstract

Achieving and maintaining sustainability in irrigated agriculture production in the era of rapidly increasing stress on our natural resources require, among other essential actions, a significant upgrade of the currently available soil water monitoring technologies to allow optimum control and management of the applied water. Here we present field test results of an emerging technology, the Actively Heated Fiber Optic (AHFO), which has the potential to simultaneously measure soil water content and fluxes many times per hour at 0.25 m spacing along cables of multiple kilometers in length. AHFO observes the heating and cooling of a buried fiber optic (FO) cable resulting from an electrical impulse using a distributed temperature sensing (DTS). We present field results based on 750 m of FO cables buried at 30, 60, and 90 cm depths in agricultural field under center pivot irrigation. The calibration curve relating soil water content to the thermal response of the soil to a heat pulse of 10 W m^{-1} for 1 minute duration was developed in the lab. This calibration curve was successively applied to the 30 and 60 cm depths cables, while the 90 cm depth cable illustrated the challenges of soil heterogeneity for this technique. The method was used to map with high spatial and temporal resolution the spatial variability of soil water content and fluxes induced by the non-uniformity of water application at the surface.

4.2 Introduction

Soil moisture is the most important factor in controlling the spatio-temporal variability of surface water and energy balances [*Western et al.*, 2003]. Soil water content is highly variable in space and time in natural systems [*Western*, 2004]. These dynamic spatial patterns of soil water content ranging from the sub-meter to 10,000 m scales are known to impact hydrological processes, but have to date been exceedingly difficult to obtain, greatly holding back scientific progress in understanding and predicting those interacting hydrological processes [e.g., *Western et al.*, 2001, 2003; *Wilson et al.*, 2004]. Processes influenced by soil-water status include, for instance, flooding, erosion, solute transport, and the overall division of rainfall between infiltration and runoff generation. These processes are significantly impacted by the soil moisture variability, exacerbated by the nonlinearities involved [*Western*, 2004]. They are reported to be controlled at scales ranging from 10 m by 2 m plots [*Bergkamp et al.*, 1996], to hill slopes [*Cerda*, 1995; *Borga et al.*, 2007] and catchments [*Imeson et al.*, 1992; *Borga et al.*, 2007]. *Arora et al*. [2001] indicated that sub-satellite-grid-scale variability in soil moisture resulted in significant changes in the magnitude, time, and frequency of surface runoff generation, partitioning of total runoff into surface runoff and infiltration. These data have yet to be obtained with sufficient spatial and temporal resolution to fully understand the dependencies.

Processes such as infiltration [*Flury et al.*, 1994; *Raats*, 2001] and plant-water dynamics [*Porporato et al*., 2004] are fundamentally controlled by soil water content at the point scale. Such processes are of a particular importance in agricultural systems management. Detailed information on soil moisture is needed for applications including improved yield forecasting and irrigation scheduling [*Shmugge*, 1980]. *Grote et al*. [2010] stated that "Accurate characterization of near-surface soil water content is vital for guiding agricultural management decisions and for reducing the potential negative environmental impacts of agriculture".

4.2.1 Challenges in monitoring dynamic scales hydraulic processes

Understanding the characteristics of scale when related to measurements and modeling methods is essential to allow proper evaluation of the performance of these methods in capturing the spatio-temporal dynamics of the different hydrological processes.

Blöschl and Sivapalan [1995] presented scale for measurements (which can also be applied to models) to be a combination of three characteristics: support, spacing, and extent. Support being the area or time over which variability is averaged in a particular measurement (this can be closely related to the resolution of the measurement in the case of spatially continuous values such as obtained by DTS). Increasing the extent of measurement support decreases observed variability due to the effect of averaging at the expense of feasible observation of features below this length scale [e.g., *Western et al.*, 2002]. Increasing spacing between measurements decreases the details resolved, similar to support, however without intrinsically decreasing the variability of values obtained [e.g., *Western and Blöschl*, 1999]. Extent is the total coverage of the measurements. *Western et al.* [2002] indicate that "As extent increases, larger scale features are included in the data, and both the variability and the average size of the features tend to increase."

To our knowledge, there is no demonstrated practical method that allows observations over all of the three scale-dependent characteristics in both spatial and temporal domains simultaneously. Available methods perform well over the range of 1 or 2 scale characteristics while compromising the third one. A good example of this is the use of remote sensing to characterize soil water content. Beside its limitation for capturing soil moisture content beyond the very top section of the soil column, if spatial support is minimized in measurement to capture processes relevant to agriculture applications, either extent in space or time will suffer greatly making the readings of limited applicability.

4.2.2 Soil moisture monitoring in agriculture

One of the major concerns regarding soil water content monitoring in the agricultural context is how to adequately deal with the associated spatial variability. Most of the widely used soil-moisture sensors are based on single-point solutions capable of measuring soil water content within a limited volume of soil i.e. electromagnetic sensor, neutron probes or gypsum blocks. Thus, small fractions of soil are taken to be representative of the total system. The matter of correctly addressing spatial variability pivots on having as many readings as possible. The number of sensors installed in the field is practically limited due to economical considerations and sensors construction characteristics. For instance, TDR sensors with cable lengths greater than 30 m suffer signal dispersion and attenuation [*Robinson et al.*, 2008]. In this sense, mobile sensor platforms are of great interest due to their ability to provide multiple reading by moving across the field of study with a single unit of measurements [e.g., *Thomsen et al*., 2007; *Sudduth et al.*, 2001].

A promising line of development is the use of distributed wireless sensor network. This technology has the potential to bridge single-point measurement techniques for agricultural purposes with a more hydrological oriented technology—geophysical methods for medium to big scale soil mapping—. As suggested in *Western et al.* [2002], these sorts of systems rely on low cost single-point, autonomous wireless devices that are capable of communicating to a base station using the minimum battery consumption within an acceptable radius of influence. Examples of different implementations and limitations are described in the literature [e.g. *Lopez-Riquelme et al.*, 2009, *Cardell-Oliver et al*., 2005, *Bogena et al.* 2008].

In the last decades, the development of electronics has also led the opportunity to improve the previously described technologies through new approaches. *Adamo et al.* [2004] describes mathematical model to relate water content with the velocity of propagation of sound waves in soil. Also, *Michot et al*. [2003] describes a non-destructive and spatially integrated multi-electrode method for measuring soil electrical resistivity and monitoring soil water content in a corn field.

Based on the same principles as the established Neutron Probe soil moisture method, a new promising non-invasive methodology is described in *Zreda et al*. [2008] where a Cosmic-Ray-neutron probe is able to read water content in the upper 10-100 cm of soil within a maximum radius of 350 m.

4.2.3 Novel distributed soil moisture monitoring using actively heated Fiber Optics

Sayde et al. [2010] provided a laboratory demonstration of the feasibility of the Actively Heated Fiber Optic (AHFO) method for distributed, 0.25-10,000 m scale measurement of soil moisture content. This approach is based on observing the heating and cooling of a buried fiber optic cable through the course of a pulse application of energy as monitored by a distributed temperature sensing (DTS) system. The objective of this work is to evaluate the performance and the applicability of this technology under field conditions.

The ability of DTS to report the temperature each meter along fiber optic cables in excess of 10,000 m in length at high temporal frequency has opened many important opportunities in environmental monitoring [e.g., *Selker et al*., 2006a, 2006b; *Tyler et* *al*., 2008; *Westhoff et al.*, 2007; *Tyler et al*., 2009; *Freifeld et al*., 2008; *Neilsen et al*., 2010; *Vogt et al.*, 2010]. For instance, passive measurement of spatially distributed soil temperature is very informative. With multiple depths, the energy balance of the soil system can be computed, allowing for estimation of the energy consumption of evapotranspiration [*Steele-Dunne et al*., 2010]. Observation of the diurnal and seasonal temperature oscillations with depth provides the data required to estimate soil water. Beyond passive reporting of temperature, a particularly exciting opportunity is presented by the possibility of observing the temperature response of a buried Fiber-Optic DTS probe when it is a source of thermal energy.

The use of actively heated fiber optics for observation of subsurface water movement has been mentioned variously [e.g., *Weiss*, 2003; *Perzlmaier et al*., 2004; *Aufleger et al*., 2005; and *Perzlmaier et al*., 2006] and recently our team demonstrated the feasibility of using AHFO for accurate distributed measurement of soil water content [*Sayde et al*., 2010]. In these applications the fiber optic is encased in a stainless steel capillary tube surrounded by copper windings or a molded aluminum encasement, all of which are enclosed in a high-voltage jacket. The metallic component of the fiber optic cable is used as an electric resistance heater to inject heat concentric to the fiber optic sensing element into the surrounding soil, while the optical fiber is used as a thermal sensor to monitor temperature changes. As the thermal properties of soils are a function of soil moisture content, soil moisture content can be inferred by analysis of thermal responses of specific soils to the heat pulse. *Sayde et al.* [2010] presents a novel interpretation of these heat pulse signals optimized for use with DTS. Here, the thermal response of the soil is calculated in the form of a cumulative temperature increase which represents the product of change in temperature and lapsed time (T_{cum}) from the start of the heat pulse. Soil moisture content is computed via T_{cum} through a calibration equation. This procedure yielded relatively accurate estimation of soil moisture content which employs all of the photons possible from the DTS laser system. *Sayde et al.* [2010] found that the accuracy of the soil water content measurements varied approximately linearly with water content. At volumetric moisture content of 0.05 m^3 m^{-3} the standard deviation of the readings was 0.001 m^3 m^{-3}, and at 0.41 m^3 m^{-3} volumetric moisture content the standard deviation was 0.046 m^3 m^{-3}. *Sayde et al.* [2010] indicated that this error could be further reduced by increasing the signal-to-noise ratio which could be accomplished by: averaging several heat-pulse results; using a more precise DTS unit; increasing the heating intensity; or increasing the duration of the heating. DTS instruments have now been developed which are approximately ten fold more precise than that used by *Sayde et al.* [2010] suggesting that much more precise measurements are now possible, though calibration of the method to specific soils will be required to achieve these limits.

The feasibility of the AHFO method has been demonstrated by *Sayde et al.* [2010] under controlled environment. In this work will explore the performance of this method under field conditions. Specifically we will test how well this method is able to capture small scale (<1m) variation in soil water content and fluxes as imposed by controlled spatially variable water application at the surface. We will also discuss methods to improve the calibration procedure and the quality of the AHFO outputs.

4.3 Materials and Methods

4.3.1 Site description

The study site is located in an operating commercial farm near Echo, OR. The 26 ha agricultural field is irrigated by a center pivot system designed to deliver up to 4 cm/d. As typically observed in center pivot systems, the spacing between consecutive emitters decreased with distance from the center while their discharge rates increased, as required to insures a spatially even application depth (Table 4.1).

Table 4.1 Emitters locations, discharges, status and section**.**

Sprinkler No.	Actual distance from center (m)	Projected position on FO cable (m)	Actual Discharge (l mn^{-1})	Emitter status	Section #
1	6.9	N/A	6.1	N/A	1
2	12.6	N/A	6.1	N/A	1
3	18.4	23.5	6.1	N/A	1
4	24.1	30.8	6.1	N/A	1
5	29.9	37.4	8.0	N/A	1
6	35.7	43.7	8.7	N/A	1
7	41.4	49.8	11.0	N/A	1
8	47.2	56.1	11.0	ON	2
9	52.2	61.3	12.1	ON	2
10	57.9	67.2	14.8	ON	2
11	63.7	73.0	15.9	ON	2
12	69.4	78.9	17.4	ON	2
13	75.2	84.7	15.9	OFF	2

Table 4.1 (Continued) Emitters locations, discharges, status and section

Sprinkler No.	Actual distance from center (m)	Projected position on FO cable (m)	Actual Discharge (l mn^{-1})	Emitter status	Section #
14	79.0	88.6	13.3	ON	2
15	82.8	92.5	13.3	ON	2
16	86.7	96.4	14.8	ON	2
17	90.5	100.2	14.8	ON	2
18	94.3	104.1	15.9	ON	2
19	98.1	107.8	14.8	OFF	2
20	101.3	111.0	15.9	OFF	3
21	105.1	114.9	17.4	ON	3
22	108.9	118.3	17.4	Paired with 23	3
23	112.7	122.1	19.0	Paired with 22	3
24	116.6	126.5	19.0	OFF	3
25	120.4	129.8	20.5	Paired with 26	3
26	124.3	133.9	20.5	Paired with 25	3
27	128.1	138.2	22.0	OFF	3
28	131.9	141.6	22.0	Paired with 29	3
29	135.8	145.4	23.9	Paired with 28	3
30	139.6	149.3	23.9	Paired with 31	3
31	143.5	153.1	23.9	Paired with 30	3
32	147.2	157.3	22.0	OFF	3
33	150.4	160.5	22.0	OFF	4
34	154.2	164.4	25.4	ON	4
35	158.0	168.2	27.3	ON	4
36	161.8	172.0	27.3	OFF	4
37	165.7	175.9	27.3	ON	4
38	169.5	179.7	28.8	OFF	4
39	173.4	183.6	28.8	OFF	4
40	177.2	187.4	28.8	ON	4

Table 4.1 (Continued) Emitters locations, discharges, status and section

Sprinkler No.	Actual distance from center (m)	Projected position on FO cable (m)	Actual Discharge (l mn^{-1})	Emitter status	Section #
41	181.0	191.2	31.1	ON	4
42	184.9	195.1	31.1	OFF	4
43	188.7	198.9	31.1	ON	4
44	192.5	202.8	33.0	OFF	4
45	196.3	206.5	28.8	ON	4
46	199.5	209.7	31.1	OFF	4
47	203.3	213.5	33.0	ON	4
48	207.1	217.4	34.9	OFF	4
49	211.0	221.2	34.9	ON	4
50	214.8	225.1	36.8	OFF	4
51	218.6	228.9	36.8	ON	4
52	222.5	232.7	36.8	OFF	4
53	226.3	236.6	38.3	ON	4
54	230.1	240.4	38.3	OFF	4

The field was planted with corn on March 17th, 2009 and harvested on September 15th, 2009. The soil is sandy loam (Table 4.2). The bulk density values measured in the field did not correspond well with the NRCS soil survey. The average bulk density obtained from a total of 26 non-disturbed soil samples from four locations was 1.67 g cm^{-3} with a standard deviation of 0.12 g cm^{-3} compared to the 1.15-1.70 g cm^{-3} range indicated by the NRCS (Table 4.2).

Table 4.2 Soil physical and hydraulic properties (USDA Natural Resources Conservation Service, 2006).

Depth (in)	Sand (%)	Silt (%)	Clay (%)	Bulk density (g/cm^3)	Sat. Hydr. Conductivity m/s	Available Water capacity (cm^3/cm^3)	Organic matter (%)
0-4			4-8	1.15-1.30	14.4-50.4 10^{-6}	0.14-0.17	0.7-1.0
4-35			4-8	1.20-1.50	14.4-50.4 10^{-6}	0.14-0.17	0.0-1.0
35-60			4-8	1.40-1.70	14.4-50.4 10^{-6}	0.14-0.17	0.0-1.0

4.3.2 Field installation and data collection procedure

In October 2007, three sets of Fiber Optic (FO) cables were installed below the tillage depth along a 240 m transect (Figure 4.1) at 30, 60, and 90 cm below the surface. A plow system was designed for this installation. The plow consisted of a thin (2.54 cm) steel blade with trailing-edge tubes through which the cables are introduced below the surface (Figure 4.2). By ganging the three tubes along the trailing edge of the plow, we installed three sets of cables at the three depths in a single pass (Figure 4.3). The most rapid possible re-establishment of native soil conditions surrounding the installed cables was critical to our considerations; therefore, the plow blade was held at a 45 degree angle as measured perpendicular to the direction of plowing, so that the weight of the soil would assist in closing the cut made in the soil.

The first 8 m of each of the three FO cables sets were gathered and submerged in an ice bath for calibration and validation purposes. The last 8 m of the three FO cables were also gathered and submerged in an ice bath during calibration. The first 8 m were kept in an enclosure near the pivot center, and the last 8 m were buried in the soil when the FO system is not in use to allow for normal field operations.

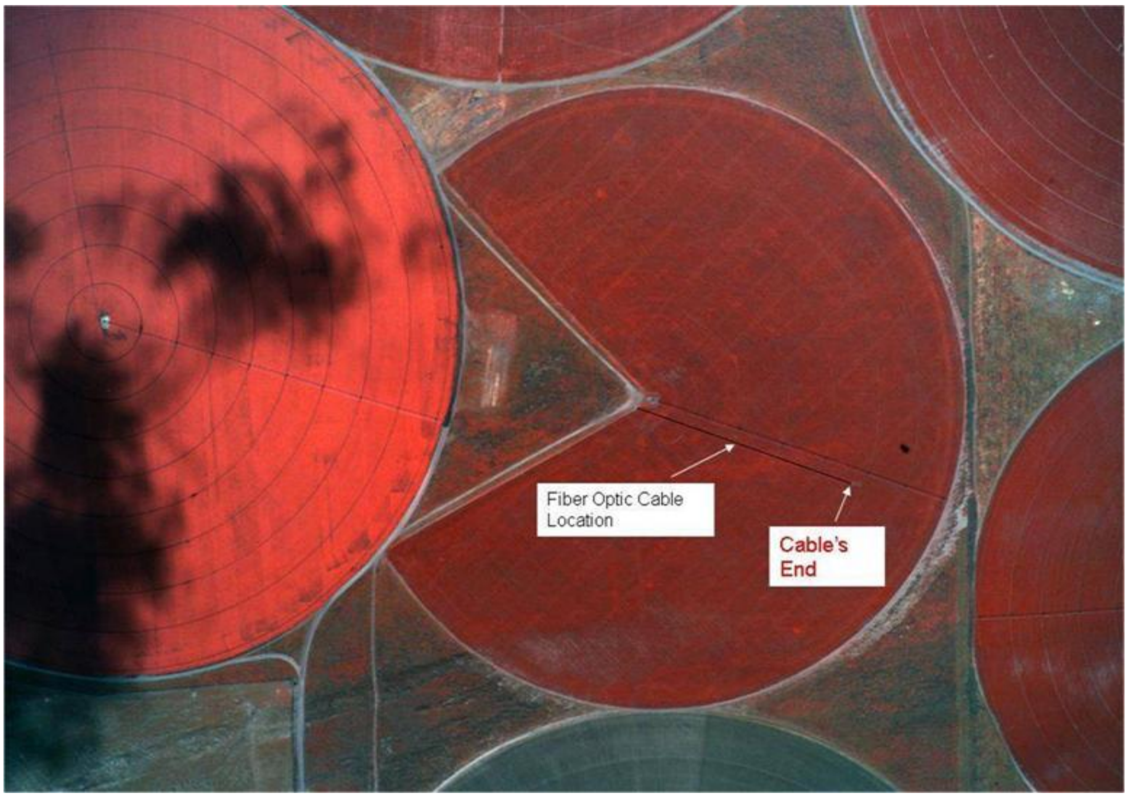

Figure 4.1 Fiber Optic transect location in the field.

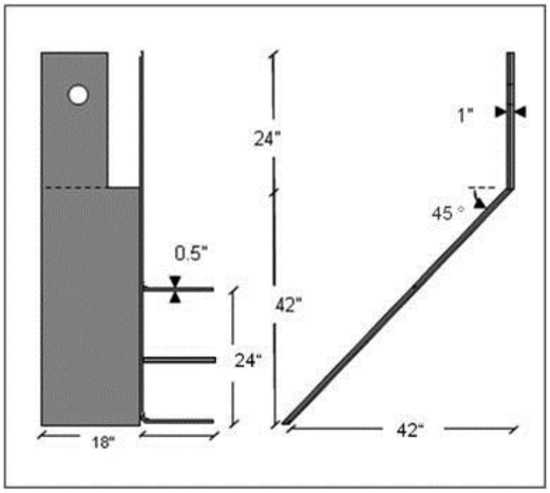

(a) (b)

Figure 4.2 (a) 45-degree "lift-plow" cable insertion tubes design (b) 45-degree "lift-plow" cable insertion tubes.

Figure 4.3 Photograph from September 2007 showing the "lift-plow" in operation.

The FO cable (BruSteel® manufactured by Brugg Cable, Brugg, Switzerland) deployed in the field had an outer diameter (OD) of 3.8 x 10^{-3} m and is composed of four optical fibers encased in a central stainless steel capillary tube (OD 1.3 x 10^{-3} m; ID 1.07 x 10^{-3} m) surrounded by stainless steel strands (12 4.2 x 10^{-4} m OD stainless steel wires), all of which were enclosed in a 0.42 x 10^{-4} m thick nylon jacket. The cable had a resistance of 0.365 Ω m^{-1} at 20 ºC.

Two of the optical fibers, located at the core of the BruSteel cable, were connected between the three different depths sections to form a continuous optical fiber allowing simultaneous temperature reading along the whole FO system.

A DTS unit (Sensortran DTS 5100 M4), connected to the FO system, recorded temperature every 0.5 m along the fiber-optic cable, with a spatial resolution of 1 m for each single measurement. The average reading frequency was 0.2 Hz.

The high voltage power supply available at the center pivot system provided an average of 490 V to heat one of the three sections with an average power intensity of 11 W m^{-1}. A series of timers and relays insured that each of the three cable section is heated separately for 1 minute duration every hour. A voltmeter located at the center pivot, provided discrete measurements of the voltage applied. The spatial variability patterns were imposed by spatially varying the water application pattern at the surface. The center pivot operation and the discharging emitters' status were modified to apply four distinct but simultaneous water application treatments along the FO cables transect location as follows:

- Section 1: From 0 to 55 m radial position. The emitters were bagged but did not discharge water over this section. The center pivot was programmed to repeatedly pass back and forth covering a 21º angle region of the center pivot circle such that only the 3 other sections under wet treatments are covered by the center pivot path. This insured that no emitters discharged water over section 1.
- Section 2: From 55 to 110 m radial position. The emitters were bagged such as water was applied directly below the emitters instead of the typical circular pattern (Figure 4.4). This insured high application rate directly below the emitters while the inter emitters locations were kept dry.
- Section 3: From 110 to 158 m. Of the 12 emitters covering this section, one was turned off, another was discharging at its regular position, while the rest formed five sets of two emitters attached together as showed in Figure 4.5.
- Section 4: From 158 to 240 m. Out of the 21 emitters covering this section, 10 were turned off and the remaining emitters were applying water at their regular positions as indicated in Table 4.1 and Figure 4.6.

The total water application duration was 7 hr. If all emitters were discharging water at their typical location and circular application pattern, the application rate would be 1.4 cm/hr.

Figure 4.4 Bagged emitters in Section 2.

Figure 4.5 A pair of emitters joined in Section 3.

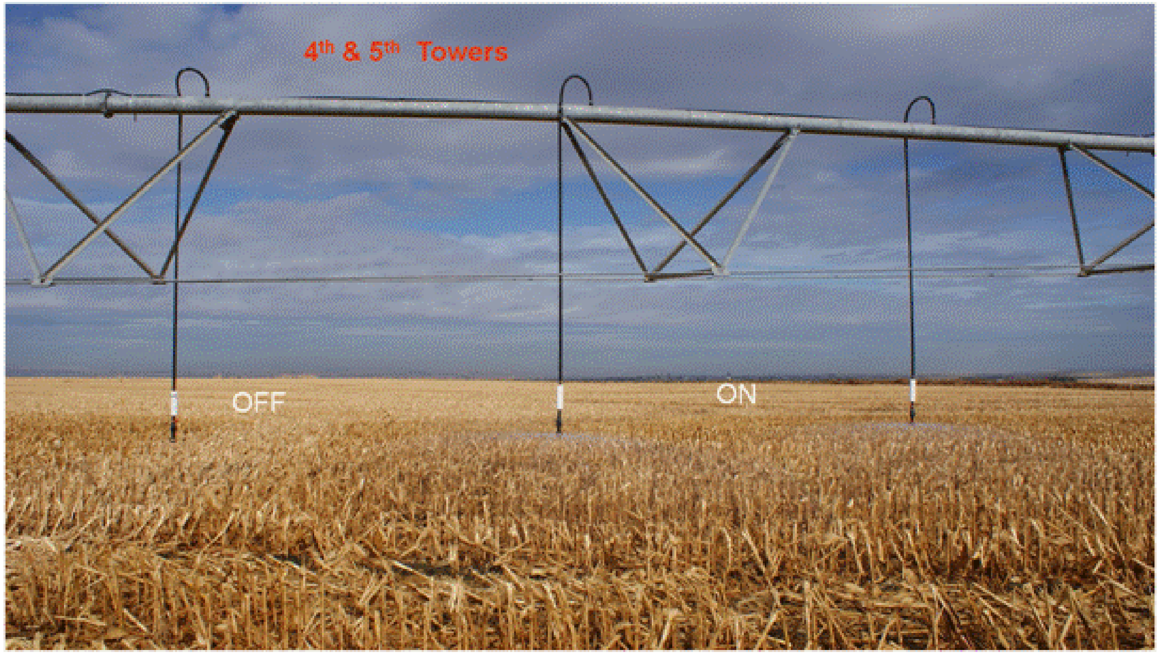

Figure 4.6 Example of emitters status in Section 4.

4.3.3 Data interpretation method

The heat pulse signals were interpreted using the same methodology described in *Sayde et al.* [2010] that is optimized for use with DTS; the thermal response of the soil is calculated in the form of a cumulative temperature increase (T_{cum}) from the start of the heat pulse as follow:

$$T_{cum} = \int_0^{t_0} \Delta T \, dt \qquad \text{Eq. 4.1}$$

where T_{cum} is the cumulative temperature increase (°C.s) during the total time of integration t_0 (s), and ΔT is the DTS reported temperature change from the pre-pulse temperature (°C).

The soil moisture content is inferred from T_{cum} through a calibration equation. This procedure yielded relatively accurate estimation of soil moisture content which employs the entire period of measurement from the DTS laser system generated by a heat-pulse experiment [*Sayde et al.*, 2010].

4.3.4 Lab calibration

The soil specific calibration of the equation relating the thermal response (T_{cum}) to soil water content was obtained from a laboratory experiment. The laboratory experiment was carried out using the same type of FO cable (BruSteel®) installed in a vessel of repacked soil from the experimental site prepared to reproduce the average bulk density observed in the field.

A 0.51 m diameter soil column was supported by a 0.91 m tall plastic barrel. An outlet was installed 0.1 m above the bottom and a 0.012 m diameter perforated hose was fitted to the inside of the drainage port and wound in a spiral laying flat on the bottom of barrel to provide an easily controlled lower boundary condition. The drainage was actively controlled using a peristaltic pump.

Within the column, 10 m of BruSteel® FO cable was distributed in a helicoidal geometry supported by three vertical 1.22 m steel rods. The cable made eight 0.3-m diameter helical coils, spaced 0.1 m vertically, starting 0.05 m from the bottom and ending at the surface of the soil (0.9 m from the bottom). Air-dried soil, obtained from the field, was added in 20 kg lifts and compacted to the desired bulk density between lifts. No further settling was observed during the remainder of the experiment.

A 4-m section of the cable is inserted in a known-temperature water bath for calibration and validation purposes. An 11.4 m section of the cable (including the section in the soil column), located downstream of the cable section that was kept in the water bath, was heated by connecting the stainless steel windings at both ends of the heated section to variable voltage AC current source (Staco® Variable Autotransformer Type 3PN1010). The drop in voltage along the 12 AWG copper connecting wires was ~ 0.1% of the total voltage, and thus was assumed to be negligible. A digital timer with a precision of ± 0.01 % (THOMAS® TRACEABLE® Countdown Controller 97373E70) controlled the duration of the heat pulse.

The calibration data were obtained in three phases: Phase I) for θ ranging from 0.23 to 0.15 $m^3\ m^{-3}$; Phase II) for θ ranging from 0.11 to 0.05 $m^3\ m^{-3}$; and Phase III) for θ at saturation (0.41 $m^3\ m^{-3}$).

In phase I, the soil column was actively saturated from the bottom using a peristaltic pump connected to the drainage outlet. Then, the same setup was used to drain the column for a 3-day period with the column top covered to reduce evaporation.

Following the final DTS measurements in the drained column, triplicate volumetric samples were obtained from seven depths from the soil surface to 10 cm from the bottom.

In phase II, the top cover of the column used in phase I was removed, and the column was left exposed to the ambient room environment for three months to generate a smooth transition from dry soil at the column top to nearly saturated conditions at the column base. After the final DTS measurements made in the air-dried column, 32 soil samples for water content determination were collected from around the cable in 12.5 cm spans along the cable starting from the surface of the soil to 50 cm from the bottom.

In phase III, the remaining 50 cm of the soil column, that was not excavated, was saturated from the bottom up using the drainage outlet. The saturated column used in phase III of the lab calibration was also used to determine the functional form relating the soil thermal response (T_{cum}) to the heat pulse power intensity (P). Eight different levels of power intensity were tested ranging from 5 to 38 W m^{-1}. For each power level a 2-minute pulse was applied.

Two DTS instruments were used during the lab calibration:

- Sensortran DTS 5100 M4 was used in phase I: This DTS unit recorded temperature every 0.5 m along the fiber-optic cable, with a spatial resolution of 1 m for each single measurement. The average reading frequency was 0.2 Hz.

- Silixa Ultima in phase II and III: This DTS unit recorded temperature every 0.125 m along the fiber-optic cable, with a spatial resolution of 0.29 m for each single measurement. The average reading frequency was 1 Hz.

Three replicates of the same combinations of power intensity and pulse duration were applied in the three phases.

4.3.5 Thermal properties of the soil column

Accurate estimation of soil thermal properties is needed to allow rigorous comparisons of the calibration equations obtained from the lab to the ones obtained from either analytical or numerical solutions of the heat transport models. To this end, thermal conductivity and specific heat were measured with an accuracy of 5% using a dual-needle probe (Decagon KD2-Pro® equipped with SH-1® dual-needle) for nine undisturbed soil samples and for soil water content ranging from saturation (0.40 m^3 m^{-3}) to dry conditions. The nine samples were randomly chosen from a set of 14 non-disturbed soil samples used for the determination of soil water content distribution across the soil column in phase I of the lab calibration. For the air-dry conditions, the previously oven dried samples were kept exposed to ambient air for a period of two months before thermal properties were measured. For the saturated conditions, the same set of samples was submerged in water for 24 hours period prior to measurements. For soil water content between saturation and dry conditions, the saturated samples were placed in a pressure chamber for three days to reach equilibrium at each of the four pressure levels (0.07, 0.33, 0.66, and 1 bar), then soil water content is determined gravimetrically and soil thermal properties are measured. Finally the samples were dried in the oven and left covered for 12 hours in ambient room temperature to cool down before thermal properties were measured.

4.3.6 Adjusting for the variation in the applied power intensity

In the field deployment, variability in the power intensity between different heat pulses is to be expected. The sources of such variability are: 1) temporal fluctuation in the applied voltage, and 2) thermal dependency of the electrical conductivity of the FO cable's heating element (the stainless steel component). With no regulation applied for the input current, the intensity of the heat pulse is sensitive to the voltage fluctuations of the power distribution network at the center pivot. The fluctuation in voltage in the field deployment was in the order of ± 2 volt over the 36 hr duration of the soil moisture readings as measured with a standard voltmeter at the center pivot. In addition, the fluctuation in the electrical resistance of the FO heating element mainly depended on the fluctuation of the cable temperature in time and with depth. When the power intensity is not strictly regulated and held constant between different heat pulses, it is essential to account for the variability in the thermal response resulting from variation in power input.

Both the cylindrical source transient and the line source transient methods suggest that the temperature increase, and in consequence T_{cum}, are proportional to the power intensity inputs as shown in the temperature change solution for both methods [see *Blackwell*, 1954; *de Vries and Peck*, 1958; *Jaeger*, 1965; *Shiozawa and Campbell*, 1990; *Bristow et al.*, 1994]

The FO cable geometry is far more complex than the geometry and dimensions assumptions of either the cylindrical source transient or the line source transient methods, and thus demonstration of the 1:1 relation of the thermal response of soil to the power intensity of the heat pulse is needed.

4.4 Results and Discussions

4.4.1 Power intensity effect on T_{cum}

In the AHFO method, if power intensity of each heat pulse is not strictly regulated, large uncertainty can be induced into the results due to the power intensity fluctuation. To reduce this uncertainty, a method is needed to allow comparison of the thermal response of soil to heat pulses with different power intensities. In this section we will demonstrate that T_{cum} can be scaled by a simple multiplicative factor to reflect a reference power intensity value. From basic principles, in absence of phase-change, the underlying thermal conduction and heat capacity processes are expected to be linear, so that any change in power level should be correctable via linear scaling to a reference power application. To verify the theory of the 1:1 relationship, the concept was tested using lab experimental data retrieved from the saturated soil column with various heating power levels. Eight different levels of power intensity were tested ranging from 5 to 38 W m^{-1}. For each power level a 2-minute pulse was applied.

We first demonstrate that the intercept of the regression line relating $\dot{P}$ to $\dot{T}_{cum}$ takes on the expected value of zero. Here $\dot{P}$ and $\dot{T}_{cum}$ are the results of standardizing P and T_{cum} by their means of 18.8 W m^{-1} and 889.4 °C s respectively in order to have both parameter at the same scale (Figure 4.7). Thereafter, we demonstrate that the slope of the resulting regression line is equal to one after setting the intercept equal to zero value. Least-Squares Methods (LSM) is applied in the two-step process to estimate the proper parameters used in formulating the linear regression model that relates the standardized power intensity level ($\dot{P}$) to the standardized thermal response ($\dot{T}_{cum}$). The first step uses a linear regression model that includes both slope and intercept to test if the intercept is different from zero. The estimated linear regression has the following form:

$$\hat{\mu}\{\dot{T}_{cum}|\dot{P}\} = \hat{\beta}_0 + \hat{\beta}_1\dot{P} \qquad \text{Eq. 4.2}$$

Where $\hat{\mu}\{\dot{T}_{cum}|\dot{P}\}$ is the estimate of the regression of $\dot{T}_{cum}$ on $\dot{P}$ (dimensionless), $\hat{\beta}_0$ is the estimated intercept of the regression line (dimensionless), $\hat{\beta}_1$ is the estimated slope of the regression line (dimensionless).

The results of the LSM fit showed that the p-value of the hypothesis that the intercept is non-zero ($\hat{\beta}_0$) is 0.938 after accounting for the slope effect (Table 4.3); therefore, there is no statistical evidence that the intercept is different from zero.

Table 4.3 Regression parameters estimate using Equation 1with both slope and intercept

	Coefficients	Standard Error	t-statistic	p-value	Lower 95%	Upper 95%
$\hat{\beta}_0$	0.002	0.026	0.081	0.938	-0.062	0.066
$\hat{\beta}_1$	0.998	0.022	44.397	8.7E-09	0.943	1.053

The second step uses the linear regression of Equation 4.2 with $\hat{\beta}_0$ set to zero. The results of LSM fit strongly support the theory of the 1:1 relation that relates power intensity to thermal response (Table 4.4 and Figure 4.7) for the range of power and conditions of the lab experimental setup.

Table 4.4 Regression parameter estimates using Equation 1 with $\boldsymbol{\hat{\beta}_0}$ set to zero

	Coefficients	Standard Error	t-statistic	p-value	Lower 95%	Upper 95%
$\hat{\beta}_1$	0.999	0.011	94.826	3.82E-12	0.975	1.024

The implication is that if there is a temporal variation in the power intensity applied, the obtained thermal response can be easily (linearly) scaled to reflect a reference power intensity. This can be achieved by knowing the power, voltage or current associated with each particular heat pulse, or by using a reference section of the heated fiber optic cable held in a medium with constant thermal properties throughout the experiment. This technique was applied in both lab calibration and field application to account for the power fluctuations.

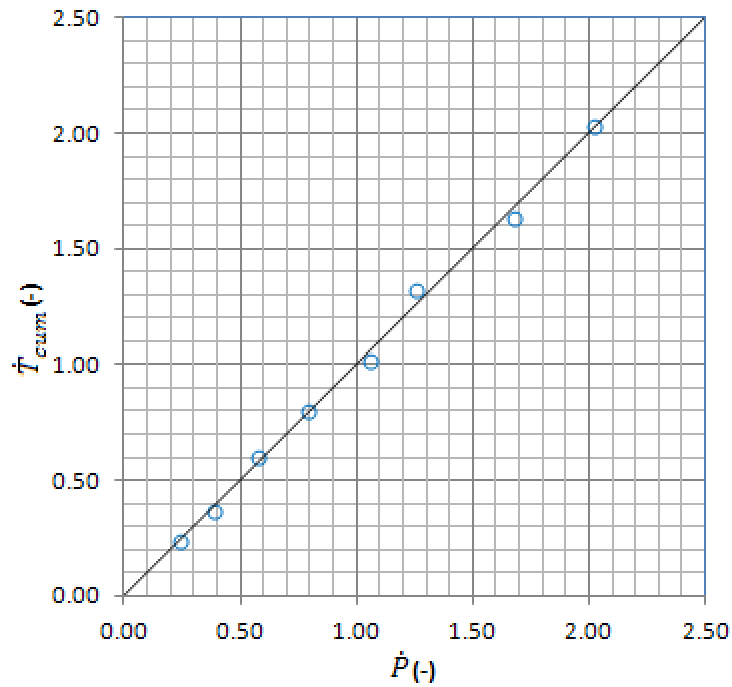

Figure 4.7 Standardized power intensity level ($\dot{\boldsymbol{P}}$) vs. standardized thermal response ($\dot{\boldsymbol{T}}_{\boldsymbol{cum}}$)

4.4.2 Lab calibration results and system performance

A calibration equation was fitted to the data relating measured soil water content to measured T_{cum} (Figure 4.8). The gravimetric samples obtained from the soil column, indicated an average bulk density (ρ_b) of 1.63 g cm^{-3} with a standard deviation (σ_b) of 0.06 g cm^{-3}. The obtained values are in the range of both measured bulk density in the field (ρ_b=1.67 g cm^{-3} and σ_b=0.12 g cm^{-3}) and just within the range suggested of this soil by the NRCS survey (1.15-1.70 g cm^{-3} range; Table 4.2).

The fitted curve showed that T_{cum} becomes insensitive to variation in soil water content both at very dry soil with degree of saturation (S) below 0.1 and high water content (S > 0.4). In the former case, this can be explained by observing the behavior of the soil thermal conductivity (λ) at low soil water content. In fact, λ has been showed to be nearly constant from zero to a critical value of soil water content (θ_{cr}) before it starts increasing when the water geometry transitions from pendular to funicular [*de Vries*, 1963; *Tarnawski and Leong*, 2000]. A similar behavior is observed in the measured λ from the calibration of the soil column, where a sharp increase in λ is observed beyond 0.03 $m^3\,m^{-3}$ (S > 0.08) of soil water content (Figure 4.9). The observed θ_{cr} value aligns with *de Veris* [1963] recommendation of using θ_{cr} values of 0.03 $m^3\,m^{-3}$ for coarse soils and 0.05 to 0.1 $m^3\,m^{-3}$ for fine soils. The value of θ_{cr} tends to be dependent on the clay content of the soil [*Tarnawski and Leong*, 2000; *McInnes*, 1981]. This behavior is also observed in the thermal diffusivity curve (Figure 4.10).

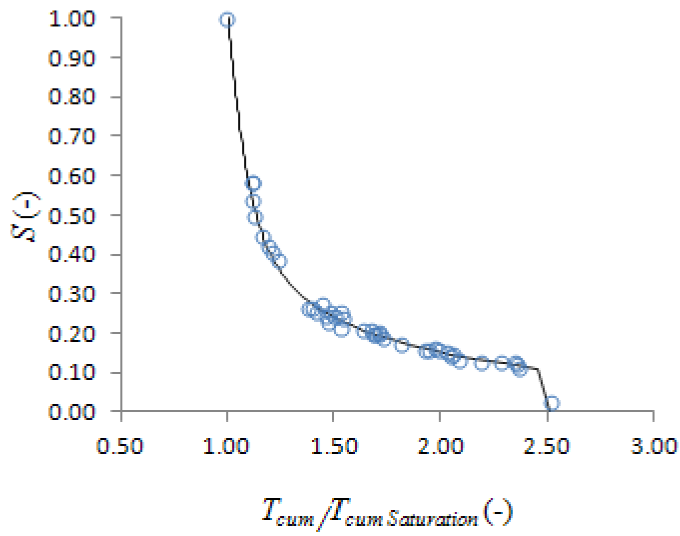

Figure 4.8 Calibration curve relating the degree of saturation (*S*) to T_{cum} normalized by its value at saturation integrated over 180 seconds for the 1–minute duration heat pulses

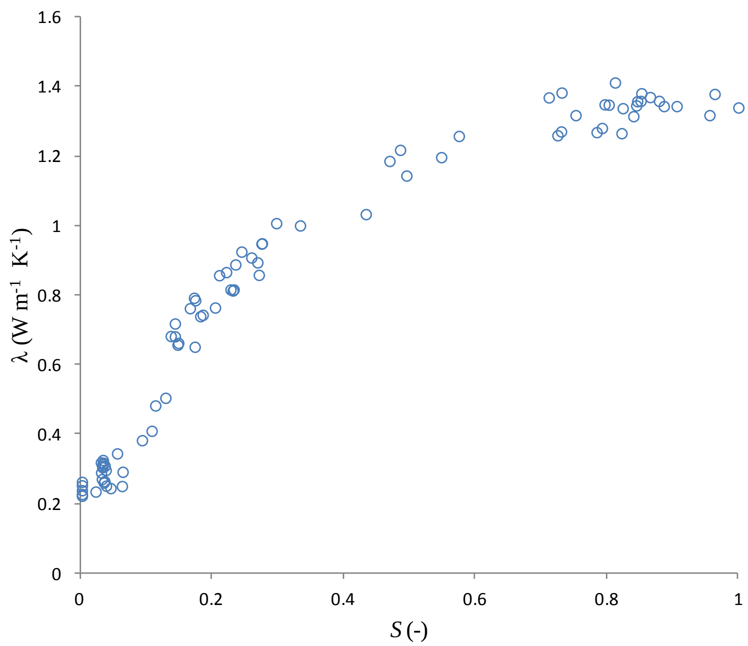

Figure 4.9 *S* vs. λ measured from non-disturbed samples collected from the calibration soil column. After saturation, the samples were drained in a pressure chamber to allow measurement of λ at different level of soil water content using a KD2 Pro.

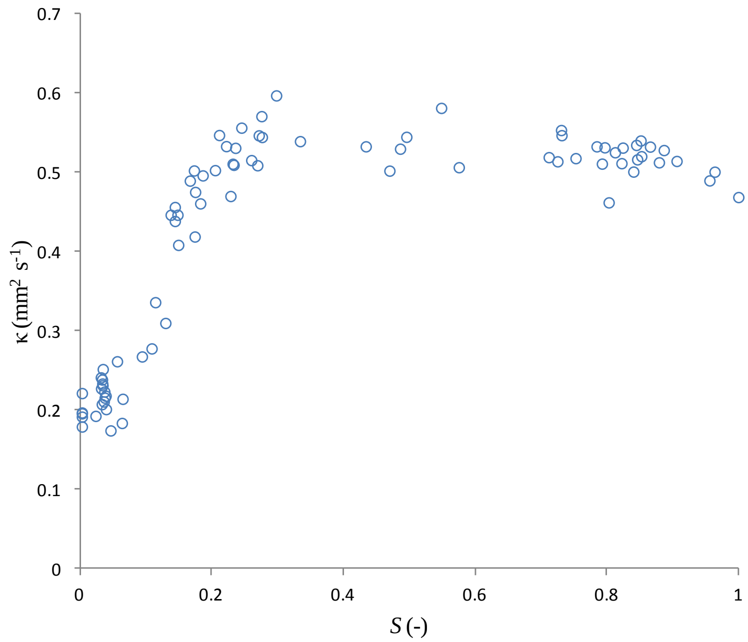

Figure 4.10 *S* vs. κ measured from non-disturbed samples collected from the calibration soil column. After saturation, the samples were drained in a pressure chamber to allow measurement of κ at different level of soil water content using a KD2 Pro.

For soil water content ranging from 0.04 to 0.40 $m^3\ m^{-3}$ ($0.1 < S < 1$) the slope in the relationship relating θ to T_{cum} decreases with soil water content (Figure 4.8) indicating that the error in soil water content estimation is expected to increase with increasing soil water content as observed in *Sayde et al.* [2010].

The same methodology described in *Sayde et al.* [2010] was applied to estimate the error in soil water content obtained from T_{cum}. For each value of θ, the estimated error (σ_θ) was calculated using the following equation:

$$\sigma_{\theta} = \frac{\sigma_{T_{cum}}}{\left| \dfrac{df(\theta)}{d\theta} \right|}$$

Eq. 4.3

Where $\sigma_{T_{cum}}$ is the error in T_{cum} (dimensionless), $\dfrac{df(\theta)}{d\theta}$ is the local slope of the T_{cum} response evaluated at θ (dimensionless).

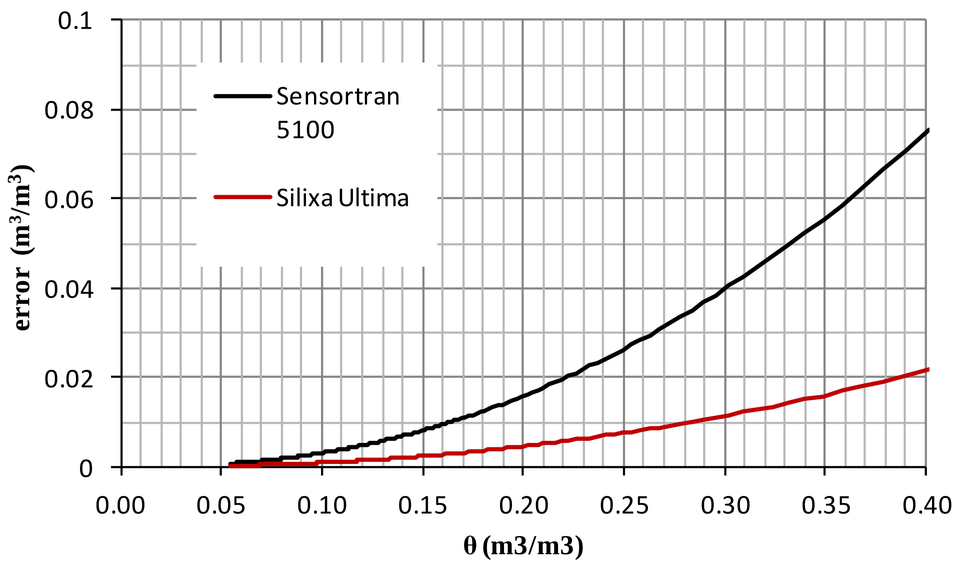

Figure 4.11 Estimated error in soil water content estimation due to the DTS system performance.

σ_{Tcum} was obtained by measuring the variability in T_{cum} over repeated measurements at constant soil moisture content. Under the lab controlled conditions, 85% of the variability in σ_{Tcum} (3.18 °Cs) is due to instrument noise, the high resolution Silixa Ultima in this case. The remaining 15% is believed to be caused by voltage fluctuation during heating and spatial variability of soil thermal properties in the soil column. The noise in Sensortran 5100 unit was around 12.60 °C, a level at which any other source of error is negligible and undetectable.

4.4.3 Field test results

In this section, the results of the field test of section 4.3.2 are presented. The calibration equation developed in section 4.4.2 (Figure 4.8), is used to translate T_{cum} values observed over the three depths cables to soil water content values. The shape of the calibration curve indicates that if error in calibration occurred it would be easily detected in the results. i.e. the calibration curve in Figure 4.8 is very steep toward high soil water content and very flat at low soil water content. As soil is wetted to near saturation in many locations in the field and if the calibration curve is slightly biased toward the wet side, the obtained soil moisture estimates from the calibration curve of the wetted location would be off the chart and easily detected. On the other hand, if the calibration curve is biased toward the dry side, then obtained soil moisture estimates from T_{cum} will indicate that the soil is very dry at all time and no significant changes in soil water content will be detected. Again here, such type of error can be easily detected in this work due to the high variability (both in space and time) in soil water content that is expected from the imposed water application spatial variability at the surface. And in fact, the 90 cm depth soil water contents as estimated using the calibration curve of Figure 4.8, clearly show the signs of biased calibration as stated in the previous paragraph for a calibration curve biased toward the dry end: the changes in T_{cum} at the 90 cm depth were of same magnitude than the one observed at the 30 and the 60 cm depths (see Figure 4.12). Nevertheless, this change in T_{cum} did not translate in significant soil water content changes when the calibration curve of Figure 4.8 is applied as observed with the 30 and the 60 cm depths.

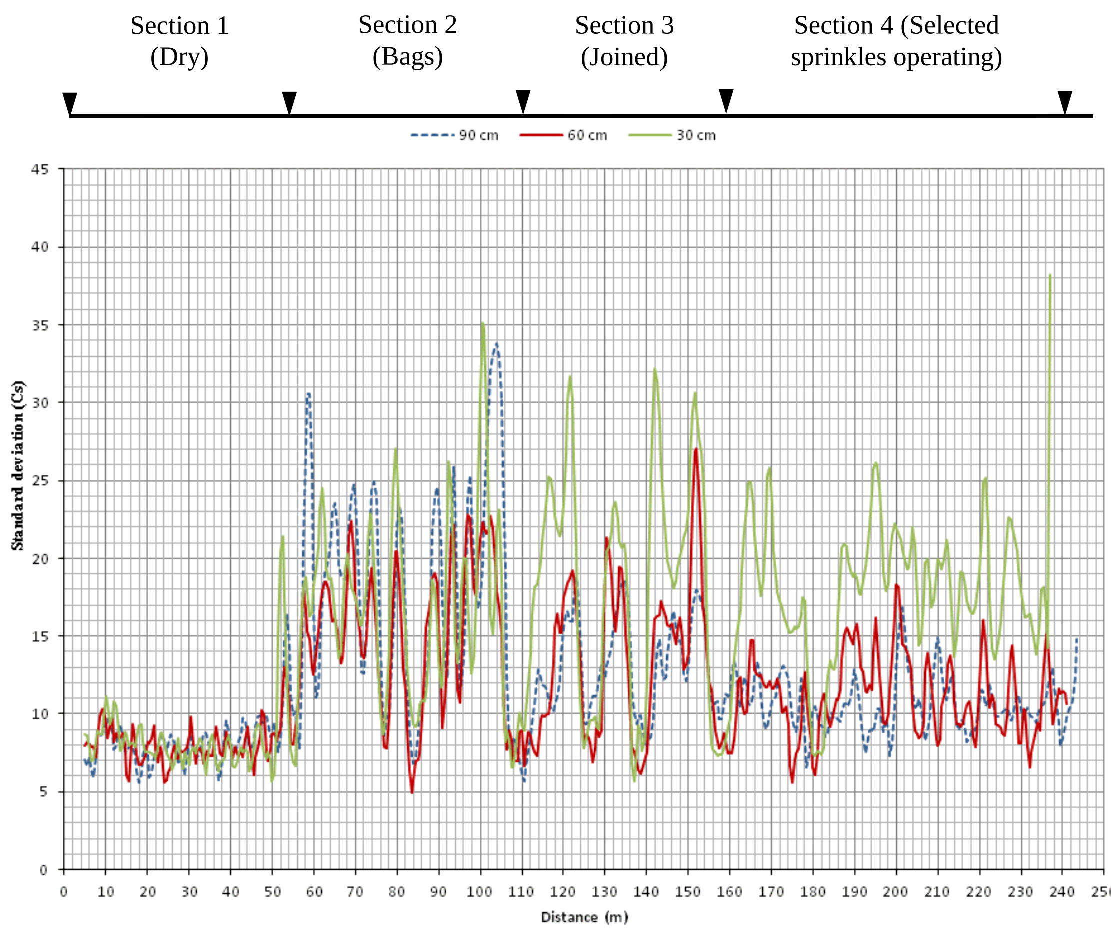

Figure 4.12 Observed standard deviation of T_{cum} at the 30, 60 and 90 cm depths during the 36 hr duration of the experiment.

The 30 and the 60 cm DTS estimated soil water content did correspond to what to be expected from the four patterns of spatial variability imposed at the surface, as shown in the followings paragraphs.

The section between 0 and 55 m (Section 1) was not irrigated, so as would be expected, no significant water change was detected at either depth (see Figure 4.13).

For the section between 55 and 110 m (Section 2), the constraining bags installed around the emitters forced the water to directly fall below the emitters instead of spreading in the typical circular pattern. This implies that water was only applied directly below the emitters and at a very high rate. This signal of a localized high application rate is captured by the FO system as shown in Figure 4.13 where we notice nine strips of high soil water content change that corresponds to the locations of the nine bagged emitters. Figures 4.14 and 4.15 show clearly the association between the highest water increase at a given time step and the location of a discharging emitter.

In section 3 (between 110 m and 158 m), four sets of two emitters were attached together resulting in high discharge over a larger area than that in the bagged sprinklers of Section 2. The location of the four wide strips of high soil water content change observed at both 30 and 60 cm depths of the fiber optic cable (Figure 4.13) correspond to the four sets of paired emitters.

In section 4 (from 158 m to the end), emitters were switched on and off in space as shown in Figures 4.14 and 4.15. The same pattern in soil water change is observed through the FO cable at the 30 cm depth, where the highest soil water content increases are observed at the location of the operating emitters.

For the 60 cm depth cable, the little variation in soil water content observed over section four is still associated with the status of the above ground emitters. We can notice that the water content increase is of similar magnitude at 30 cm depth and is much smaller at the 60 cm depth than the one observed with the two other wet treatments. This is to be expected as this section received a lower water application treatment than the two other sections.

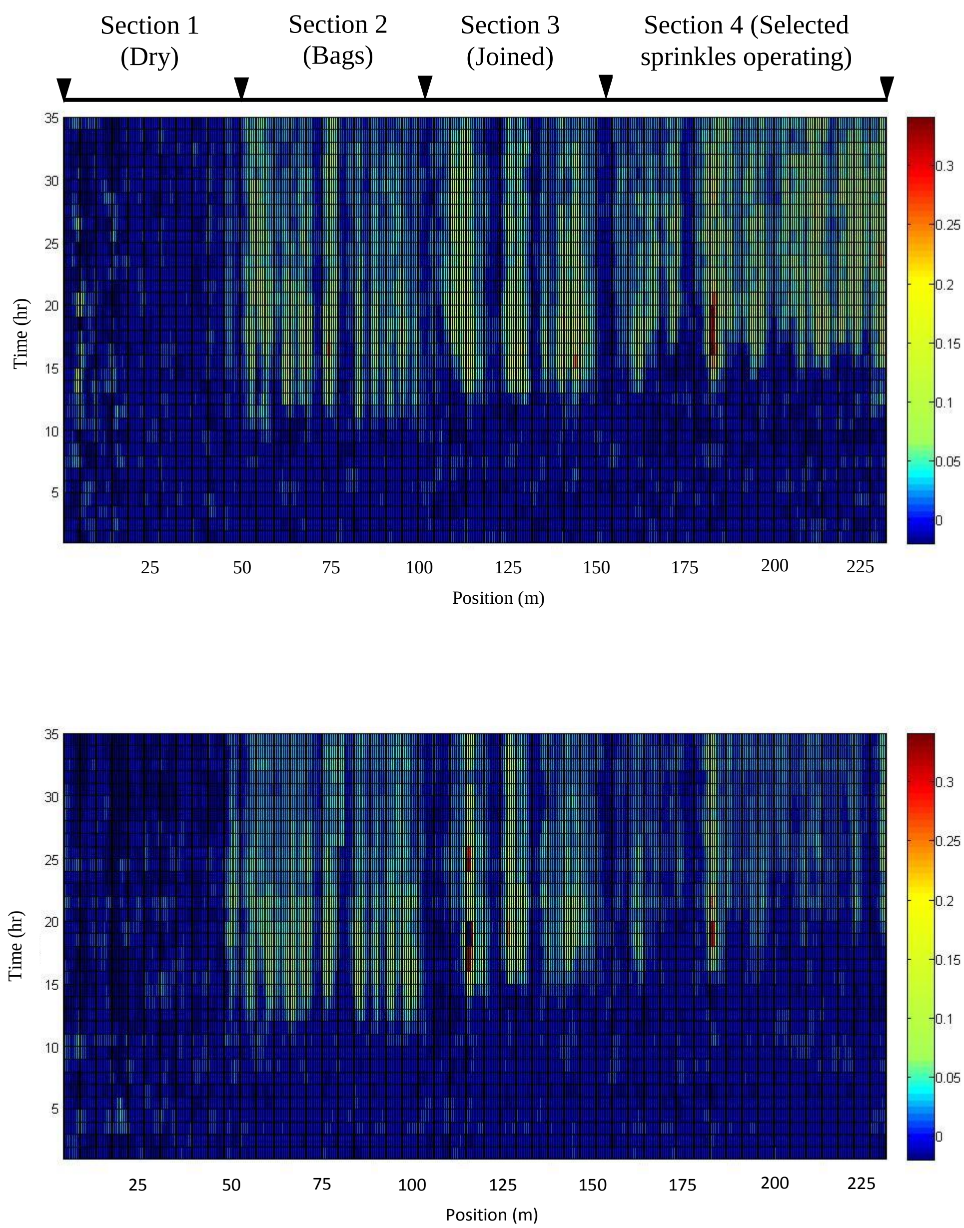

Figure 4.13 Soil water content change at the 30 cm (top figure) and 60 cm depths (bottom figure).

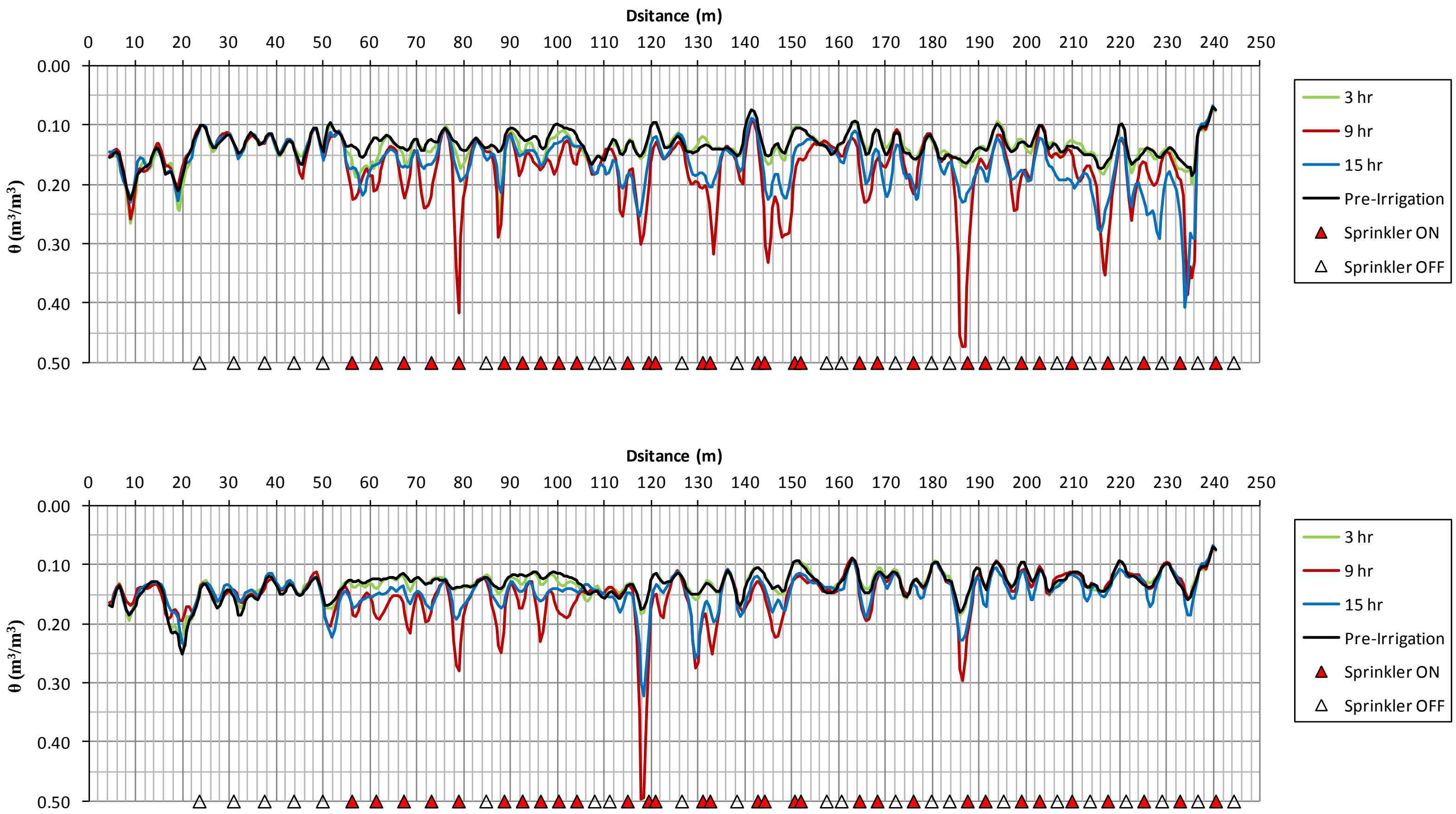

Figure 4.14 DTS-estimated soil water content at 30 cm depth (top figure) and 60 cm depth (bottom figure) with emitter positions shown before irrigation, and 3, 9, and 15 hours after the 7 hr irrigation set started.

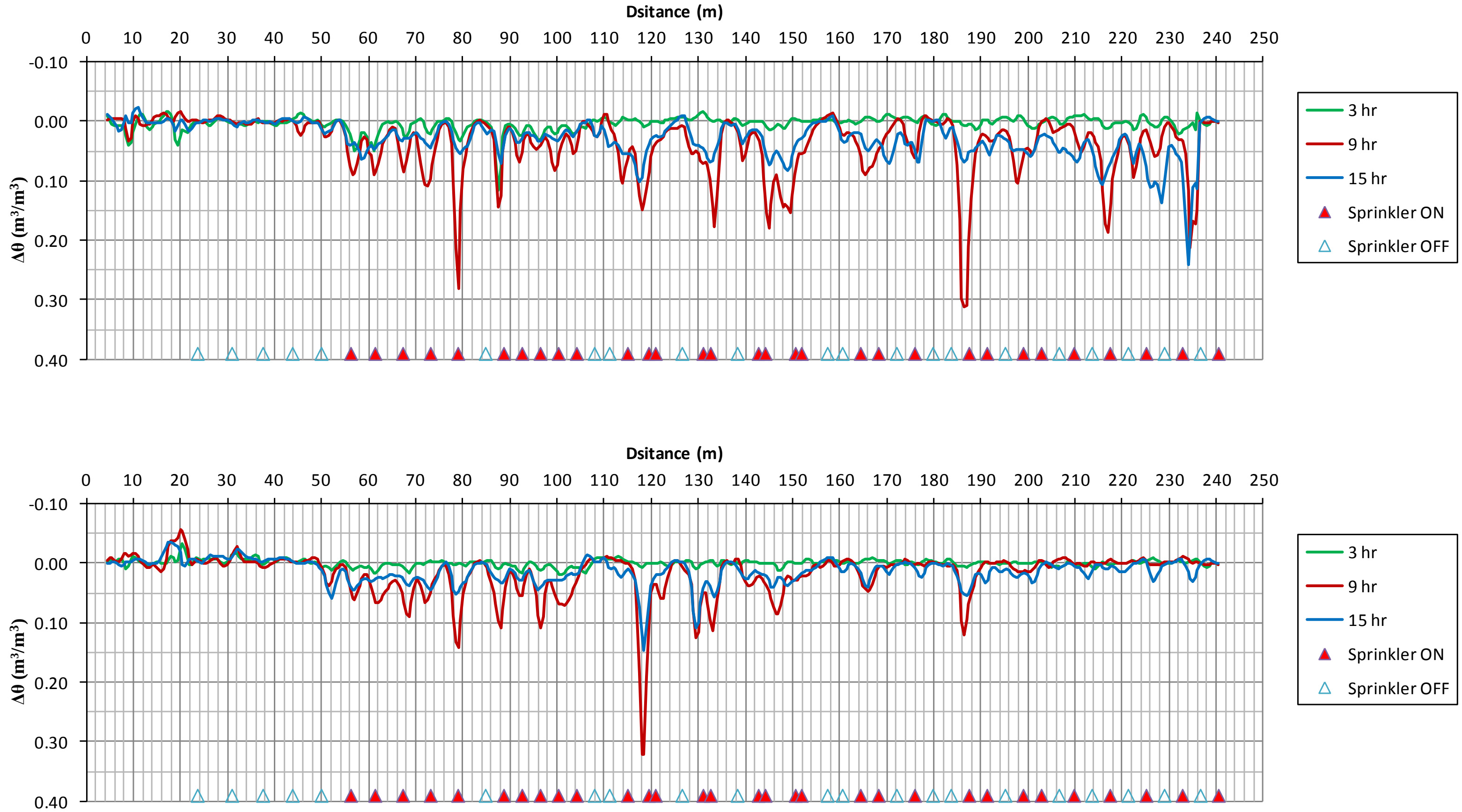

Figure 4.15 Change in soil water content at 30 cm depth (top figure) and 60 cm depth (bottom figure) with emitter positions shown before irrigation, and 3, 9, and 15 hours after the 7 hr irrigation set started.

To compare the soil water content response for the different wetting regimes, a time-lagged cross-correlation analysis was performed between the time series of soil moisture change at each particular position along the FO cable installed at 30 cm depth and those of its corresponding position along the FO cable at the 60 cm depth. The cross-correlation method has been employed successfully to study time-lag relationship between soil moisture content at variable depths [*Georgakakos et al.*, 1995; *Mahmood and Hubbard*, 2007; *Mahmood et al.*, 2012].

Matlab function "Xcorr" is used to calculate the cross-correlation coefficient, $\hat{R}_{xy}(m)$, associated with each time lag (m) tested as follows:

$$\hat{R}_{xy}(m) = \begin{cases} \sum_{n=0}^{N-m-1} x_{n+m}\, y_n^* & m \geq 0 \\ \hat{R}_{yx(-m)}^* & m < 0 \qquad \text{Eq. 4.4} \\ \hat{R}_{yx(-m)}^* & m < 0 \qquad \text{Eq. 4.4} \end{cases}$$

Here x and y are soil water content at the 30 and the 60 cm depth respectively that are normalized by their value at time m = 0. N is the length of the x and y vectors.

The maximum correlation coefficient value is used to identify the appropriate time lag to represent the wetting-front travel time at each location (see Annex 1 for a list of maximum correlation coefficient per location and its corresponding time lag value). The analysis results were separated into two groups based on the maximum change in soil water content observed at the 30 cm depth locations. The first group of data represents data retrieved from locations where $\Delta\theta > 0.05$ m^3 m^{-3} is observed at the 30 cm depth during the experiment, while the second group is composed from those at the remaining locations (see Figure 4.16). The reasoning behind this separation is that at the three wetted sections along the FO cables, transect water was applied at a set of discrete locations, causing a vertically-progressing soil water content change where water was applied, when compared to the inter-emitters locations where the observed lower soil water content change is expected to be driven by lateral redistribution. For the first group, the average time lags were 0.64 hr (Standard deviation of 0.97 hr), 2.55 hr (Standard deviation of 1.21 hr), and 3.46 hr (Standard deviation of 2.91 hr) hr for section 2, section 3, and section 4 respectively. This variation can be explained by the pattern of water application at the surface for the three different wet treatment sections, with section 2 is expected to be receiving the highest application rate for the locations of group 1, and section 4 receiving the lowest application rate.

The same correlation method was used to calculate the wetting front travel time from depth 60 cm to depth 90 cm. Since the T_{cum} to moisture content calibration developed for the upper soil was not found to be suitable for the 90 cm depth, the time series of change in T_{cum} (from pre-irrigation conditions) for both 60 and 90 cm depths are employed instead of the time series of change in soil water content. As before, the calculated time lag was separated into two groups; Group 1 includes the time lag for location where $\Delta\theta$ at 60 cm was > 0.05 m^3 m^{-3}, and Group 2 for where $\Delta\theta$ at 60 cm was < 0.05 m^3 m^{-3} (Figure 4.17). For the Group 1, the average time lags were 0.93 hr (Standard deviation of 1.72 hr), 3.33 hr (Standard deviation of 1.49 hr), and 5.89 hr (Standard deviation of 1.83 hr) for section 2, section 3, and section 4 respectively. On average, the wetting front velocity was 32% faster between the 30 and the 60 cm depths than between the 60 and the 90 cm depths.

That said, readers should be aware of the high uncertainty associated with the use of the time lag to estimates the wetting front traveling time for section 2 of the fiber optic cable location. In section 2, about half of the time lag values calculated for the different positions in for the 30 cm depth and for a lesser extent for the 60 cm depth have either negative or zero values. This is a clear indication that the transit times were not long enough to be accurately quantified based on 1-hr measurement intervals at the highest fluxes. Thus, the time lag results of section 2 were considered non-reliable to estimate the water front traveling time and will not be used in the further analysis.

The estimates of the wetting front traveling times in section 3 and section 4 are used to calculate the wetting front velocity and associated fluxes. For each particular location (i) along the fiber optic cables and for each particular depth (d) a wetting front velocity (V_{id}) and a flux (F_{id}) can be calculated as follows:

$$V_{id} = D_{id}\, l_{id}^{-1} \qquad \text{Eq. 4.5}$$

and

$$F_{id} = V_{id}\, \Delta\theta max_{id} \qquad \text{Eq. 4.6}$$

Where:

- D_{id} is the distance between two successive depths, D_{id} = 30 cm in our case,
- l_{id}^{-1} is the time period elapsed between the wetting front arrival at two successive depths (hr). l_{id}^{-1} is estimated by the calculated time lag that have positive values shown in Figure 4.16 for the 30 cm depth and Figure 4.17 for the 60 cm depth with 1 hr added to each time lag. . The reasoning behind adding 1 hr to the time lag is due to the hourly time resolution of the heat pulses applied; as water front is moving in depth from one cable location to another, the arrival time captured by the 1-hr measurement interval could have happen anytime between the beginning and the end of this particular hour. Adding 1 hr will insure a lower (conservative) boundary on all possible values of water front velocity and flux . This also will allow us to avoid dividing by zero value in equation [5]. The obtained values of velocity and fluxes will be considered as being the minimum possibly observed.
- $\Delta\theta max_{id}$ is the maximum change in volumetric water content ($m^3\,m^{-3}$)

As expected, larger water fluxes are observed below the locations that showed higher increase in water content (Figure 4.18 , Figure 4.19 and Table 4.5), which in turn are associated with the locations of the discharging emitters as discussed in a previous section. The Fluxes seem to get smaller with depth. The magnitude in flux reduction with depth can be associated with the pattern of water application at the surface. In fact the fluxes average was reduced by 41% over section 3, and 71% over section 4 (see Table 4.5). This is to be expected, as the applied water discharge rate was the largest, and localized over a wetted area that was smaller in section 3 when compared to section 4.

Table 4.5 Averages Fluxes (cm hr^{-1}) by section observed at different depths

	Section 3			**Section 4**		
	$\Delta\theta \geq 0.5$ $m^3\ m^{-3}$	$\Delta\theta < 0.5$ $m^3\ m^{-3}$	All locations	$\Delta\theta \geq 0.5$ $m^3\ m^{-3}$	$\Delta\theta < 0.5$ $m^3\ m^{-3}$	All locations
Average Flux at 30 cm depth (cm hr^{-1})	>1.3	>0.2	>0.8	>0.9	>0.2	>0.8
Average Flux at 60cm depth (cm hr^{-1})	>1.1	>0.3	>0.5	>1.0	>0.1	>0.2
Average Flux applied at the surface (cm hr^{-1})	-	-	1.0	-	-	0.8

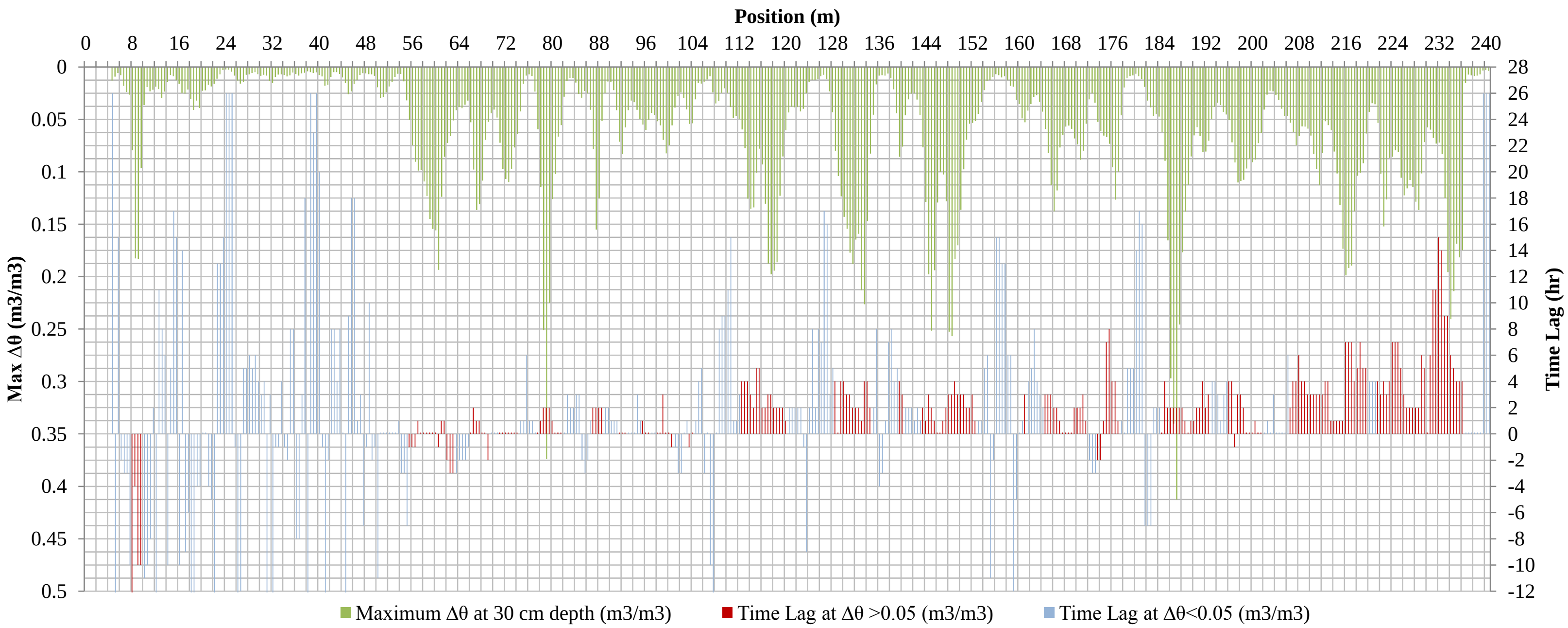

Figure 4.16 Time lag at the highest time-lagged correlation value between Δθ at 30cm and Δθ at 60 cm.

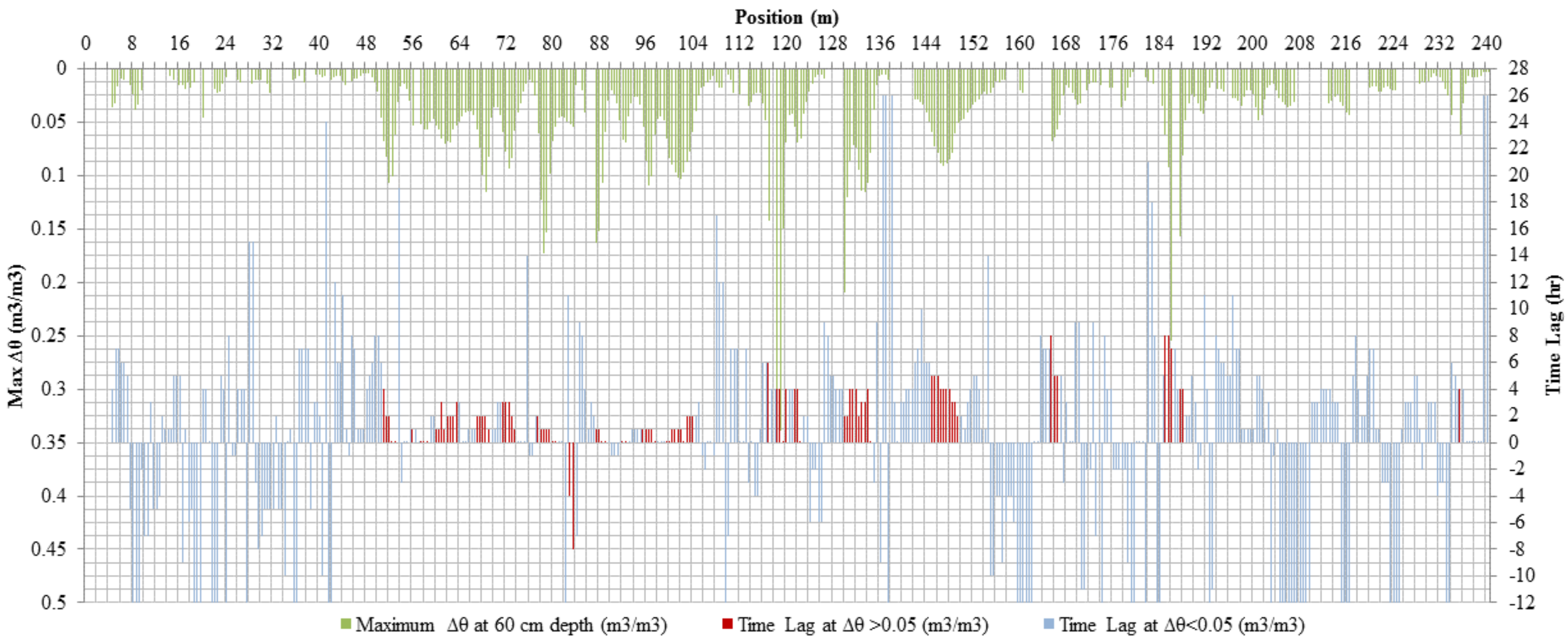

Figure 4.17 Time lag at the highest time-lagged correlation value between ΔT_{cum} at 60cm and ΔT_{cum} at 90 cm

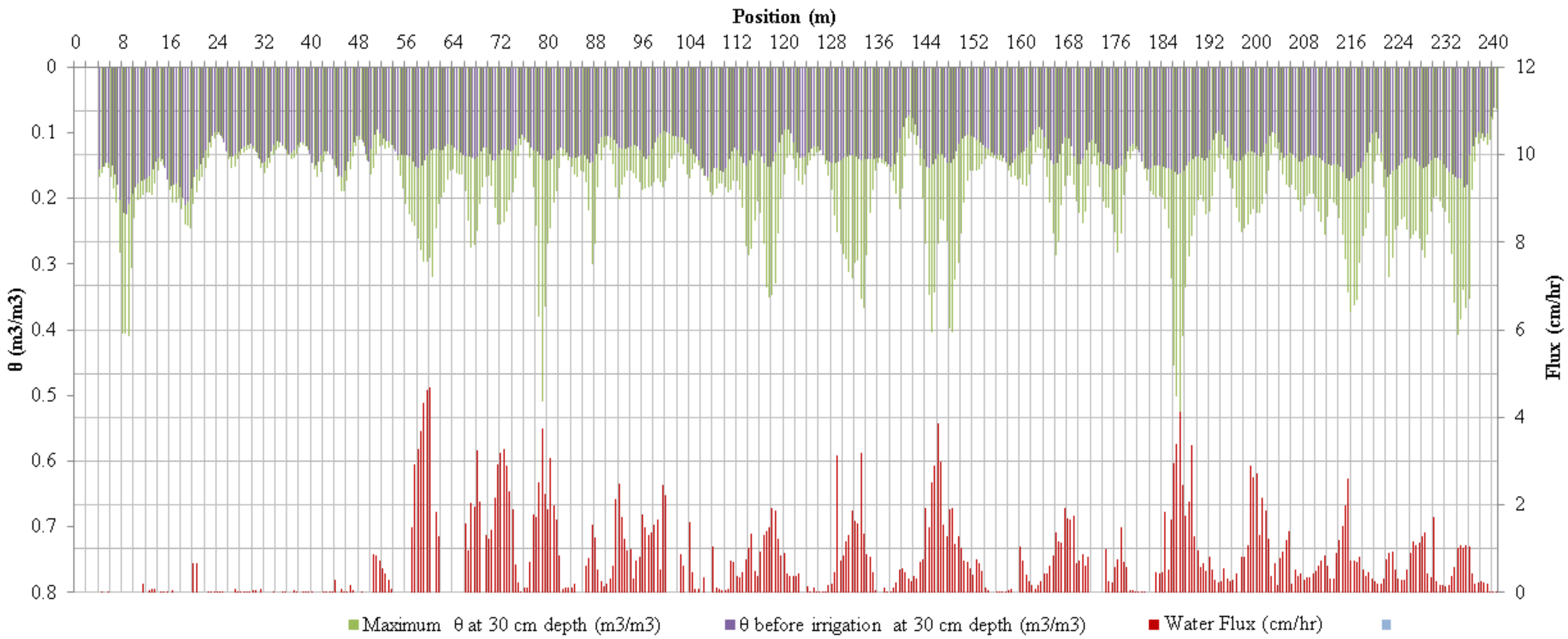

Figure 4.18 Water flux, pre-irrigation soil water content, and maximum soil water content at the 30 cm depth.

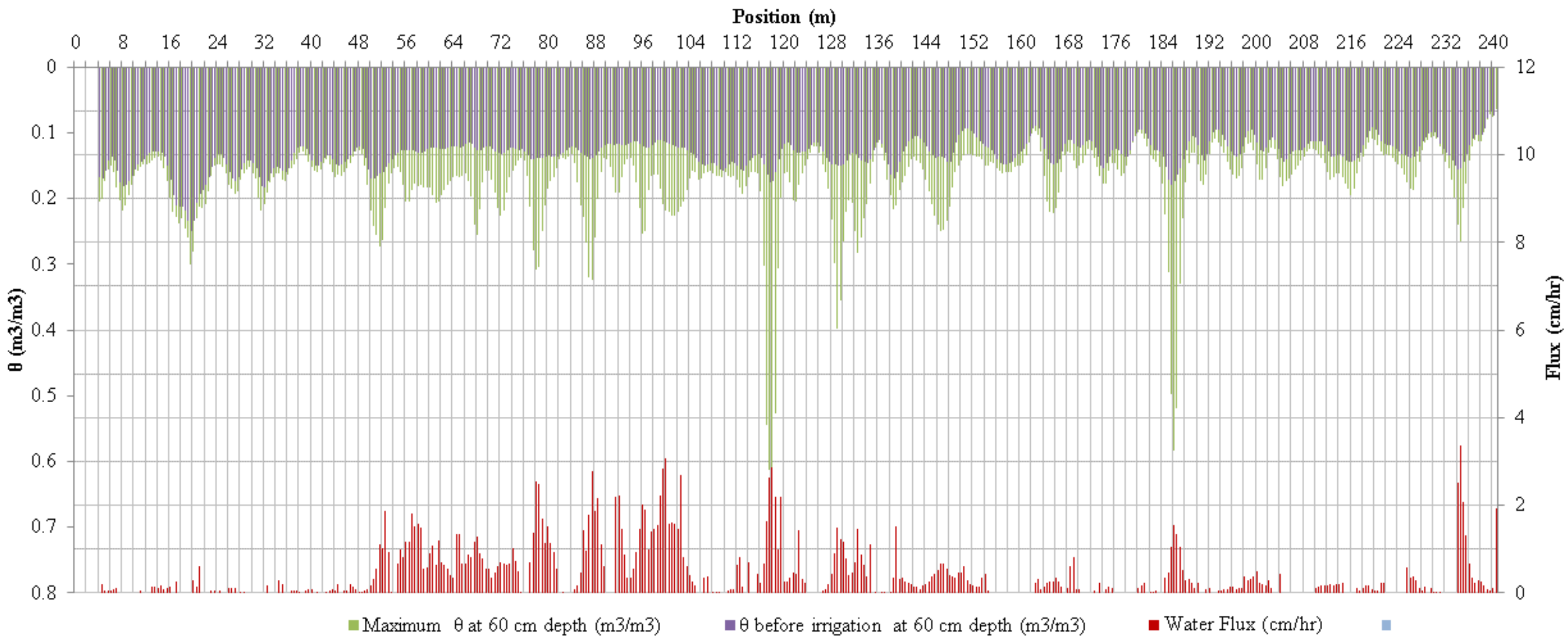

Figure 4.19 Water flux, pre-irrigation soil water content, and maximum soil water content at the 60 cm depth.

4.4.4 Addressing the challenge of field calibration

In this work, the calibration curve (in Figure 4.8) relating DTS measured T_{cum} to soil water content was obtained in a laboratory experiment. Soil was collected from the field where the FO system installed and repacked to the observed bulk density in the field in a 0.5 m diameter soil column. This operation was tedious and time consuming; to cover the whole range of soil moisture conditions; the soil column has to be saturated, drained for several weeks, and then left drying over several months. In addition, the soil column was only representative of the top 70 cm of the soil, the maximum depth in the field from which soil was collected. In keeping with unpublished observations of a textural transition observed during the installation of neutron probe tubes, beyond 70 cm depth the soil had different thermal properties and thus the calibration equation obtained in laboratory experiment were not directly applicable. These results reiterate that a more practical calibration methodology of the AHFO method will be needed for the method to find broad adoption.

The most direct, if time intensive, method is to measure the thermal conductivity and diffusivity of the soil of interest over the full range of soil moisture conditions (as in Figure 4.9 and Figure 4.10). Samples that were typical of all major soils seen at the site would need to be included. One could then use heat transport models to generate calibration curve relating T_{cum} to soil water content for this particular soil, FO cable design, and operating conditions. But measuring thermal properties of soil over the full range of soil water content presents a daunting challenging regard the effort and time required to complete such a procedure.

Practical lessons can be learned from looking at how curves relating the thermal conductivity (λ) to soil water content (θ). Most models relating λ to θ we use a same core assumption that the relationship between λ and θ for all types of soils and bulk densities has the same fundamental shape that is scaled by a set of parameters that is particular for each soil [see *Johansen* 1975; *Campbell* 1985; *Cote and Kon*rad 2005; *Lu et al.* 2006]. Apparently those sets of parameters can be easily obtained by couple of simultaneous λ and θ measurements for the soil of interest in the case of the models described by *Johansen* [1975], *Cote and Kon*rad [2005] and *Lu et al.* [2006]. For the model described by *Campbell* [1985] a single non-disturbed sample that provides information on λ for a wet and for the dry condition, and on the bulk density of the soil will be enough to generate the curve relating λ to θ for a particular soil.

In principle, calibration curves relating T_{cum} to soil water content should have also a same basic shape; steep slope toward high water content and flat toward low soil water content, as observed in this work and in *Sayde et al.* [2010]. This information suggests that calibrations curves for different soil types could be scaled from one reference curve using couple of measurements in the field. The only fundamental difference in shape that we might expect between curves of different soil types is the θ_{cr} value below which T_{cum} is held nearly constant (see section 4.3.1. for more information).

The thermal response (T_{cum} in our case) of the FO cable to a heat pulse is a function of how rapidly heat was conducted into the surrounding medium i.e. the thermal conductivity of the soil [*Weiss*, 2003] especially for long heat pulse where the effect of the finite dimensions of the FO cable will diminish with time and thus the long time solution of the line source transient methods can be applied [*Weiss*, 2003; *Perzlmaier et al.*, 2004]. *De Vries* [1952] showed that this solution has the following form for the heating period:

$$\Delta T \approx (q/4\pi\lambda)\ln(t) + b \qquad \text{For } t < t_0 \qquad \text{Eq. 4.7}$$

Here ΔT is the change in temperature (°C), q is the energy input (W m^{-1}), λ is thermal conductivity of the medium (W m^{-1} K^{-1}), t is time (s), t_0 is the duration of the heating pulse (s), b is a constant independent from time.

The integral with respect of time of Equation 4.7 is:

$$T_{cum} \approx (q/4\pi\lambda)t\{\ln(t) - 1\} + tb \qquad \text{Eq. 4.8}$$

Here, the *tb* term can be easily accounted for with basic algebra if data is available for two heating times. For example, take T'_{cum} to be the T_{cum} for an integration time of t duration, and T''_{cum} to be the T_{cum} for an integration time of $2t$ duration such as $2t \leq$ heating time, then the difference between those two entities, ΔT_{cum}, is:

$$\Delta T_{cum} = 2(q/4\pi\lambda)t[\ln(1/2)] \qquad \text{Eq. 4.9}$$

Following this approach a result is obtained wherein an inverse proportionality holds between λ and a form of T_{cum} that can be used in theory to derive a calibration curve relating T_{cum} to θ with few simultaneous measurements of θ with either λ and T_{cum}.

4.4.5 How to improve the quality of the AHFO method results?

In the previous section, the uncertainty level for a particular measurement was shown to improve considerably when a high performance DTS unit is employed for the temperature measurements. This led to explore the possibilities of improving measurements' performance and its limitations.

In fact, when planning for an AHFO installation, we seek to optimize the quality of the measurement while dealing with a constraining budget. The aim of this section is to provide guidance for future design and operation of AHFO applications. This guidance based on a theoretical analysis of the nature of the sources of error in DTS heat-pulse moisture content measurements, as well as being drawn from extensive lab and field operations during the past three years.

Assuming that the calibration was performed correctly, and there is no drift in calibration over time, the quality of the soil moisture measurements using the AHFO method will depend mainly on the signal-to-noise ratio delivered by the system.

Here, T_{cum} is the signal magnitude. As demonstrated in section 3.1., T_{cum} increases linearly with the power intensity level.

The noise magnitude will depend on the spatial and temporal lengths of a measurement. In fact, the DTS reported temperature is calculated from the ratio of the magnitudes of anti-Stokes to Stocks scattered light. Thus, the noise level of a single measurement will depends on the accuracy of this ratio, which in turn is a function of total number of reflected photons observed. By the law of large number, those observed photons follow a normal distribution with a standard deviation decreasing by the square root of the total number of photons observed [*Selker et al.*, 2006]. Since the number of photons observed will be a 1:1 function of the fiber volume that are emitted from and the length of time they are integrated over, the noise level (i.e. precision) will decrease by the square root of both spatial and temporal lengths of a measurement.

Here we introduce a quality factor index (F_Q) that reflects the impact of different combinations of heat pulse, data collection, and sensing system characteristics on magnitude of the signal-to-noise ratio, such as:

$$F_Q = \frac{P}{E} \left[\frac{L_R\, H\, N}{L_M\, t_T}\right]^{0.5} f(\theta, t_0\,, t_T) \qquad \text{Eq. 4.10}$$

Where :

- P is the power applied (W m^{-1}). As demonstrated in the previous section, the thermal response, T_{cum} in this case, will increase linearly with applied power.
- E is the temperature reading error per temperature reading cycle (°C). Here the reading cycle refers to the time between the start of successive temperature readings on the DTS.
- L_R is the spatial resolution of the temperature readings (m) such as $L_R > L_M$,. Increasing L_R will increase the length over which the measurement is averaged over, and thus increasing its precision by square root of the length. L_M is the DTS spatial resolution (m). It is closely related to E; to understand the effect of L_M on the potential precision, think about comparing two DTS unit with the same E level but different L_M . The one with the lowest L_M value has the potential to deliver a better precision, proportionally to the square root of L_M .
- N is the number of heat pulses (dimensionless). As errors in T_{cum} are considered normally distributed then precision should increase with square root of N.
- H is the temperature reading frequency (Hz). The precision will increase the square root of H. i.e., If two DTS units has the same E value but different H, the one with higher H has the potential of delivering more precise reading of T_{cum}, proportionally to the square root of the higher on the lower H ratio.
- t_0 is the heat pulse duration (s),
- t_T is the total reading duration (s). Increasing t_T will increase the total error values accumulated by square root of t_T. Increasing t_T will also increase the

signal amount captured. This is accounted for in the function$f\ (\theta, t_0, t_T\ )$,the functional form relating the thermal response of a particular soil, FO cable design, and moisture content to t_0 and t_T (dimensionless). $f\ (\theta, t_0, t_T\ )$ is independent from the power applied. It reflects how T_{cum} evolves in time. e.g. For the geometry of the FO cable and soil employed in this work, and considering that $t_0 = t_T$, $f\ (\theta, t_0, t_T\ ) = t_0^{1.27}$ at saturation. This has been obtained by fitting a function to a numerical simulation of the heat response of a cable with the same geometry and thermal properties of the FO cable employed in this experiment, and with a surrounding material with the same thermal properties as the one observed in the soil column at saturation.

F_Q Limitations

To increase the expected quality factor index (F_Q) of the data in a field deployment, one can increase any of the nominator parameters or/and decreases any of the denominator parameters in Equation 4.10. Each of these eight parameters has either an upper (For Eq. 4.10 nominators) or lower (For Eq. 4.10 denominators) constraining value imposed by practical and economical considerations (see Table 4.6). For instance, an excessive power application in principle could cause water to evaporate and/or diffuse away from the heat source, i.e., the FO cable [*Farouki*, 1986]. The upper limit of P and t_0 will depend on:

- Cable physical properties, i.e., cable's dimension and thermal properties: The thinner the cable or larger the cable thermal conductivity is, the larger the thermal increase at the soil-cable interface will be expected and by consequence the higher the risk of observing water displacement from around the cable.

- Soil water content: For a similar P not only a higher temperature increase is expected at the soil-cable interface with decreasing soil water content, but also if some drying due to the previous heating may have occurred, hydraulic conductivity might be too low to redistribute the water back to original before the start of the next heating pulse.

It is noteworthy to indicate that for the range of soil moisture content (0.05-0.40m^3m^{-3}) observed in the soil column of the laboratory experiment, no signs of water displacement due to heating were detected for combinations of power intensity and heating duration ranging from 5 to 20 W and 1 to 2 minutes respectively.

L_M, H, and E depend mainly on the performance of the DTS unit employed, which is usually selected based on economical and/or logistical assessments. Note that E will increase with distance away from the DTS unit. E also depends on the quality of the sensing cable, i.e., a sensing cable with high light losses can degrade the measured signal.

Averaging through space and time will increase L_R, and N will basically increases the extent of measurement support and thus decreases observed variability due to the effect of averaging but nevertheless at the expense of feasible observation of features below this length scale (As discussed in section 4.2.1). Another method to increase N is to inject heat pulses at higher frequency while allowing enough cooling time between two consecutive heat pulses in order for pre-heat pulse conditions to reestablish (i.e., compute an hourly value of moisture content from the data arising from six pulses that were conducted on 10-minute intervals).

Increasing t_T will increase the total heat signal captured by the $f(\theta, t_0, t_T)$ function in [9]. When $t_T > t_0$, $f(\theta, t_0, t_T)$ will capture both the heating and the cooling signal of the heated cable. The additional signal captured during cooling will decrease with increasing t_T. In this case, it exists a value of t_T where the additional gain in $f(\theta, t_0, t_T)$ will be smaller than the additional noise added by the increasing reading time (that is adding up by the square root of time).

Table 4.6 Main limitations for the different parameters in the F_Q equation

F_Q Parameter	**Main Limitations**
P, t_0	Excessive heating may cause water displacement
L_M, E, H	Economical/logistical limitations due to the instrument
L_R	Reduced spatial information
t_T	Rate of change in T_{cum} with $t_T <$ instrument noise per second
N	Pre-heat pulse condition not reestablished between heating pulses

4.5 Conclusions

The results of the field testing showed that AHFO method is capable of capturing a complex spatial pattern of soil water content and soil water fluxes. Similar spatial patterns are challenging to depict using few measurements at the point scale. Larger scale measurements techniques, such as Cosmic-Ray probes and remote sensing, might be able to provide an average picture of the change in soil water content at a reasonable accuracy. Nevertheless, they will fail to capture all the important small scale processes observed in this experiment. The monitoring such small scale processes are of particular importance in irrigated agriculture (e.g. localized irrigation), and natural systems (e.g. preferential flows and contaminant transport).

The results showed that soil moisture contents and fluxes can be measured and monitored at a range of values (ranging from dry to saturated conditions) that is significantly larger than the <0.06 range $m^3 m^{-3}$ reported by *Weiss* [2003] and more informative than the qualitative “dry, wet or saturated” assessment reported by *Perzlmaier et al.* [2004; 2006]. This improvement is mainly due to the use of a data interpretation method (i.e. *The time integral of temperature deviation* developed by *Sayde et al.* [2010]) that is appropriate to the DTS method wherein precision of temperature reporting is a direct function of the interval of photon integration.

AHFO applications allow operator control over the heat signal that is injected into the soil. This is a significant advantage over the diurnal cycle driven heat signal employed by the passive distributed temperature sensing method for soil moisture estimation described by *Steele-Dunne et al*. [2010] i.e. A heat signal that can be significantly attenuated under several conditions (e.g. Increasing soil depth, under dense vegetative canopy, cloudy days, or other surface energy flux limited systems).

Laboratory experiments showed that the power intensity of the injected heat is 1:1 proportional to the T_{cum} response of the FO cable. This can be used to improve the quality of the measured data by accounting for fluctuation in power. The deviation from the 1:1 line can be used also as an indicator of water displacement due to overheating.

The calibration of the AHFO method remains challenging. A calibration method that is much less labor and time intensive than the one currently used in this experiment needs to be developed in order to allow practical application of the AHFO method. In principle, a possible alternative calibration procedure could be based on the theory that the calibration curves relating T_{cum} to θ should have a similar characteristic shape that is scalable to fit a particular soil by few measured T_{cum}-θ couples; similar to what is observed with the relationship between thermal conductivity and θ.

Error in soil water content estimates due to instrumentation was reduced considerably (from 0.07 to 0.02 m^3m^{-3} at saturation) when a DTS with better performance is employed in the laboratory experiment. This is due to the increase in the signal to noise ratio of measured T_{cum}. A quality factor index (F_Q) is introduced to quantify the impact of different design and operation decisions and their interactions on the signal to noise level.

4.6 References

Adamo, F., G. Andria, F. Attivissimo, and N. Giaquinto. 2004. An acoustic method for soil moisture measurement. *IEEE Trans. Instrum. Meas., 53*:891-898.

Arora, V.K., Chiew, F.H.S., and Grayson, R.B. 2001. Effect of sub-grid variability of soil moisture and precipitation intensity on surface runoff and streamflow. *J. Geophys. Res.* 106 (D15):17073–17091.

Aufleger, M., Conrad, M., Perzlmaier, S., and Porras, P. 2005. Improving a Fiber Optics tool for monitoring leakage. *Hydro Review Worldwide*, 13(4):18-23.

Bergkamp, G., Cammeraat, L.H., and Martinez-Fernandez, J. 1996. Water movement and vegetation patterns on shrubland and an abandoned field in two desertification-threatened areas in Spain. *Earth Surf. Proc.* 21:1073–1090.

Blöschl, G., and M. Sivapalan. 1995. Scale issues in hydrological modelling: a review. *Hydrological Processes* 9:251-290.

Bogena, H.R., J.A. Huisman, U. Rosenbaum, A. Weuthen, and H. Vereecken. 2008. Evaluation of the ZigBee based wireless soil moisture network SoilNet. *Proceedings of the joint workshop of DBG commissions I, VI and VIII*,May 29/30 2008 in Kiel, Germany.

Borga, M., Boscolo, P., Zanon, F., and Sangati, M. 2007. Hydrometeorological analysis of the August 29, 2003 flash flood in the eastern Italian Alps. *Journal of Hydrometeorology* 8 (5):1049–1067.

Campbell, G. S. 1985. Soil Physics with BASIC. Elsevier: New York.

Cardell-Oliver, R., Kranz, M., Smetten, K., and Mayer. 2005. A reactive soil moisture sensor network: design and field evaluation. *International Journal of Distributed Sensor Networks*, 1:149–162.

Cerda, A., 1995. Spatial distribution of infiltration on the matorral slopes in a Mediterranean environment, Genoves, Spain. In: Fantechi., R., Peter, D., Blabanis, P., Rubio, J.L. _Eds.., *Desertification in a European Context: Physical and Socio-economic Impacts. European Commission*, 427–436.

Cote, Jean, and Konrad, J.M. 2005. Thermal conductivity of base-course materials: *Canadian Geotechnical Journal*, 42:61-78.

Farouki, O.T. 1986. Thermal properties of soils. Series on rock and soil mechanics. Vol. 11. Trans Tech Publications, Clausthal-Zeller- feld, Germany.

Flury, M., Flüler, H., Jury, W.A., Leuenberger, J. 1994. Susceptibility of soils to preferential flow of water: a field study. *Water Resour. Res*. 30, 1945–1954.

Freifeld, B.M., Finsterle, S., Onstott, T.C., Toole, P., Pratt, M. 2008. Ground surface temperature reconstructions: Using in situ estimates for thermal conductivity acquired with a fiber-optic distributed thermal perturbation sensor. *Geophysical Research Letters*, 35, L14309, doi:10.1029/2008GL034762.

GeorgakakosK, . P., D.-H. Bae, and D. R. Cayan. 1995. H ydroclimatologoyf continental watersheds, 1, Temporal analyses. *Water Resour. Res*., 31(3), 655-675.

Grote, K., C. Anger, B. Kelly, S. Hubbard and Y. Rubin. 2010. Characterization of soil water content variability and soil texture using GPR ground wave techniques. *J. Environ. Eng. Geophys.*, 15: 93-110.

Imeson, A.C., Verstraten, J.M., van Mulligen, E.J., and Sevink, J. 1992. The effects of fire and water repellency on infiltration and runoff under Mediterranean type forest. *Catena* 19:345–361.

Johansen, O. 1975. Thermal conductivity of soils. Ph.D. thesis,University of Trondheim, Trondheim, Norway. US Army Corps ofEngineers, Cold Regions Research and Engineering Laboratory, Hanover, N.H. CRREL Draft English Translation 637.

López-Riquelmea, J.A., F. Sotoa, J. Suardíaza, P. Sáncheza and A. Iborraa. 2009. Wireless Sensor Networks for precision horticulture in Southern Spain. *Computers and Electronics in Agriculture.*, 68(1):25-35

Lu, H., Moran, C.J. and Prosser, I.P. 2006: Modeling sediment delivery ratio over the Murray Darling Basin. *Environmental Modeling and Software* 21:1297–308.

Mahmood. R. and Hubbard, K. G. 2007. Relationship between soil moisture of near surface and multiple depths of the root zone under heterogeneous land uses and varying hydroclimatic conditions. *Hydrological Processes* 21(25):3449-3462.

Mahmood R., A. Littell, K.G. Hubbard , J. You. 2012. Observed data-based assessment of relationships among soil moisture at various depths, precipitation, and temperature. *Applied Geography* 34:255-264

McInnes, K.J. 1981. Thermal conductivities of soils from dryland wheat regions of Eastern Washington. MS Thesis, Washington State Univ., Pullman, WA.

Michot, D., Y. Benderitter, A. Dorigny, B. Nicoullaud, D. King, and A. Tabbagh. 2003. Spatial and temporal monitoring of soil water content with an irrigated corn crop cover using surface electrical resistivity tomography. *Water Resour. Res. 39*:1138.

Neilson, B.T., C.E. Hatch and S.W. Tyler. 2010 .. Effects of solar radiative heating on fiber optic cables used in aquatic settings. doi:10.1029/2009WR008354. *Water Resources Res*.

Perzlmaier, S., Aufleger, M., and Conrad, M. 2004. Distributed fibre optic temperature measurements in hydraulic engineering. - Prospects of the heat-up method. In: Proceedings of the 72nd ICOLD Annual Meeting - Workshop on Dam Safety Problems and Solutions-Sharing Experience, Seoul, South Korea, May 16-22, 2004, Korean National Committee on Large Dams (KNCOLD), Seoul.

Perzlmaier, S., Straßer, K.-H., Strobl, Th., and Aufleger, M. 2006. Integral seepage monitoring on open channel embankment dams by the DFOT heat pulse method. 22nd ICOLD, Barcelona. Q. 86 – R. 12.

Porporato, A., Daly, E., and Rodríguez-Iturbe, I. 2004. Soil water balance and ecosystem response to climate change. *American Naturalist* 164 (5):625–633.

Raats, P.A.C. 2001. Developments in soil–water physics since the mid 1960s. *Geoderma* 100:355–387.

Robinson, D. A., C. S. Campbell, J. W. Hopmans, B. K. Hornbuckle, S. B. Jones, R. Knight, F. Ogden, J. Selker, and O. Wendroth. 2008. Soil moisture measurement for ecological and hydrological watershed-scale observatories: A review, Vadose Zone J., 7(1):358–389.

Sayde. C., C. Gregory, M. Gil-Rodriguez, N.Tufillaro, S. Tyler, N.van de Giesen, M. English, R. Cuenca, and J. Selker, 2010. Feasibility of soil moisture monitoring with heated fiber optics. *Water Resources Research*, 46, W06201, doi:10.1029/2009WR007846.

Selker, J.S., Thévenaz, L., Huwald, H., Mallet, A., Luxemburg, W., van de Giesen, N.,Stejskal, M., Zeman, J., Westhoff, M., and Parlange, M.B. 2006a. Distributed Fiber Optic Temperature Sensing for Hydrologic Systems. *Wat. Resour. Res.*, 42, W12202, doi:10.1029/2006WR005326.

Selker, J., N. van de Giesen, M. Westhoff, W. Luxemburg, and M. B. Parlange. 2006b. *Geophysical Research Letters*, 33, L24401, doi:10.1029/2006GL027979.

Schmugge, T. J. 1980. Effect of texture on microwave emission from soils. *IEEE Trans. Geosci. Remote Sens.*, GE-18:353-361.

SteelelDunne, S. C., M. M. Rutten, D. M. Krzeminska, M. Hausner, S. W.Tyler, J. S. Selker, T. A. Bogaard, and N. C. van de Giesen. 2010. Feasibility of soil moisture estimation using passive distributed temperature sensing, *Water Resour. Res*., 46, W03534, doi:10.1029/2009WR008272.

Sudduth, K.A., S.T. Drummond, N.R. Kitchen and K.A. Sudduth. 2001. Accuracy issues in electromagnetic induction sensing of soil electrical conductivity for precision agriculture. *Computers and Electronics in Agriculture., 31*:239–264.

Tarnawski V.R., Leong W.H. 2000. Thermal conductivity of soils at very low moisture content and moderate temperatures. Transport in Porous Media. 41(2):137-147.

Thomsen, A., K. Schelde, P. Droser and S. Flemming. 2007. A Mobile TDR for geo-referenced measurement of soil water content and electrical conductivity. *Precision Agric.*, 8:213-223.

Tyler, S., Burak, S., McNamara, J., Lamontagne, A., Dozier, J., and Selker, J. 2008. Spatially distributed temperatures at the base of two mountain snowpacks measured with Fiber Optic sensors. *I. J. Glaciology*. 54(187):673-679.

Tyler, S. W., J. S. Selker, M. B. Hausner, C. E. Hatch, T. Torgersen, C. E. Thodal, and G. Schladow. 2009. Environmental temperature sensing using raman spectra DTS fiber-optic methods. *Wat. Resour. Res*., doi:10.1029/2008WR007052.

USDA Natural Resources Conservation Service, accessed in 2006.

Vogt, T.; Philipp Schneider, Lisa Hahn-Woernle, Olaf A. Cirpka, Estimation of seepage rates in a losing stream by means of fiber-optic high-resolution vertical temperature profiling, *Journal of Hydrology*, Volume 380, Issues 1-2, 15 January 2010, Pages 154-164, ISSN 0022-1694, DOI: 10.1016/j.jhydrol.2009.10.033.

de Vries, D.A. 1952. A nonstationary method for determining thermal conductivity of soil in situ. *Soil Sci.*, 73:83-9.

de Vries, D.A. 1963. Thermal properties of soils. *Physics of Plant Environment*. Ed. W.R. Van Wijk., 210-35. North-Holland: Amsterdam.

Weiss, J. D. 2003. Using fiber optics to detect moisture intrusion into a landfill cap consisting of a vegetative soil barrier. *J. Air & Waste Manage. Assoc*., 53:1130-1148.

Western, A.W. and Blo¨schl, G. 1999. On the spatial scaling of soil moisture. *Journal of Hydrology* 217:203–224.

Western AW, Bl¨oschl G, Grayson RB. 2001. Towards capturing hydrologically significant connectivity in spatial patterns. *Water Resour. Res.* 37:83–97.

Western, A.W., R.B. Grayson, and G. Bloschl. 2002. Scaling of soil moisture: A hydrologic perspective. *Annu. Rev. Earth Planet. Sc.*, *30*:149-180.

Western, A.W., Grayson, R.B., Blöschl, G., and Wilson, D.J. 2003. Spatial variability of soil moisture and its implications for scaling. In: Perchepsky, Y., Selim, M., Radcliffe, A. (Eds.), Scaling Methods in Soil Physics. CRC Press, Boca Raton, 119–142.

Western, A.W., Zhou, S., Grayson, R.B., McMahon, T.A., Blöschl, G., Wilson, D.J. 2004. Spatial correlation of soil moisture in small catchments and its relationship to dominant spatial hydrological processes. *Journal of Hydrology*, 286:113–134.

Westhoff, M.C., Savenije, H. H. G., Luxemburg, W. M. J, Stelling, G. S., van de Giesen, N. C., Selker, J. S., Pfister, L., and Uhlenbrook, S. 2007. A distributed stream temperature model using high resolution temperature observations. *Hydrol. Earth Syst. Sci.*, 11:1469–1480.

Wilson, J.D., Western, A.W., and Grayson, R.B., 2004. Identifying and quantifying sources of variability in temporal and spatial soil moisture observations. *Water Resources Research* 40, W02507.

Zreda, M., D. Desilets, T. P. A. Ferré, and R. L. Scott. 2008. Measuring soil moisture content non-invasively at intermediate spatial scale using cosmic-ray neutrons. *Geophys. Res. Lett.*, 35, L21402.

5. General Conclusions and Future Directions

The objectives of this research were to characterize and reduce the uncertainty associated with determination of spatially variable soil moisture conditions. These objectives were to be achieved using two approaches: 1) by implicitly accounting for spatial variability using a Bayesian decision model, and 2) by explicitly measuring spatial variability using the Actively Heated Fiber Optic (AHFO) method.

The content of this research was presented in three core chapters. First, Chapter 2 discussed a concept approach of using a Bayesian decision model to integrate information embodied in estimates of soil water depletion generated from an ET based model with the information obtained from soil moisture measurements in the field to derive a posterior estimation of soil water status that has the potential to provide a better basis for irrigation decisions. Second, Chapter 3 presented the feasibility analysis of implementation of a new and simple interpretation of heat data to retrieve high resolution soil water content along Fiber Optic cable using the AHFO method.
Third, Chapter 4 presented the field testing methodology and results of the AHFO method.

For the Bayesian decision model, insights derived from the analysis lead to an important general conclusion, that scientific irrigation scheduling can be made more effective by explicitly accounting for the uncertainties of both ET estimates and soil water determinations.

Additionally, the results showed that:

- Analytical tools for irrigation scheduling need not only estimate the most probable levels of depletion; they must also quantify the uncertainties of such predictions.
- Uncertainty in field scale estimates of soil water conditions derived from measurements can be substantially large. For the specific case of the numerical example, 37% of the measurements were located outside the ± 50% of the average range. The task of quantifying such uncertainty may be challenging.

The feasibility analysis showed that the AHFO method became feasible for determination of soil water content across a much broader range of values than previously reported using a response metric that has not been previously employed: the time integral of temperature deviation.

The key finding of the feasibility analysis is to confirm the potential to employ DTS systems to monitor soil water content at temporal resolutions well under one hour and at high spatial resolution (≤ 1 m). In principle, this DTS method could monitor soil moisture along cables exceeding several km in extent. This would allow for concurrent observation of thousands of adjacent locations, which will likely provide new insights into the spatial structure of infiltration and evaporation.

Additional work is required to develop optimal heating and interpretation strategies for DTS-based heat pulse methods, building upon the rich literature related to needle heat pulse systems

The results of the field testing showed that AHFO method is capable of capturing a complex spatial pattern of soil water content and soil water fluxes.

Laboratory experiments showed that the power intensity of the injected heat is 1:1 proportional to the T_{cum} response of the FO cable. This can be used to improve the quality of the measured data by accounting for fluctuation in power. The deviation from the 1:1 line can be used also as an indicator of water displacement due to overheating.

Future directions for the Bayesian decision model:

Several simplifying assumptions are used in the development of the Bayesian decision model; assumptions such the normality and statistical independencies of the different parameters in the model. Further studies are recommended to investigate and account for possible divergences in the assumptions.

There are additional sources of information that could be integrated in this analysis to provide additional insights on the status of soil moisture depletion in the field. In specific, we would expect that most experienced farmers could judge how representative is a particular measurement location to the soil moisture depletion status observed across a particular field. In principle such additional information could be easily adaptable in the model when using a model that explicitly account for spatial variability in the field (e.g. IMO). This will allow generating a prior and a posterior distribution that reflects defined conditions in the field (e.g. driest 25%, average, wettest 25%, etc…). Another advantage of including such information is that it will allow additional flexibility for decision makers to adapt wide range of irrigation scheduling strategies instead of targeting the average condition in the field as the current version of the model suggests.

Future directions for the AHFO model:

The calibration of the AHFO method remains challenging. A calibration method that is much less labor and time intensive than the one currently used in this experiment needs to be developed in order to allow practical application of the AHFO method. In theory, curves relating T_{cum} to soil water content should have a same basic shape. This suggests that calibration curves for different soil types could be scaled from one reference curve using couple of measurements in the field. Field demonstration of this methodology is required in future work.

In the AHFO method, the errors in soil water content estimates due instrumentation and operation can be reduced by increasing the signal-to-noise ratio of T_{cum} readings. The design and operation of the FO system can be specifically optimized to meet the specific output resolution requirements in all three dimensions: time, space, and accuracy. This is can be achieved by economically optimizing a Quality Factor Index (F_Q), that is presented in this thesis, under a set of constraining values for the eight different interacting parameters that are used to calculate F_Q. Those parameters are: the power intensity applied, the DTS temperature reading error per temperature reading cycle, the spatial resolution of the temperature readings, the DTS spatial resolution, the rate at which the DTS soil water is measured, the DTS temperature reading frequency, the heat pulse duration, and the total T_{cum} reading duration. Future studies should focus on defining the constraining values of the eight parameters described above. In addition, the geometry and components of the FO sensing cable are known to affect the signal-to-noise ratio of T_{cum} readings. The design of the FO cable sensors should be optimized for the soil moisture measurement application.

BIBLIOGRAPHY

Abourached, C., C. Hillyer, C. Sayde, M. English, and J. Bosch. 2007. A web-based advisory service for optimum irrigation management. *ASABE* Paper No. 072253. Minneapolis, MN.: ASABE.

Adamo, F., G. Andria, F. Attivissimo, and N. Giaquinto. 2004. An acoustic method for soil moisture measurement. *IEEE Trans. Instrum. Meas.*, *53*:891-898.

Arora, V.K., Chiew, F.H.S., and Grayson, R.B. 2001. Effect of sub-grid variability of soil moisture and precipitation intensity on surface runoff and streamflow. *J. Geophys. Res.* 106 (D15):17073–17091.

Aufleger, M., Conrad, M., Perzlmaier, S., and Porras, P. 2005. Improving a Fiber Optics Tool for Monitoring Leakage. *Hydro Review Worldwide*, 13(4):18-23.

Bergkamp, G., Cammeraat, L.H., and Martinez-Fernandez, J. 1996. Water movement and vegetation patterns on shrubland and an abandoned field in two desertification-threatened areas in Spain. *Earth Surf. Proc.* 21:1073–1090.

Blackwell, J. H. 1954. A transient-flow method for determination of thermal constants of insulating materials in bulk. *J. Appl. Phys.*, 25:137–144.

Blöschl, G., and M. Sivapalan. 1995. Scale issues in hydrological modelling: a review. *Hydrological Processes* 9:251-290.

Bogena, H.R., J.A. Huisman, U. Rosenbaum, A. Weuthen, and H. Vereecken. 2008. Evaluation of the ZigBee based wireless soil moisture network SoilNet. *Proceedings of the joint workshop of DBG commissions I, VI and VIII*,May 29/30 2008 in Kiel, Germany.

Borga, M., Boscolo, P., Zanon, F., and Sangati, M. 2007. Hydrometeorological analysis of the August 29, 2003 flash flood in the eastern Italian Alps. *Journal of Hydrometeorology* 8 (5):1049–1067.

Bristow, K. L., Campbell, G. S., and Calissendorff, C. 1993. Test of a heat-pulse probe for measuring changes in soil water content. *Soil Sci. Soc. Am. J.,* 57:930-4.

Bristow, K. L., R. D. White, and G. J. Kluitenberg. 1994. Comparison of single and dual probes for measuring soil thermal properties with transient heating. *Australian Journal of Soil Research,* 32:447-464.

Bristow, K. L. 1998. Measurement of thermal properties and water content of unsaturated sandy soil using dual-probe heat-pulse probes. *Agricultural and Forest Meteorology*, 89:75-84.

Bristow, K.L., G.J.Kluitenberg, C.J.Goding, and T.S. Fitzgerald. 2001. A small multi-sensor probe for measuring soil thermal properties, water content and electrical conductivity. *Comput. Electron. Agric.*, 31:265–280.

Campbell, G. S. 1985. Soil Physics with BASIC. Elsevier: New York.

Campbell, G. S., Calissendorff, K., and Williams, J. H. 1991. Probe for measuring soil specific heat using a heat-pulse method. *Soil Sci. Soc. Am. J*., 55: 291-293.

Carslaw, H.S. and Jaeger, J.C., Conduction of Heat in Solids, Oxford Univ. Press, NJ, 1959, pp. 262.

Cardell-Oliver, R., Kranz, M., Smetten, K., and Mayer. 2005. A reactive soil moisture sensor network: design and field evaluation. *International Journal of Distributed Sensor Networks,* 1:149–162.

Cerda, A., 1995. Spatial distribution of infiltration on the matorral slopes in a Mediterranean environment, Genoves, Spain. In: Fantechi., R., Peter, D., Blabanis, P., Rubio, J.L. _Eds.., *Desertification in a European Context: Physical and Socio-economic Impacts. European Commission*, 427–436.

Charlesworth, P. 2005. Soil water monitoring. Irrigation Insights No. 1, CSIRO. Land & Water Australia (2nd Edition) 96p.

Coleman, T.F. and Y. Li. 1996. An Interior, Trust Region Approach for Nonlinear Minimization Subject to Bounds, *SIAM Journal on Optimization*, 6:418-445.

Cote, Jean, and Konrad, J.M. 2005. Thermal conductivity of base-course materials: *Canadian Geotechnical Journal*, 42:61-78.

Debaeke, P., Aboudrare, A., 2004. Adaptation of crop management to water-limited environments. *Eur. J. Agron*. 21:433–446.

English, M. 1981. The uncertainty of crop models in irrigation optimization. *Agricultural Water Management* 32(1):1-14.

English, M., 1990. Deficit irrigation. I. Analytical framework. *J. Irrig. Drain E. ASCE* 116 :399–412

English, M. and Orlob, G. 1978. Decision theory applications and irrigation optimization. Technical Completion report Contribution No. 174, University of California

English, M. and S. Navaid Raja. 1996. Perspectives on deficit irrigation. *Transactions of the American Society of Agricultural Engineers* 24(4): 917–921 and 928.

English, M. J., K. H. Solomon, and G. J. Hoffman. 2002. A paradigm shift in irrigation management. *Journal of Irrigation and Drainage Engineering* 128(5):267-277.

English, M., C. Sayde, A. Gitelman, and L. Khoury. 2008. A feedback system to optimize crop water use estimates in irrigation scheduling. In *World Environmental & Water Resources Congress*, May 13-16, 2008, Honolulu, Hawaii

Farouki, O.T. 1986. Thermal properties of soils. Series on rock and soil mechanics. Vol. 11. Trans Tech Publications, Clausthal-Zeller- feld, Germany.

Fereres, E., and M. A. Soriano. 2006. Deficit irrigation for reducing agricultural water use. *Journal of Experimental Botany* 58(2):147-159, doi:10.1093/jxb/erl165.

Fereres E, Goldhamer DA, Parsons LR. 2003. Irrigation water management of horticultural crops. Historical review compiled for the American Society of Horticultural Science's 100th Anniversary. *HortScience*, 38:1036-1042.

Flury, M., Flüler, H., Jury, W.A., Leuenberger, J. 1994. Susceptibility of soils to preferential flow of water: a field study. *Water Resour. Res*. 30:1945–1954.

Freifeld, B.M., Finsterle, S., Onstott, T.C., Toole, P., Pratt, M. 2008. Ground surface temperature reconstructions: Using in situ estimates for thermal conductivity acquired with a fiber-optic distributed thermal perturbation sensor. *Geophysical Research Letters,* Vol. 35, L14309, doi:10.1029/2008GL034762.

Geerts, S., and D. Raes. 2009. Deficit irrigation as an on-farm strategy to maximize crop water productivity in dry areas. *Agricultural Water Management* 96(9):1275-1284, doi: 10.1016/j.agwat.2009.04.009

GeorgakakosK, . P., D.-H. Bae, and D. R. Cayan. 1995. H ydroclimatologoyf continental watersheds, 1, Temporal analyses. *Water Resour. Res*., 31(3):655-675.

Grattan, K.T.L. and Sun T. 2000. Fiber optic sensor technology: an overview. *Sens. Actuat. A.*, 82:40-61.

Green, S., B. Clothier, and Jardine B. 2003, Theory and Practical Application of Heat Pulse to Measure Sap Flow, *Agron. J.*, *95*(6):1371-1379.

Grote, K., C. Anger, B. Kelly, S. Hubbard and Y. Rubin. 2010. Characterization of soil water content variability and soil texture using GPR ground wave techniques. *J. Environ. Eng. Geophys.*, 15:93-110.

Haverkamp, R., M. Vauclin, and G. Vachaud. 1984. Error analysis in estimating soil water content from neutron probe measurements. 1. Local standpoint. *Soil Sci.* 137: 78–90

Heitman, J. L., J. M. Basinger, G. J. Kluitenberg, J. M. Ham, J. M. Frank and P. L. Barnes. 2003. Field Evaluation of the Dual-Probe Heat-Pulse Method for Measuring Soil Water Content. *Vadose Zone J.*, 2:552-560.

Hillyer C., English M., Sayde C., Hutchinson K., and Busch J. 2009. A Web-Based Advisory Service For Optimum Irrigation Management. World Environmental & Water Resources Congress, *ASCE*, Kansas City, MO.

Hillyer C., and Robinson P. 2010. Envisioning The Next Generation Of Irrigation Schedulers. 5th National Decennial Irrigation Conference Proceedings, *ASABE*, St. Joseph, Michigan, Phoenix, Arizona.

Hopmans, J. W., J. Simunek, and K. L. Bristow. 2002. Indirect estimation of soil thermal properties and water flux using heat pulse probe measurements: Geometry and dispersion effects. *Wat. Resour. Res.* 38(1), DOI 10.1029/2000WR000071.

Hupet, F., P. Bogaert, and M. Vanclooster. 2004. Quantifying the local scale uncertainty of estimated actual evapotranspiration. *Hydrol. Processes* 18:3415–3434, doi:10.1002/hyp.1504.

Imeson, A.C., Verstraten, J.M., van Mulligen, E.J., and Sevink, J. 1992. The effects of fire and water repellency on infiltration and runoff under Mediterranean type forest. *Catena* 19:345–361.

Jaeger, J. C. 1965. Application of the theory of heat conduction to geothermal measurements. In 'Terrestrial Heat Flow.' (Ed. W. H. K. Lee.) *American Geophysical Union Monograph*, 8:7-23.

Johansen, O. 1975. Thermal conductivity of soils. Ph.D. thesis,University of Trondheim, Trondheim, Norway. US Army Corps ofEngineers, Cold Regions Research and Engineering Laboratory, Hanover, N.H. CRREL Draft English Translation 637.

Kluitenberg, G. J., Ham, J. M., and Bristow, K. L. 1993. Error analysis of the heat pulse method for measuring soil volumetric heat capacity. *Soil Sci. Soc. Am. J.*, 57:1444-1451.

Kluitenberg, G. J., Ochsner, T. E., and Horton, R. 2007. Improved Analysis of Heat Pulse Signals for Soil Water Flux Determination, *Soil Sci. Soc. Am. J.*, *71*(1): 53-55.

Larson, T. H. 1988. Thermal measurement of soils using a multineedle probe with a pulsed point-source. *Geophysics*, 53:266-70.

López-Riquelmea, J.A., F. Sotoa, J. Suardíaza, P. Sáncheza and A. Iborraa. 2009. Wireless Sensor Networks for precision horticulture in Southern Spain. *Computers and Electronics in Agriculture.*, 68(1):25-35

Lu, H., Moran, C.J. and Prosser, I.P. 2006: Modeling sediment delivery ratio over the Murray Darling Basin. Environmental Modeling and Software 21:1297–308.

Lubimova, H. A., Lusova, L. M., Firsov, F. V., Starikova, G. N. and Shushpanov, A. P. 1961. Determination of surface heat flow in Mazesta (USSR*). Annali di Geophys.* XIV, 157-167.

Mori, Y., Hopmans, J. W., Mortensen, A. P., and Kluitenberg, G. J. 2003, Multi-Functional Heat Pulse Probe for the Simultaneous Measurement of Soil Water Content, Solute Concentration, and Heat Transport Parameters, *Vadose Zone J.*, 2(4): 561-571.

Mahmood. R. and Hubbard, K. G. 2007. Relationship between soil moisture of near surface and multiple depths of the root zone under heterogeneous land uses and varying hydroclimatic conditions. *Hydrological Processes* 21(25):3449-3462.

Mahmood R., A. Littell, K.G. Hubbard , J. You. 2012. Observed data-based assessment of relationships among soil moisture at various depths, precipitation, and temperature. *Applied Geography* 34:255-264

McInnes, K.J. 1981. Thermal conductivities of soils from dryland wheat regions of Eastern Washington. MS Thesis, Washington State Univ., Pullman, WA.

Michot, D., Y. Benderitter, A. Dorigny, B. Nicoullaud, D. King, and A. Tabbagh. 2003. Spatial and temporal monitoring of soil water content with an irrigated corn crop cover using surface electrical resistivity tomography. *Water Resour. Res.* 39:1138.

Mori, Y., Hopmans, J. W., Mortensen, A. P., and Kluitenberg, G. J. 2005. Estimation of Vadose Zone Water Flux from Multi-Functional Heat Pulse Probe Measurements, *Soil Sci. Soc. Am. J.*, 69(3):599-606.

Mortensen, A.P., Hopmans, J.W., Mori, Y., and Simunek, J. 2006. Multi-functional heat pulse probe measurements of coupled vadose zone flow and transport. *Adv. Water Resour.* 29:250–267.

Neilson, B.T., C.E. Hatch and S.W. Tyler. 2010 .. Effects of solar radiative heating on fiber optic cables used in aquatic settings. doi:10.1029/2009WR008354. *Water Resources Res*.

Olmanson, O.K., and Ochsner, T.E. 2006. Comparing ambient temperature effects on heat pulse and time domain reflectometry soil water content measurements. *Vadose Zone J.*, 5:751–756.

Perzlmaier, S., Aufleger, M., and Conrad, M. 2004. Distributed fibre optic temperature measurements in hydraulic engineering. - Prospects of the heat-up method. In: Proceedings of the 72nd ICOLD Annual Meeting - Workshop on Dam Safety Problems and Solutions-Sharing Experience, Seoul, South Korea, May 16-22, 2004, Korean National Committee on Large Dams (KNCOLD), Seoul.

Perzlmaier, S., Straßer, K.-H., Strobl, Th., and Aufleger, M. 2006. Integral Seepage Monitoring on Open Channel Embankment Dams by the DFOT Heat Pulse Method. 22nd ICOLD, Barcelona. Q. 86 – R. 12.

Porporato, A., Daly, E., and Rodríguez-Iturbe, I. 2004. Soil water balance and ecosystem response to climate change. *American Naturalist* 164 (5):625–633.

Raats, P.A.C. 2001. Developments in soil–water physics since the mid 1960s. *Geoderma* 100:355–387.

Ren, T., Kluitenberg, G. J., and Horton, R. 2000. Determining soil water flux and pore water velocity by a heat pulse technique. *Soil Sci. Soc. Am. J.,* 64:552-560.

Ren, T., T. Y. Ochsner and R. Horton. 2003. Development of Termo-Time Domain Reflectometry for Vadose Zone Measurements. *Vadose Zone J.*, 2:544-551.

Ren, T., Z. Ju, Y Gong and R. Horton. 2005. Comparing Heat-Pulse and Time Domain Reflectometry Soil Water Contents from Thermo-Time Domain Reflectometry Probes. *Vadose Zone J.*, 4:1080-1086.

Robinson, D. A., C. S. Campbell, J. W. Hopmans, B. K. Hornbuckle, S. B. Jones, R. Knight, F. Ogden, J. Selker, and O. Wendroth. 2008. Soil moisture measurement for ecological and hydrological watershed-scale observatories: A review, Vadose Zone J., 7(1):358–389.

Sayde. C., C. Gregory, M. Gil-Rodriguez, N.Tufillaro, S. Tyler, N.van de Giesen, M. English, R. Cuenca, and J. Selker, 2010. Feasibility of soil moisture monitoring with heated fiber optics. *Water Resources Research*, 46, W06201, doi:10.1029/2009WR007846.

Sayde, C., L. Khoury, A. Gitelman, and M. English. 2008. Optimizing estimates of soil moisture for irrigation scheduling. *ASABE* Paper No. 084699. St. Joseph, MI.

Schmitz, M., and H. Sourell. 2000. Variability in soil moisture measurements. *Irrigation Science*, 19, 147–151.

Selker, J.S., Thévenaz, L., Huwald, H., Mallet, A., Luxemburg, W., van de Giesen, N.,Stejskal, M., Zeman, J., Westhoff, M., and Parlange, M.B. 2006a. Distributed Fiber Optic Temperature Sensing for Hydrologic Systems. *Wat. Resour. Res.,* 42, W12202, doi:10.1029/2006WR005326.

Selker, J., N. van de Giesen, M. Westhoff, W. Luxemburg, M. B. Parlange. 2006b. *Geophysical Research Letters*, 2006, 33, L24401, doi:10.1029/2006GL027979.

Shaw, B. and L.D. Baver. 1940. An electrothermal method for following moisture changes on the soil in situ. Proc. Soil Sci. Soc. Am. 4:78-83.

Shiozawa, S., and G.S. Campbell. 1990. Soil thermal conductivity. *Remote Sens. Rev.,* 5:301–310.

Schmugge, T. J. 1980. Effect of texture on microwave emission from soils. *IEEE Trans. Geosci. Remote Sens.,* GE-18:353-361.

Steele, D. D., T. F. Scherer, L. D. Prunty, and E. C. Stegman. 1997. Water balance irrigation scheduling: Comparing crop curve accuracies and determining the frequency of corrections to soil moisture estimates. *Trans. ASAE* 13(5): 599-599.

Steele-Dunne, S. C., M. M. Rutten, D. M. Krzeminska, M. Hausner, S. W. Tyler, J. S. Selker, T. A. Bogaard, and N. C. van de Giesen. 2009 Feasibility of Soil Moisture Estimation using Passive Distributed Temperature Sensing. *Water Resour. Res.*, doi:10.1029/2009WR008272.

Sudduth, K.A., S.T. Drummond, N.R. Kitchen and K.A. Sudduth. 2001. Accuracy issues in electromagnetic induction sensing of soil electrical conductivity for precision agriculture. *Computers and Electronics in Agriculture., 31*:239–264.

Tarara, J. M., and J. M. Ham. 1997. Measuring soil water content in the laboratory and field with dual-probe heat-capacity sensors. *Agronomy Journal*, 89:535-542.

Tarnawski V.R., Leong W.H. 2000. Thermal conductivity of soils at very low moisture content and moderate temperatures. *Transport in Porous Media*, 41(2):137-147.

Thomsen, A., K. Schelde, P. Droser and S. Flemming. 2007. A Mobile TDR for geo-referenced measurement of soil water content and electrical conductivity. *Precision Agric.*, 8:213-223.

Tyler, S., Burak, S., McNamara, J., Lamontagne, A., Dozier, J., Selker, J. 2008. Spatially Distributed Temperatures at the Base of Two Mountain Snowpacks Measured with Fiber Optic Sensors. *I. J. Glaciology*. 54(187):673-679.

Tyler, S. W., J. S. Selker, M. B. Hausner, C. E. Hatch, T. Torgersen, C. E. Thodal, and G. Schladow. 2009. Environmental Temperature Sensing using Raman Spectra DTS Fiber-Optic Methods. *Wat. Resour. Res*., doi:10.1029/2008WR007052.

de Vries, D.A. 1952. A nonstationary method for determining thermal conductivity of soil in situ. *Soil Sci.*, 73:83-9.

Vogt, T.; Philipp Schneider, Lisa Hahn-Woernle, Olaf A. Cirpka. 2010. Estimation of seepage rates in a losing stream by means of fiber-optic high-resolution vertical temperature profiling. *Journal of Hydrology*, 380(1-2)154-164.

de Vries, D A., and Peck, A. J. 1958. On the cylindrical probe method of measuring thermal conductivity with special reference to soils. Part 1. Extension of theory and discussion of probe characteristics. *Aust. J. Phys.*, 11: 255-71.

de Vries, D.A. 1963. Thermal properties of soils. Physics of Plant Environment. Ed. W.R. Van Wijk. pp. 210-35. North-Holland: Amsterdam.

Weiss, J. D. 2003. Using Fiber Optics to Detect Moisture Intrusion into a Landfill Cap Consisting of a Vegetative Soil Barrier. *J. Air & Waste Manage. Assoc*., 53:1130-1148.

Western, A.W. and Blo¨schl, G. 1999. On the spatial scaling of soil moisture. *Journal of Hydrology* 217:203–224.

Western AW, Bl¨oschl G, Grayson RB. 2001. Towards capturing hydrologically significant connectivity in spatial patterns. *Water Resour. Res.* 37:83–97.

Western, A.W., R.B. Grayson, and G. Bloschl. 2002. Scaling of soil moisture: A hydrologic perspective. *Annu. Rev. Earth Planet. Sc.*, *30*:149-180.

Western, A.W., Grayson, R.B., Blöschl, G., and Wilson, D.J. 2003. Spatial variability of soil moisture and its implications for scaling. In: Perchepsky, Y., Selim, M., Radcliffe, A. (Eds.), Scaling Methods in Soil Physics. CRC Press, Boca Raton, 119–142.

Western, A.W., Zhou, S., Grayson, R.B., McMahon, T.A., Blöschl, G., Wilson, D.J. 2004. Spatial correlation of soil moisture in small catchments and its relationship to dominant spatial hydrological processes. *Journal of Hydrology*, 286:113–134.

Westhoff, M.C., Savenije, H. H. G., Luxemburg, W. M. J, Stelling, G. S., van de Giesen, N. C., Selker, J. S., Pfister, L., and Uhlenbrook, S. 2007. A distributed stream temperature model using high resolution temperature observations. *Hydrol. Earth Syst. Sci.*, 11:1469–1480.

Wilson, J.D., Western, A.W., and Grayson, R.B. 2004. Identifying and quantifying sources of variability in temporal and spatial soil moisture observations. *Water Resources Research* 40, W02507.

Youngs, E.G. 1956. A laboratory method of following moisture content changes. Trans. 6th Int. Congr. Soil Sci., Paris I: 89-93.

Zreda, M., D. Desilets, T. P. A. Ferré, and R. L. Scott. 2008. Measuring soil moisture content non-invasively at intermediate spatial scale using cosmic-ray neutrons. *Geophys. Res. Lett.*, 35, L21402.

APPENDICES

APPENDIX A - CALCULATION OF THE POSTERIOR DISTRIBUTIONS OF THE SOIL WATER DEPLETION AT A PARTICULAR LOCATION IN THE FIELD

Using Bayes rule to combine the data distribution $p(D_i \mid \delta_i, \sigma_{Di}^2)$ and the prior distribution $p(\delta_i \mid m, s^2, \alpha^2)$, the posterior distribution of the true soil water depletion at a particular location in the field (δ_i) is given up to a constant of proportionality as:

$$p(\delta_i \mid D_i, m, \sigma_{Di}^2, s^2, \alpha^2) \propto p(\delta_i \middle| m, s^2, \alpha^2) \times p(D_i \mid \delta_i, \sigma_{Di}^2)$$

$$p(\delta_i \mid D_i, m, \sigma_{Di}^2, s^2, \alpha^2) \propto \frac{1}{\sqrt{2\pi(s^2+\alpha^2)}} \exp\left[-\frac{1}{2(s^2+\alpha^2)}(\delta_i - m)\right] \times \frac{1}{\sqrt{2\pi\sigma_{Di}^2}} \exp\left[-\frac{1}{2\sigma_{Di}^2}(D_i - \delta_i)^2\right]$$

$$\propto \exp\left[-\frac{1}{2(s^2+\alpha^2)}(\delta_i - m)^2\right] \times \left[\exp[-\frac{1}{2\sigma_{Di}^2}(D_i - \delta_i)^2\right]$$

$$= \exp\left[-\frac{1}{2(s^2+\alpha^2)}(\delta_i{}^2 - 2\delta_i m + m^2) - \frac{1}{2\sigma_{Di}^2}(D_i{}^2 - 2D_i\delta_i + \delta_i{}^2)\right]$$

$$= \exp\left[-\frac{1}{2(s^2+\alpha^2)\sigma_{Di}^2}\left[\sigma_{Di}^2\delta_i{}^2 - 2\sigma_{Di}^2\delta_i m + \sigma_{Di}^2 m^2 - (s^2+\alpha^2)D_i{}^2 + 2(s^2+\alpha^2)D_i\delta_i + (s^2+\alpha^2)\delta_i{}^2\right]\right]$$

$$= \exp\left[-\frac{1}{2(s^2+\alpha^2)\sigma_{Di}^2}[\delta_i{}^2(\sigma_{Di}^2 + (s^2+\alpha^2)) - 2\delta_i(\sigma_{Di}^2 m + (s^2+\alpha^2)D_i) + (\sigma_{Di}^2 m^2 - (s^2+\alpha^2)D_i{}^2)]\right]$$

$$\propto \exp\left[-\frac{1}{2(s^2+\alpha^2)\sigma_{Di}^2}[\delta_i{}^2(\sigma_{Di}^2 + (s^2+\alpha^2)) - 2\delta_i(\sigma_{Di}^2 m + (s^2+\alpha^2)D_i)]\right]$$

$$= \exp\left[-\frac{1}{2}\left[\delta_i{}^2\left(\frac{1}{(s^2+\alpha^2)}+\frac{1}{\sigma_{Di}^2}\right)-2\delta_i\left(\frac{m}{(s^2+\alpha^2)}+\frac{D_i}{\sigma_{Di}^2}\right)\right]\right]$$

$$= \exp\left[-\frac{1}{2}\left(\frac{1}{(s^2+\alpha^2)}+\frac{1}{\sigma_{Di}^2}\right)\left[\frac{\delta_i{}^2\left(\frac{1}{(s^2+\alpha^2)}+\frac{1}{\sigma_{Di}^2}\right)}{\left(\frac{1}{(s^2+\alpha^2)}+\frac{1}{\sigma_{Di}^2}\right)}-\frac{2\delta_i\left(\frac{m}{(s^2+\alpha^2)}+\frac{D_i}{\sigma_{Di}^2}\right)}{\left(\frac{1}{(s^2+\alpha^2)}+\frac{1}{\sigma_{Di}^2}\right)}\right]\right]$$

$$= \exp\left[-\frac{1}{2}\left(\frac{1}{(s^2+\alpha^2)}+\frac{1}{\sigma_{Di}^2}\right)\left[\delta_i{}^2-\frac{2\delta_i\left(\frac{m}{(s^2+\alpha^2)}+\frac{D_i}{\sigma_{Di}^2}\right)}{\left(\frac{1}{(s^2+\alpha^2)}+\frac{1}{\sigma_{Di}^2}\right)}\right]\right]$$

$$= \exp\left[-\frac{1}{2}\left(\frac{1}{(s^2+\alpha^2)}+\frac{1}{\sigma_{Di}^2}\right)\left[\delta_i{}^2-\frac{2\delta_i\left(\frac{m}{(s^2+\alpha^2)}+\frac{D_i}{\sigma_{Di}^2}\right)}{\left(\frac{1}{(s^2+\alpha^2)}+\frac{1}{\sigma_{Di}^2}\right)}\right]+\left(\frac{\left(\frac{m}{(s^2+\alpha^2)}+\frac{D_i}{\sigma_{Di}^2}\right)}{\left(\frac{1}{(s^2+\alpha^2)}+\frac{1}{\sigma_{Di}^2}\right)}\right)^2-\left(\frac{\left(\frac{m}{(s^2+\alpha^2)}+\frac{D_i}{\sigma_{Di}^2}\right)}{\left(\frac{1}{(s^2+\alpha^2)}+\frac{1}{\sigma_{Di}^2}\right)}\right)^2\right]$$

$$= \exp\left[-\frac{1}{2}\left(\frac{1}{(s^2+\alpha^2)}+\frac{1}{\sigma_{Di}^2}\right)\left[\delta_i{}^2 - \frac{2\delta_i\left(\frac{m}{(s^2+\alpha^2)}+\frac{D_i}{\sigma_{Di}^2}\right)}{\left(\frac{1}{(s^2+\alpha^2)}+\frac{1}{\sigma_{Di}^2}\right)}\right]+\left(\frac{\left(\frac{m}{(s^2+\alpha^2)}+\frac{D_i}{\sigma_{Di}^2}\right)}{\left(\frac{1}{(s^2+\alpha^2)}+\frac{1}{\sigma_{Di}^2}\right)}\right)^2\right]\exp\left[-\left(\frac{\left(\frac{m}{(s^2+\alpha^2)}+\frac{D_i}{\sigma_{Di}^2}\right)}{\left(\frac{1}{(s^2+\alpha^2)}+\frac{1}{\sigma_{Di}^2}\right)}\right)^2\right]$$

$$\propto \exp\left[-\frac{1}{2}\left(\frac{1}{(s^2+\alpha^2)}+\frac{1}{\sigma_{Di}^2}\right)\left[\delta_i{}^2 - \frac{2\delta_i\left(\frac{m}{(s^2+\alpha^2)}+\frac{D_i}{\sigma_{Di}^2}\right)}{\left(\frac{1}{(s^2+\alpha^2)}+\frac{1}{\sigma_{Di}^2}\right)}\right]+\left(\frac{\left(\frac{m}{(s^2+\alpha^2)}+\frac{D_i}{\sigma_{Di}^2}\right)}{\left(\frac{1}{(s^2+\alpha^2)}+\frac{1}{\sigma_{Di}^2}\right)}\right)^2\right]$$

$$= \exp\left[-\frac{1}{2}\left(\frac{1}{(s^2+\alpha^2)}+\frac{1}{\sigma_{Di}^2}\right)\left(\delta_i - \frac{\left(\frac{m}{(s^2+\alpha^2)}+\frac{D_i}{\sigma_{Di}^2}\right)}{\left(\frac{1}{(s^2+\alpha^2)}+\frac{1}{\sigma_{Di}^2}\right)}\right)^2\right]$$

Thus,

$$P\left(\hat{\delta}_i \middle| D_i, m, s^2, \alpha^2\right) \sim N\left(\hat{\delta}_i, \hat{\sigma}^2_{\hat{\delta}i}\right)$$

where:

$$\hat{\delta}_i = \frac{\dfrac{m}{s^2+\alpha^2} + \dfrac{D_i}{\sigma^2_{Di}}}{\dfrac{1}{s^2+\alpha^2} + \dfrac{1}{\sigma^2_{Di}}}$$

and

$$\frac{1}{\hat{\sigma}^2_{\hat{\delta}i}} = \frac{1}{s^2+\alpha^2} + \frac{1}{\sigma^2_{Di}}$$

δ_i is the true soil water depletion at a particular location (*i*) in the field,
D_i is the measured soil water depletion at location (*i*),
$\sigma_{Di}{}^2$ is the error/uncertainty of this particular measurement of soil water depletion at location (*i*),
m is the prior for the true field-average soil water depletion (ω),
s^2 is the prior for true variance of soil water depletion in the field (τ^2),
α is added to the prior *s* to reflect the uncertainty in the *IMO* model outputs.

APPENDIX B - CALCULATION OF THE POSTERIOR DISTRIBUTIONS OF THE AVERAGE SOIL WATER DEPLETION IN THE FIELD USING THE HEIRARCHICAL MODEL

The measured soil moisture depletion at a particular location *i* can be expressed as:

$D_i \mid \delta_i , \sigma^2_{Di} \sim N(\delta_i , \sigma^2_{Di})$ σ^2_{Di} assumed known

The true soil water depletion at at a particular location *i* can be expressed as:

$\delta_i \mid \omega , \sigma^2_{\delta} \sim N(\omega , \sigma^2_{\delta})$ $\sigma^2_{\delta} = s^2$ assumed known from IMO

The prior distribution of the average soil water depletion in the field can be expressed as:

$\omega \sim N(m , \alpha^2)$ m assumed known from IMO
α^2 is a user input based on an educated guess

Then:

$$f(D_i \mid \delta_i , \sigma^2_{Di}) = \frac{1}{\sqrt{2\pi\sigma^2_{Di}}} \exp\left[-\frac{1}{2\sigma^2_{Di}}(D_i - \delta_i)^2\right]$$

$$=> L(\tilde{D} \mid \tilde{\delta}, \tilde{\sigma}^2_D) = \prod_{i=1}^{n} \frac{1}{\sqrt{2\pi\sigma^2_{Di}}} exp\left[\frac{-1}{2\sigma^2_{Di}}(D_i - \delta_i)^2\right]$$

$$\propto exp\left[\frac{-1}{2}\sum_{i=1}^{n}\frac{1}{\sigma^2_{Di}}(D_i - \delta_i)^2\right]$$

And,

$$f(\delta_i \mid \omega , \sigma^2_{\delta}) = \frac{1}{\sqrt{2\pi\sigma^2_{\delta}}} exp\left[\frac{-1}{2\sigma^2_{\delta}}(\delta_i - \omega)^2\right]$$

$$f(\tilde{\delta} \mid \omega , \sigma^2_{\delta}) \propto exp\left[\frac{-1}{2\sigma^2_{\delta}} \sum_{i=1}^{n}(\delta_i - \omega)^2\right]$$

$$f(\omega) = \frac{1}{\sqrt{2\pi\alpha^2}} exp\left[\frac{-1}{2\alpha^2}(\omega - m)^2\right]$$

$$\propto exp\left[\frac{-1}{2\alpha^2}(\omega - m)^2\right]$$

$$=> f\left(\tilde{\delta}, \omega \,\middle|\, \tilde{D}\right)$$

$$\propto exp\left[\frac{-1}{2}\sum_{i=1}^{n}\frac{1}{\sigma_{Di}^2}(D_i - \delta_i)^2\right] exp\left[\frac{-1}{2\sigma_\delta^2}\sum_{i=1}^{n}(\delta_i - \omega)^2\right] exp\left[\frac{-1}{2\alpha^2}(\omega - m)^2\right]$$

We want: $f\left(\omega \,\middle|\, \tilde{D}\right)$

$$f\left(\omega \,\middle|\, \tilde{D}\right) \propto exp\left[\frac{-1}{2\alpha^2}(\omega - m)^2\right]\prod_{i=1}^{n} N\left(\delta_i \,\middle|\, \omega, \sigma_\delta^2 + \sigma_{Di}^2\right)$$

$$\propto exp\left[\frac{-1}{\alpha^2}(\omega - m)^2\right] exp\left[\frac{-1}{2}\sum_{i=1}^{n}\frac{1}{\sigma_{Di}^2 + \sigma_\delta^2}(D_i - \omega)^2\right]$$

$$Q = \frac{-1}{2}\left[\frac{1}{2\alpha^2}(\omega^2 - 2\omega m + m^2) \quad + \sum_{i=1}^{n}\frac{1}{\sigma_{Di}^2 + \sigma_\delta^2}\left(\omega^2 - 2\omega D_i + {D_i}^2\right) \quad \right]$$

$$\propto \frac{-1}{2}\left[\frac{1}{\alpha^2}(\omega^2 - 2\omega m) \quad + \sum_{i=1}^{n}\frac{1}{\sigma_{Di}^2 + \sigma_\delta^2}(\omega^2 - 2\omega D_i) \quad \right]$$

$$= \frac{-1}{2}\left(\left\{\frac{1}{\alpha^2} + \sum_{i=1}^{n}\frac{1}{\sigma_{Di}^2 + \sigma_\delta^2}\right\}\left\{\omega^2 - 2\omega\left[\frac{\frac{m}{\alpha^2} + \sum_{i=1}^{n}\frac{D_i}{\sigma_{Di}^2 + \sigma_\delta^2}}{\frac{1}{\alpha^2} + \sum_{i=1}^{n}\frac{1}{\sigma_{Di}^2 + \sigma_\delta^2}}\right]\right\}\right)$$

$$=> \hat{\omega} = \frac{\frac{m}{\alpha^2} + \sum_{i=1}^{n}\frac{D_i}{\sigma_{Di}^2 + \sigma_\delta^2}}{\frac{1}{\alpha^2} + \sum_{i=1}^{n}\frac{1}{\sigma_{Di}^2 + \sigma_\delta^2}}$$

$$\hat{\alpha}^2 = \frac{\frac{m}{\alpha^2} + \sum_{i=1}^{n}\frac{D_i}{\sigma_{Di}^2 + \sigma_\delta^2}}{\frac{1}{\alpha^2} + \sum_{i=1}^{n}\frac{1}{\sigma_{Di}^2 + \sigma_\delta^2}}$$

Where $\omega \,\middle|\, \tilde{D} \sim N(\hat{\omega}, \hat{\alpha}^2)$ is the posterior distribution of the average soil moisture depletion in the field

APPENDIX C– TIME-LAGGED CROSS-CORRELATION RESULTS

Table 1: Time lag at maximum correlation level, maximum correlation value, maximum observed Δθ at the 30 cam depth, and section number for each position along the FO cable transect.

Position (m)	Corr. Coef.	Time Lag (hr)	Max Δθ (m^3/m^3)	Section
4.5	0.00	26	0.01	1
5	0.08	-22	0.01	1
5.5	0.13	15	0.01	1
6	0.33	-2	0.01	1
6.5	0.53	-3	0.02	1
7	0.30	-3	0.02	1
7.5	0.13	-10	0.03	1
8	0.17	-16	0.08	1
8.5	0.35	-4	0.18	1
9	0.30	-10	0.18	1
9.5	0.29	-10	0.10	1
10	0.50	-11	0.04	1
10.5	0.61	-10	0.02	1
11	0.65	-8	0.02	1
11.5	0.48	2	0.02	1
12	0.25	-16	0.02	1
12.5	0.34	11	0.02	1
13	0.39	8	0.03	1
13.5	0.51	6	0.02	1
14	0.27	-10	0.01	1
14.5	0.38	5	0.01	1
15	0.31	17	0.01	1
15.5	0.27	15	0.01	1
16	0.29	-10	0.02	1
16.5	0.30	14	0.02	1
17	0.37	-9	0.03	1
17.5	0.27	-6	0.02	1
18	0.17	-18	0.03	1
18.5	0.18	-18	0.04	1
19	0.31	-4	0.03	1
19.5	0.60	-4	0.04	1

Position (m)	**Corr. Coef.**	**Time Lag (hr)**	**Max Δθ (m^3/m^3)**	**Section**
20	0.66	0	0.02	1
20.5	0.62	0	0.02	1
21	0.37	-4	0.02	1
21.5	0.25	-5	0.02	1
22	0.27	-13	0.02	1
22.5	0.38	13	0.01	1
23	0.40	13	0.01	1
23.5	0.30	15	0.00	1
24	N/A	26	0.00	1
24.5	N/A	26	0.00	1
25	N/A	26	0.00	1
25.5	0.40	-1	0.01	1
26	0.08	-13	0.01	1
26.5	0.07	-12	0.02	1
27	0.40	5	0.01	1
27.5	0.31	5	0.01	1
28	0.33	6	0.01	1
28.5	0.44	5	0.01	1
29	0.35	6	0.00	1
29.5	0.45	4	0.01	1
30	0.45	3	0.01	1
30.5	0.29	4	0.01	1
31	0.38	-18	0.01	1
31.5	0.35	3	0.01	1
32	0.37	-19	0.02	1
32.5	0.34	-1	0.01	1
33	0.46	-1	0.01	1
33.5	0.33	4	0.01	1
34	0.25	-1	0.01	1
34.5	0.38	-2	0.01	1
35	0.12	8	0.01	1
35.5	0.20	8	0.01	1
36	0.19	-8	0.01	1
36.5	0.42	-8	0.01	1
37	0.35	3	0.01	1
37.5	0.18	18	0.01	1

Position (m)	Corr. Coef.	Time Lag (hr)	Max $\Delta\theta$ (m^3/m^3)	Section
38	0.00	-17	0.00	1
38.5	N/A	26	0.00	1
39	0.00	23	0.01	1
39.5	N/A	26	0.00	1
40	0.35	20	0.01	1
40.5	0.46	-1	0.01	1
41	0.37	-17	0.02	1
41.5	0.33	-2	0.02	1
42	0.57	8	0.01	1
42.5	0.59	8	0.00	1
43	0.64	4	0.00	1
43.5	0.48	8	0.01	1
44	0.37	0	0.01	1
44.5	0.38	-15	0.02	1
45	0.27	9	0.03	1
45.5	0.35	18	0.02	1
46	0.32	18	0.02	1
46.5	0.38	1	0.01	1
47	0.31	3	0.01	1
47.5	0.00	-7	0.01	1
48	0.00	-1	0.01	1
48.5	0.00	10	0.01	1
49	0.33	-2	0.01	1
49.5	0.35	-1	0.01	1
50	0.41	-11	0.02	1
50.5	0.67	0	0.03	1
51	0.85	0	0.03	1
51.5	0.94	0	0.02	1
52	0.92	0	0.02	1
52.5	0.874	0	0.01	2
53	0.667	0	0.01	2
53.5	0.540	1	0.01	2
54	0.560	-3	0.01	2
54.5	0.564	-3	0.01	2
55	0.742	-7	0.03	2
55.5	0.833	-1	0.05	2
56	0.870	-1	0.07	2
56.5	0.926	-1	0.09	2

Position (m)	Corr. Coef.	Time Lag (hr)	Max Δθ (m^3/m^3)	Section
57	0.948	1	0.10	2
57.5	0.921	0	0.10	2
58	0.903	0	0.11	2
58.5	0.915	0	0.12	2
59	0.906	0	0.14	2
59.5	0.902	0	0.15	2
60	0.948	0	0.16	2
60.5	0.905	-1	0.19	2
61	0.960	1	0.12	2
61.5	0.962	1	0.09	2
62	0.945	-2	0.07	2
62.5	0.963	-3	0.07	2
63	0.952	-3	0.05	2
63.5	0.939	-3	0.04	2
64	0.923	-2	0.04	2
64.5	0.906	-2	0.04	2
65	0.870	-2	0.04	2
65.5	0.877	-1	0.03	2
66	0.905	0	0.05	2
66.5	0.924	2	0.10	2
67	0.934	1	0.14	2
67.5	0.946	1	0.13	2
68	0.961	0	0.11	2
68.5	0.937	0	0.07	2
69	0.916	-2	0.05	2
69.5	0.907	0	0.04	2
70	0.929	0	0.04	2
70.5	0.953	0	0.05	2
71	0.962	0	0.07	2
71.5	0.978	0	0.10	2
72	0.971	0	0.11	2
72.5	0.946	0	0.11	2
73	0.933	0	0.10	2
73.5	0.936	0	0.08	2
74	0.930	0	0.06	2
74.5	0.930	1	0.04	2
75	0.827	1	0.02	2

Position (m)	**Corr. Coef.**	**Time Lag (hr)**	**Max Δθ (m^3/m^3)**	**Section**
75.5	0.510	6	0.01	2
76	0.500	1	0.01	2
76.5	0.686	1	0.01	2
77	0.872	0	0.02	2
77.5	0.950	0	0.06	2
78	0.954	1	0.11	2
78.5	0.958	2	0.25	2
79	0.913	2	0.37	2
79.5	0.920	2	0.23	2
80	0.939	1	0.13	2
80.5	0.971	0	0.10	2
81	0.960	0	0.07	2
81.5	0.900	0	0.06	2
82	0.866	0	0.03	2
82.5	0.522	3	0.01	2
83	0.667	2	0.01	2
83.5	0.522	2	0.01	2
84	0.404	3	0.01	2
84.5	0.588	3	0.03	2
85	0.611	-2	0.03	2
85.5	0.830	-3	0.02	2
86	0.773	-2	0.03	2
86.5	0.880	1	0.04	2
87	0.893	2	0.08	2
87.5	0.918	2	0.15	2
88	0.892	2	0.13	2
88.5	0.899	2	0.05	2
89	0.922	2	0.02	2
89.5	0.881	2	0.01	2
90	0.879	1	0.01	2
90.5	0.883	1	0.02	2
91	0.896	1	0.04	2
91.5	0.971	0	0.07	2
92	0.982	0	0.08	2
92.5	0.971	0	0.06	2
93	0.974	0	0.04	2
93.5	0.942	0	0.03	2

Position (m)	**Corr. Coef.**	**Time Lag (hr)**	**Max Δθ (m^3/m^3)**	**Section**
94	0.888	0	0.03	2
94.5	0.929	3	0.04	2
95	0.949	1	0.05	2
95.5	0.962	1	0.05	2
96	0.924	0	0.06	2
96.5	0.861	0	0.05	2
97	0.854	0	0.04	2
97.5	0.890	0	0.05	2
98	0.952	0	0.05	2
98.5	0.941	0	0.06	2
99	0.922	3	0.07	2
99.5	0.957	0	0.08	2
100	0.971	0	0.07	2
100.5	0.979	-1	0.06	2
101	0.956	-1	0.04	2
101.5	0.929	-3	0.03	2
102	0.889	-3	0.02	2
102.5	0.840	0	0.03	2
103	0.847	1	0.04	2
103.5	0.891	-1	0.05	2
104	0.921	0	0.05	2
104.5	0.893	1	0.03	2
105	0.718	4	0.02	2
105.5	0.566	5	0.02	2
106	0.480	-3	0.01	2
106.5	0.263	0	0.01	2
107	0.175	-10	0.01	2
107.5	0.105	-19	0.02	2
108	0.448	0	0.03	3
108.5	0.498	8	0.03	3
109	0.479	9	0.02	3
109.5	0.183	9	0.02	3
110	0.077	11	0.02	3
110.5	0.033	15	0.04	3
111	0.309	1	0.05	3
111.5	0.567	1	0.05	3

Position (m)	Corr. Coef.	Time Lag (hr)	Max Δθ (m^3/m^3)	Section
112	0.659	3	0.05	3
112.5	0.733	4	0.06	3
113	0.776	4	0.08	3
113.5	0.823	4	0.13	3
114	0.842	3	0.14	3
114.5	0.841	2	0.13	3
115	0.879	5	0.10	3
115.5	0.883	5	0.08	3
116	0.909	2	0.09	3
116.5	0.912	2	0.13	3
117	0.867	3	0.19	3
117.5	0.836	3	0.20	3
118	0.904	2	0.19	3
118.5	0.931	2	0.19	3
119	0.928	2	0.12	3
119.5	0.942	2	0.09	3
120	0.945	1	0.06	3
120.5	0.958	2	0.04	3
121	0.934	2	0.04	3
121.5	0.950	2	0.04	3
122	0.933	2	0.04	3
122.5	0.888	2	0.04	3
123	0.823	-1	0.04	3
123.5	0.733	-9	0.03	3
124	0.623	2	0.01	3
124.5	0.333	8	0.01	3
125	0.286	2	0.01	3
125.5	0.289	8	0.01	3
126	0.348	7	0.01	3
126.5	0.112	17	0.01	3
127	0.067	16	0.01	3
127.5	0.620	3	0.02	3
128	0.817	5	0.04	3
128.5	0.850	4	0.08	3
129	0.841	0	0.10	3
129.5	0.843	4	0.12	3
130	0.887	4	0.14	3
130.5	0.898	3	0.15	3

Position (m)	Corr. Coef.	Time Lag (hr)	Max $\Delta\theta$ (m^3/m^3)	Section
131	0.861	3	0.18	3
131.5	0.891	2	0.19	3
132	0.955	2	0.16	3
132.5	0.934	2	0.16	3
133	0.903	1	0.21	3
133.5	0.878	4	0.23	3
134	0.900	4	0.15	3
134.5	0.879	2	0.08	3
135	0.742	2	0.05	3
135.5	0.382	8	0.02	3
136	0.816	-4	0.01	3
136.5	0.354	-3	0.01	3
137	0.160	1	0.01	3
137.5	0.134	7	0.01	3
138	0.280	8	0.01	3
138.5	0.571	4	0.02	3
139	0.782	5	0.04	3
139.5	0.857	4	0.09	3
140	0.877	3	0.08	3
140.5	0.931	2	0.05	3
141	0.949	2	0.03	3
141.5	0.938	2	0.03	3
142	0.938	1	0.03	3
142.5	0.910	2	0.03	3
143	0.922	1	0.05	3
143.5	0.928	2	0.08	3
144	0.922	1	0.13	3
144.5	0.923	3	0.20	3
145	0.911	2	0.25	3
145.5	0.946	1	0.19	3
146	0.954	0	0.13	3
146.5	0.955	0	0.10	3
147	0.934	1	0.10	3
147.5	0.940	2	0.13	3
148	0.960	3	0.25	3
148.5	0.943	3	0.26	3
149	0.967	4	0.18	3
149.5	0.965	3	0.17	3

Position (m)	Corr. Coef.	Time Lag (hr)	Max $\Delta\theta$ (m^3/m^3)	Section
150	0.947	3	0.14	3
150.5	0.943	3	0.10	3
151	0.966	2	0.07	3
151.5	0.962	2	0.05	3
152	0.954	3	0.05	3
152.5	0.945	1	0.05	3
153	0.925	1	0.04	3
153.5	0.902	1	0.03	3
154	0.837	5	0.02	3
154.5	0.805	6	0.01	3
155	0.408	-11	0.01	3
155.5	0.286	-2	0.01	3
156	0.263	15	0.01	3
156.5	0.286	15	0.01	3
157	0.445	13	0.01	3
157.5	0.445	13	0.01	3
158	0.615	6	0.01	3
158.5	0.356	6	0.02	4
159	0.492	-12	0.02	4
159.5	0.627	-5	0.03	4
160	0.839	0	0.04	4
160.5	0.873	1	0.05	4
161	0.834	3	0.05	4
161.5	0.767	4	0.04	4
162	0.578	5	0.04	4
162.5	0.624	8	0.03	4
163	0.762	4	0.03	4
163.5	0.890	3	0.03	4
164	0.924	2	0.04	4
164.5	0.904	3	0.06	4
165	0.896	3	0.08	4
165.5	0.887	3	0.11	4
166	0.879	2	0.14	4
166.5	0.940	2	0.12	4
167	0.924	1	0.08	4
167.5	0.891	0	0.06	4
168	0.833	0	0.06	4
168.5	0.850	0	0.06	4

Position (m)	Corr. Coef.	Time Lag (hr)	Max $\Delta\theta$ (m^3/m^3)	Section
169	0.861	0	0.06	4
169.5	0.881	2	0.07	4
170	0.902	2	0.07	4
170.5	0.878	2	0.09	4
171	0.853	3	0.08	4
171.5	0.896	1	0.05	4
172	0.832	-2	0.03	4
172.5	0.738	-3	0.03	4
173	0.660	-3	0.03	4
173.5	0.747	-2	0.05	4
174	0.590	-2	0.06	4
174.5	0.696	1	0.07	4
175	0.778	7	0.07	4
175.5	0.767	8	0.07	4
176	0.854	4	0.10	4
176.5	0.822	4	0.13	4
177	0.825	1	0.10	4
177.5	0.770	1	0.05	4
178	0.564	0	0.02	4
178.5	0.404	5	0.01	4
179	0.169	5	0.01	4
179.5	0.204	5	0.01	4
180	0.333	14	0.01	4
180.5	0.316	17	0.01	4
181	0.213	16	0.01	4
181.5	0.540	-7	0.02	4
182	0.655	-7	0.03	4
182.5	0.632	-7	0.04	4
183	0.535	2	0.05	4
183.5	0.638	2	0.05	4
184	0.742	2	0.05	4
184.5	0.837	0	0.06	4
185	0.847	4	0.09	4
185.5	0.920	2	0.17	4
186	0.969	2	0.30	4
186.5	0.965	2	0.34	4
187	0.916	2	0.41	4
187.5	0.920	2	0.25	4

Position (m)	Corr. Coef.	Time Lag (hr)	Max Δθ (m^3/m^3)	Section
188	0.922	2	0.18	4
188.5	0.914	1	0.14	4
189	0.916	0	0.11	4
189.5	0.939	1	0.09	4
190	0.933	1	0.07	4
190.5	0.935	2	0.06	4
191	0.889	2	0.07	4
191.5	0.888	4	0.08	4
192	0.873	2	0.08	4
192.5	0.848	3	0.07	4
193	0.909	4	0.05	4
193.5	0.879	4	0.04	4
194	0.895	3	0.03	4
194.5	0.872	1	0.04	4
195	0.867	3	0.04	4
195.5	0.869	4	0.05	4
196	0.818	4	0.05	4
196.5	0.841	4	0.07	4
197	0.843	-1	0.09	4
197.5	0.876	3	0.11	4
198	0.912	3	0.11	4
198.5	0.928	2	0.11	4
199	0.920	0	0.10	4
199.5	0.941	0	0.09	4
200	0.925	0	0.09	4
200.5	0.930	1	0.09	4
201	0.933	0	0.07	4
201.5	0.899	0	0.06	4
202	0.878	0	0.04	4
202.5	0.892	1	0.03	4
203	0.809	0	0.02	4
203.5	0.808	3	0.02	4
204	0.791	0	0.03	4
204.5	0.700	0	0.03	4
205	0.735	0	0.04	4
205.5	0.722	0	0.05	4
206	0.782	6	0.05	4
206.5	0.811	2	0.05	4

Position (m)	**Corr. Coef.**	**Time Lag (hr)**	**Max Δθ (m^3/m^3)**	**Section**
207	0.828	4	0.06	4
207.5	0.819	4	0.07	4
208	0.803	6	0.07	4
208.5	0.833	4	0.06	4
209	0.769	4	0.06	4
209.5	0.724	3	0.06	4
210	0.773	3	0.07	4
210.5	0.776	3	0.08	4
211	0.851	3	0.10	4
211.5	0.898	3	0.11	4
212	0.912	3	0.08	4
212.5	0.895	4	0.05	4
213	0.838	4	0.06	4
213.5	0.855	1	0.06	4
214	0.811	1	0.08	4
214.5	0.842	1	0.10	4
215	0.868	1	0.13	4
215.5	0.877	1	0.17	4
216	0.884	7	0.20	4
216.5	0.866	7	0.19	4
217	0.864	7	0.19	4
217.5	0.777	4	0.14	4
218	0.629	5	0.10	4
218.5	0.773	7	0.10	4
219	0.838	5	0.09	4
219.5	0.901	5	0.06	4
220	0.907	4	0.04	4
220.5	0.884	4	0.03	4
221	0.809	4	0.04	4
221.5	0.856	4	0.05	4
222	0.785	3	0.10	4
222.5	0.704	4	0.15	4
223	0.702	3	0.13	4
223.5	0.644	4	0.09	4
224	0.680	7	0.09	4
224.5	0.666	7	0.08	4
225	0.731	7	0.08	4
225.5	0.817	5	0.11	4

Position (m)	**Corr. Coef.**	**Time Lag (hr)**	**Max Δθ (m^3/m^3)**	**Section**
226	0.938	3	0.12	4
226.5	0.963	2	0.12	4
227	0.961	2	0.11	4
227.5	0.939	2	0.11	4
228	0.883	2	0.13	4
228.5	0.892	2	0.14	4
229	0.696	6	0.10	4
229.5	0.626	5	0.07	4
230	0.572	0	0.06	4
230.5	0.383	6	0.06	4
231	0.055	11	0.07	4
231.5	0.021	11	0.07	4
232	0.074	15	0.07	4
232.5	0.220	14	0.08	4
233	0.662	9	0.12	4
233.5	0.856	9	0.20	4
234	0.840	6	0.24	4
234.5	0.856	5	0.21	4
235	0.875	4	0.17	4
235.5	0.891	4	0.18	4
236	0.879	4	0.17	4
236.5	1.000	0	0.01	4
237	1.000	0	0.01	4
237.5	1.000	0	0.01	4
238	1.000	0	0.01	4
238.5	1.000	0	0.01	4
239	1.000	0	0.01	4
239.5	N/A	26	0.00	4
240	N/A	26	0.00	4
240.5	N/A	26	0.00	4